Hydration and Durability Characteristics of a New Composite Cementitious Binder Containing Slag and Calcite

スラグとカルサイトを含む新しい複合セメントバインダーの水和と耐久性に関する研究

Chuang LI

Supervised by Associate Prof. Yogarajah ELAKNESWARAN

Doctor of Philosophy

in

Division of Sustainable Resources Engineering

Graduate School of Engineering

of the

HOKKAIDO UNIVERSITY

Japan

Abstract

In past years, the most widely used cementitious material is cement, which is produced by burning limestone to a temperature over 950 degree along with other materials such as chalk, clay and iron core, emitting a significant amount of CO_2. For instance, 1000 kg of cement production releases around 900 kg CO_2 gas. Subsequently, cement production accounts for 5% - 7% of total CO_2 emissions. Therefore, in recent years, cement has been blended with different cementitious materials such as fly ash and blast furnace slag, which are primarily by-products from coal power plants and steel manufacturing, respectively, to reduce the carbon footprint associated with cement production. In addition, blended cement improved the mechanical and durability of concrete by altering its microstructure and hydration products. However, research reported a minimum of 35% cement content by volume in the blended cement. Therefore, this study aims to develop a new composite cementitious binder containing slag and calcite towards low-carbon and sustainable cementitious materials. To use this new composite as an alternative to cement, the mechanical and durability properties of the new composite are explored in detail for the short and long term.

In chapter 3, a new composite cementitious material consists of calcium hydroxide, blast furnace slag (BFS), calcite and expansive agent, where calcite acts as a filler material. The influence of the filler content, its fineness and water-to-powder ratio (W/P) on hydration kinetics and microstructure behaviour are experimentally studied in this study. The experiment tests include X-ray diffraction (XRD), TG-differential thermal analysis (DTA), selective dissolution measurement and mercury intrusion porosimetry (MIP). The experimental results revealed that the slag reaction degree is enhanced by increasing the filler content and fineness of the filler in high W/P ratio. However, the filler fineness does not show significant improvement in the hydration degree of slag with low W/P ratio in later curing period. This can be attributed to the reduced amount of available water for the hydration reaction. Moreover, it should be noted that, unlike in other studies, hemicarboaluminate,

which is thermodynamically unstable than monocarboaluminate is formed even at the later age of hydration reaction in the presence of calcium carbonate. Furthermore, an existing hydration model, which was developed primarily to predict the hydration of portland cement, is modified to predict the hydration behaviour of slag in the new composite over the hydration age. The predicted results showed good agreement with the experimental results in terms of hydration products and porosity.

Carbon dioxide penetration into the cementitious material causes numerous chemo-mechanical changes and effects the strength, porosity, pore size distribution, and chemistry. Hence, in the chapter 4, the carbonation behaviour of the new composite under an environment of 5% CO_2 and 60% humidity is examined. The phase changes due to the carbonation are quantified through XRD and TG tests as a function of carbonation period. The experimental results revealed that calcite is formed during the carbonation, where ettringite, hemicarboaluminate, and portlandite react with carbon dioxide. In addition, the fineness of calcite filler does not show a significant influence on carbonation behaviour. However, the carbonation rate increases with an increase in calcite dosage.

The influence of chloride uptake by the new composite is studied in chapter 5. To study the chloride ingress profiles, 28-day aged hydrated specimen is covered by epoxy resin except for the bottom of the circular surface, which faced 500 mL 0.5M NaCl solution for up to 12 months. The chloride penetration characteristics of the proposed material are investigated by experimental programmes, including XRD, titration, ion chromatography, TG-DTA methods. Based on the experimental results, the amount of chemical bound chloride in Afm phases, physical bound chloride in C-S-H, and free chloride in pore solution are established as a function of the immersion period, as well as a function of the distance from the exposed surface. The experimental results show that the amount of free chloride in pore solution is enhanced by increasing the fineness of the calcite filler, as well as the addition rate. However, the filler fineness does not show a significant influence in chemical bound chloride in Afm phase. Moreover, it should be noted that hemicrboaluminate converted into the

Friedel's salt when exposure to the chloride. However, immersion period does not show a significant influence on the chloride penetration distance. In other word, the new composite cementitious binder resists the chloride ingression.

In the last chapter, the hydration and durability characteristics of this new composite cementitious binder are summarised, and the issues are critically discussed for future studies.

概要

セメントは、モルタルやコンクリートの原料として年間 40 億トン以上使用されている。従来のセメントは、カルサイト($CaCO_3$)の焼成物である酸化カルシウムが主要な原料の一つであり、その製造工程で地球温暖化ガスである二酸化炭素を多量に排出する。この量は世界の総排出量の約 8%に相当するので、地球温暖化を抑制するために、従来のセメントを代替する新しい材料を開発することが重要な課題となっている。本論文では、従来のセメントの代替物として、スラグ、カルサイト、水酸化カルシウムと膨張剤を原料とする新しい複合バインダーを開発し、バインダーの水和挙動を理解することを目的として水和生成物、空隙率、相組成、化学収縮などを詳細に調べている。また、このバインダーを用いたコンクリートの長期耐久性に関わる因子として、炭素化や塩化物イオンの浸透性についても検討している。

本論文は全六章で構成され、各章の概要及び内容は以下のとおりである。

第一章では、本研究の背景と目的及び論文の構成を整理している。

第二章では、セメント系材料(ポルトランドセメント、高炉水砕スラグとポルトランドセメントを混合したスラグセメント、カルサイトセメント及びアルカリ活性化スラグ)の水和反応における生成物に関する先行研究を調査し、まとめている。また、コンクリート中の鉄筋の腐食の支配的な要因であるセメント系硬化体の炭酸化や塩化物イオンの浸透性について従来の研究をまとめている。

第三章では、スラグ、カルサイト、水酸化カルシウムと膨張剤を含む新しい複合セメントバインダーを提案し、その水和機構を解明することを目的として、カルサイトの添加量や粒子径の影響を調べている。バインダーの養生産物を X 線回折(XRD)-Rietveld 法、選択溶解法、熱重量分析(TG-DTA)、水銀圧入(MIP)などの手法で調べ、1)スラグの反応率は 35%から 45%であること、2)高い水粉体比ではカルサイト含有量の増加、粒子径の減少に伴ってスラグの反応率が向上すること、3)熱力学的に安定なエトリンガイト(Ettringite)のほかに、熱力学的に準安定なヘミカーボネット(Hemicarboaluminate)が生成することを明らかにしている。また、水和産物、空隙率、化学収縮に関して、熱力学モデルに基づく予測と実験結果がよく一致することを確認している。

第四章では、新しい複合セメントバインダーの炭酸化について検討し、強度、空隙率、空隙分布および化学的性質に対する影響を調べている。X 線回折(XRD)-Rietveld 法および 熱重量分析(TG-DTA)法による測定の結果、時間の経過に伴ってバインダー中のエトリンガイト、ヘミカーボネート、水酸化カルシウムが外部から侵入した炭酸ガスと反応し、カルサイトが生成することを確認している。 炭酸化の速度は、バインダーに添加したカルサイトの粒子径にはほとんど依存しないが、カルサイトの添加量の増加に伴い加速した。

第五章では、新しい複合セメントバインダーを塩水中に浸漬した際の塩化物イオンの拡散について検討している。X 線回折(XRD)-Rietveld 法や、Ag 滴定法、イオンクロマトグラフ

ィー、熱重量分析(TG-DTA)法などの複数の実験を組み合わせて評価を行い、バインダー中の鉱物種に化学的に結合した塩化物イオン(Chemically bound chloride)、物理的に吸着した塩化物イオン(Physically bound chloride)およびバインダー細孔溶液中の自由塩化物イオン(Free chloride)の量を個別に定量し、浸漬時間や浸漬面からの距離の関数として評価している。実験の結果から、1)自由塩化物イオンの量はバインダに添加したカルサイトの粒子径が小さくなり、添加量が増加するのに従って増加すること、2)ヘミカーボネート相は塩化物イオンと反応し、フリーデル氏塩相に転移する可能性があることを確認している。さらに、通常のセメントペーストとは異なり、本論文で提案したバインダーの場合、長時間が経過しても塩化物イオンが表面近傍にとどまり、深部には浸透しないことを新たに見出している。このことは、この新しい複合セメントバインダーが強い塩化物耐性を持つことを示唆している。

第六章では、まとめとして本研究の成果及び今後の課題について総括して述べている。また、この新しい複合材料の水和と耐久性の挙動を総括し、今後の研究の方向性についても議論している。

Acknowledgements

I would first like to thank my supervisor, Prof. Yogarajah ELAKNESWARAN, for guiding and supporting throughout all my study from my master period. The door of his office was always open whenever I had some troubles in experiments or paper writing, even when I lost my destination in my life. It is my honor to benefit from his personality and diligence, which I will treasure my whole life. His insightful feedback pushed me to sharpen my thinking and brought my horizons to a higher level. It has been a great privilege and joy to study under his guidance and supervision. Without his keen insights and constant encouragement, it would not have been completed. My gratitude to him knows no bounds.

I also express my appreciation to Professor Naoki HIROYOSHI, who have given me kind encouragement and useful instruction which are great benefit to me in my research. His clear comments and suggestions have inspired me and helped me a lot to finish this research. I believe that his invaluable advice and kindness will have a strong influence to me on how to behave myself in better.

I would also like to thank Professor Tsutomu SATO, Ryoma KITAGAKI as members of the dissertation evaluation committee. The rich experiment and knowledge in their respective field also improve my study. The experience and profit I obtained will be of grand importance to my further life.

Special thanks should go to Technology & Solution, TAISEI CORPORATION for providing the research opportunity and giving financial support for this study.

Particularly, I am the recipient of a scholarship provided by Hokkaido University DX Doctoral Fellowship. I am writing to express my sincere gratitude to Hokkaido University for making the Hokkaido University DX Doctoral Fellowship possible. I am thrilled to learn of my selection for this honor, and I am deeply appreciative of the support from Hokkaido University.

Last but not the least, my gratitude also extends to my laboratory. It was a wonderful place to study and improve my skills the my last past 5 years. Everyone here shares their happiness and gladness to each other, making our team like a home. I am truly blessed to have so many great things in my life.

Contents

List of figures

List of tables

CHAPTER 1

General introduction

1.1 Background

Concrete made of OPC (Ordinary Portland Cement) and aggregates mixed with water is the most secondly consumed material in the industrialized world, only surpassed by water and performs an indispensable role in the field of civil engineering construction. The rising population and urbanization upsurge the demand for concrete across the globe. Even though the concrete remains as cost and energy efficient material compared to other construction materials, the concrete production is accountable for 9% of the total greenhouse gas emission, in which around 5-7% is reported to be during the large-scale cement production (Cadavid-Giraldo, Velez-Gallego, and Restrepo-Boland 2020; Coffetti et al. 2022). During the Portland cement manufacturing process, the CO_2 mainly emits because of the decarbonation of limestone in the clinkering process followed by releasing from fuel and electricity used for heating and milling purposes (Skibsted and Snellings 2019). The accumulation of emitted greenhouse gases is the most serious threat in the recent decades, as it directly affects the climate changing. Therefore, numerous methods, e.g. the use of supplementary cementitious materials (SCMs), process optimization, and alternative clinker production with a reduced amount of limestone, have been recently used in the cement manufacturing plants and concrete industry for the mitigation of anthropogenic carbon dioxide emission and to improve the sustainability of the concrete production (Benhelal, Zahedi, and Hashim 2012; Noguchi et al. 2021).

The conventional attempt to decrease the CO_2 emission is the partial or complete replacement of clinker with SCMs in cement or replacement of cement with SCMs in concrete mixture. The commonly used SCMs as alternative binders include mainly inert material like limestone and reactive material from industrial by products including blast furnace slag (BFS) from iron and steel production, fly ash from coal power plant and silica fume from the silicon or ferrosilicon industry. It is also notable that using SCMs as building materials has another merit for the problems associated with waste management of industrial by-products such as reducing the land occupation for disposal and other severe environmental issues related to the landfills. In the fly ash blended cement, the fly ash

acts as filler or inert due to low reactivity during the early stage of hydration period, which leads to the provision of additional nucleation site and increases the effective water content for the cement hydration reaction, and performs as active pozzolanic material in later age as fly ash reacts with precipitated portlandite by cement reaction to form C-S-H (Deschner et al. 2012; Yu and Ye 2013). Despite the positive effects of fly ash, the field application of large amounts of fly ash is limited due to the low reactivity of fly ash at the early stage of curing period, which leads to the much lower development of mechanical properties of fly ash mixture compared to the pure concrete (Gunasekara et al. 2020; Nochaiya, Wongkeo, and Chaipanich 2010; J. Yang et al. 2019). The silica fume which consists of >80 wt% of amorphous silica is generally used with pure cement or blended cement containing slag or fly ash to improve the pozzolanic reaction (Yajun and Cahyadi 2003). Even though the silica fume exists high reactivity because of high amorphous content and fine particles, high degree agglomeration of silica fume was reported in the past research works owing to the very fine particles of silica fume i.e., 0.1-0.5 μm, and it is difficult to disperse the particles due to the high interparticle forces, thus it reduces the effectiveness of the replacement of silica fume in the cement mixture (Yajun and Cahyadi 2003; Z. Zhang, Zhang, and Yan 2016).

Among the SCMs, the BFS is most commonly used to produce sustainable blended cement, as it shows better intrinsic properties compared to other blended cement paste (Briki et al. 2021; Escalante et al. 2001a; He et al. 2021). The BFS is the only SCM that behaves as a latent hydraulic material, i.e., reacts with water once activated and portlandite is not required for the hydration reaction of BFS (Juenger, Snellings, and Bernal 2019; Skibsted and Snellings 2019). Therefore, the extensive use of BFS upsurges, and which can even be used for the total replacement of OPC binders i.e., clinker free paste as well (Brough and Atkinson 2002; Kashani et al. 2014). When slag particles get in exposure to water, the aluminosilicate forms rapidly on the surfaces of the slag grains, and it fully covers the reactive materials within a few minutes. Thus, further slag reaction is hindered by aluminosilicate formation as it is impermeable to water (Altan and Erdoğan 2012; Song et al. 2000). However, in the

presence of clinker, the reaction of BFS is triggered by the high alkaline pore solution from the early cement hydration as this impermeable layer dissolves in the high alkaline environment. On the other hand, in the case of total substitution of clinker, a chemical activator to increase the pH of the pore solution is essential to initiate the hydraulic reaction (i.e., to breakdown the aluminosilicate coating) (Deir, Gebregziabiher, and Peethamparan 2014; Song et al. 2000). Alkali hydroxides, carbonates and silicates are generally used as activators for BFS mixture (Cheah, Tan, and Ramli 2021; Deir, Gebregziabiher, and Peethamparan 2014). It is reported in numerous studies that the alkali activated slag exhibits excellent mechanical and durability properties including high early strength, high resistant against to sulphate and other acid attack (Bakharev, Sanjayan, and Cheng 2003; Provis, Palomo, and Shi 2015; Song et al. 2000; X. Zhu et al. 2018). However, the hydration reaction, setting time and development of mechanical and durability characteristics are mainly varied depending on the alkali activators and their magnitudes for a specific curing condition and Water/Binder ratio (W/B) (Altan and Erdoğan 2012; Gebregziabiher, Thomas, and Peethamparan 2015; Kashani et al. 2014; N. Li et al. 2018). Li et al., (N. Li et al. 2018) reported that increasing the Na_2O to binder ratio in the slag mixture results in increasing the compressive strength and reducing the setting time owing to the increased extent of the more dissolution of solid particles in the high concentration of Na_2O solution. The effect of different type of activators such as alkali hydroxide and alkali silicate on the yield stress and rate of hydration reaction were investigated by Kashani et al., (Kashani et al. 2014), and they concluded that alkali hydroxide activators show a significant increase in the yield stress and reaction rate compared to the silicate activated slag system. Nevertheless, the alkali activated slag binders have some drawbacks such as fast setting time and subsequent shrinkage, which might be attributed to the fast dissolution and reaction due to the addition of chemical activators and high rate of carbonation (Brough and Atkinson 2002; N. Li et al. 2018; K. H. Yang et al. 2012; X. Zhu et al. 2018). The aforementioned limitations can be improved by adding calcium hydroxide activator. The Previous studies highlighted that the calcium hydroxide activated slag mixtures are beneficial for the

practical application due to the low cost and good mechanical and durability properties (Dai et al. 2021; He et al. 2018; X. Zhu et al. 2018).

Adding an inert or low-reactivity material into the SCMs mixture enhances the hydration reaction and subsequently improves the intrinsic properties of the hardened matrix, as the particles surface of the filler materials provide additional nucleation site for the formation of hydration products and increase the effective available water for hydration reaction (Adu-Amankwah et al. 2017; Y. Han, Lin, and Wang 2021; Knop, Peled, and Cohen 2014; Snellings et al. 2022). In addition to the filler effect, a significant amount of limestone/ calcite behaves as active reactant, limestone and calcite are often used as filler materials in the alumina rich SCMs (Adu-Amankwah et al. 2017; Y. Han, Lin, and Wang 2021; Snellings et al. 2022). Generally, in the Al-rich binder, the ettringite forms until the depletion of gypsum (which is the sulphate ion source for the ettringite reaction), followed by the formation of monosulfate due to reaction between additional alumina phases and formed ettringite. However, this mineralogy of the harden mixture is altered by the addition of limestone/ calcite. Because, the formation of monosulfate is inhibited in the presence of calcium carbonate which leads to the stabilization of ettringite and other carboaluminate phases (hemi carboaluminate and monocarboaluminate) (Jeong et al. 2017; Schöler et al. 2015; MacIej Zajac et al. 2014). Due to the stably formed ettringite and carboaluminate phases instead of monosulfate in the existence of calcium carbonate, the pore space of the matrix is lower compared to that without calcite/ limestone mixture, which in turn leading to the improved mechanical and durability properties (Lothenbach et al. 2008; Matschei, Lothenbach, and Glasser 2007; Ramezanianpour and Hooton 2014). Numerous research works have been carried out recently to investigate the effects of adding limestone/ calcite on microstructure and mechanical properties of blended cement mixture (Adu-Amankwah et al. 2017; Avet and Scrivener 2018; Y. Han, Lin, and Wang 2021; Rakhimova et al. 2016; Ramezanianpour and Hooton 2014; Snellings et al. 2022; MacIej Zajac et al. 2014). It was reported that the porosity of the matrix decreases with calcium carbonate content up to a certain level, followed by an increase

depending on the sulphate content and alumina phases of the mixture, and this tendency is inverse to the development of mechanical properties (Adu-Amankwah et al. 2017; Rakhimova et al. 2016; Ramezanianpour and Hooton 2014; MacIej Zajac et al. 2014). However, only a limited number of studies focused on the hydration behaviour and microstructures of cement free binders with substitution of a large amount of calcite/ limestone filler.

The durability performance of cementitious materials is related to the binder, as well as the chemical reactions between the hydration products under a service environment. Since cementitious materials are often exposed to severe environments, their long-term performance is of concern. Hydrated cementitious materials exposed to aggressive environments, such as aqueous chloride, magnesium or sulfate solutions, often sustain irreversible damage as a result of paste softening and excessive volume change (Maltais, Samson, and Marchand 2004). In the presence of sulfate ions, sulfate attack occurs in cementitious materials, which can be groundwater, soil, or rainwater. Sulfate attack usually manifests itself by cracking and spalling of concrete accompanied by expansion and/or loss of strength (Shanahan and Zayed 2007). Ettringite and gypsum are the primary products of the chemical reaction between a sulfate-bearing solution and cement hydration products. Even This fact has been recognized for a long time, there has been little research on gypsum formation. Although the formation of gypsum is important, there is no clear documentation of the nature of disruption caused by gypsum (Santhanam, Cohen, and Olek 2001). In order to improve the sulfate resistance of concrete, blending slag with cement for reducing the CH and tricalcium aluminate contents. Slag has pozzolanic properties, with the application of slag in concrete decreases the amount of cement, which leads to the reduction of both heat hydration and CO_2 emission. It is reported that a replacement rate of 50% of slag by cement lower the sulfate attack around 10% under $MgSO_4$ solution compared to ordinary cement and a large amount of slag resisted the Na_2SO_4 attack but degraded strongly in $MgSO_4$ (Yan et al. 2020). Actually, in a higher slag proportion, the durability and mechanical properties of the mortar were decreased due to the small amount of clinker, which made the mortar

more susceptible to $MgSO_4$ attack. On the opposite, in a lower slag proportion, the behavior of the final mixtures in $MgSO_4$ environments was better (Yan et al. 2020). In the case of adding limestone filler to Portland cement, a low proportion (lower than10%) of limestone filler causes no significant changes in sulfate resistance of parent Portland cement, while a large proportion (more than 15%) worsened sulfate performance (Irassar 2009). Besides, the durability of alkali-activated slag (AAS) concrete in sulfate environment shows some differences compared to OPC. Both of AAS and OPC had a similar products of degradation, which are ettringite and gypsum under $MgSO_4$ environment, OPC samples had significant expansion, cracking, and loss of concrete, while AAS samples were not expanded but cracked (Bakharev, Sanjayan, and Cheng 2002).

Steel bars damaged by chloride corrosion are the main reason for the deterioration of the reinforced structure (Cai et al. 2022). The chloride resistance of OPC, slag-blend cement, limestone-cement and alkali-activated slag has been reported (Ababneh, Benboudjema, and Xi 2003; Caré 2008; Hawkins, Tennis, and Detwiler n.d.; Ogirigbo and Black 2017; Otieno, Beushausen, and Alexander 2014; Park, Ann, and Cho 2015; Z. Shi et al. 2017; Sui et al. 2019; Y. Zhu et al. 2022). In all cases, the chloride diffusion is strongly dependent on the duration of exposure to a chloride environment, as well as water to powder ratio and mixture conditions. Compared to OPC, when the slag content increased from 0% to 50%, chloride permeability diminished significantly at 90 days and a replacement rate of 60% of slag can reduce the rate of chloride transport to the lowest level (H. J. Chen et al. 2012). It indicates that the presence of slag results in a continuous reduction in diffusivity with time. Therefore, the slag-blended concretes showed considerably better resistance to chlorides ion penetration than the OPC concretes. Nevertheless, Partial replacement of clinker with limestone provides environmental and economic benefits to the concrete industry. Since limestone replaces part of the clinker, the system has a higher effective water-to-cement ratio (W/C) that can lead to an increased hydration degree of the clinker. In addition to the filler effect and the dilution effect, limestone was found to react with aluminum-rich phases of both the clinker and Supplementary Cementitious Materials

(SCMs), so that it affected the chloride binding capacity (Sui et al. 2019). However, due to its filler effect without pozzolanic proporties, large limestone content decreases strengths and increases the porosity. As a result, limestone-blended cement gives a different chloride binding capacity compared to OPC. The development of alkali-activated slag under chloride-containing environments has also been widely investigated by academia and industry for decades. Among alkali-activated slag, the alkali activator type strongly influences chloride resistance (Y. Zhu et al. 2022). AAS generally has better chloride resistance than OPC. The physical and chemical properties of precursors, as well as the type and concentration of alkaline components in activators are important parameters for the chloride resistance of AAS (Jingxiao Zhang et al. 2022).

The interactions of chloride with saturated cementitious materials are dominated by its diffusion through the pore structure of hardened paste. Chloride exists in three different forms inside of the cementitious materials, which are chemically bound chloride, physically bound chloride and free chloride. In OPC, the chloride ions can be chemically bound in alumina, ferric oxide, monsulfate (AFm)-type phases through the formation of Friedel's and Kuzel's salts as well as physically bound onto the outer surfaces of calcium-silicate-hydrate (C-S-H) gel (Z. Shi et al. 2017), and free chloride exists in the pore solution. Generally speaking, the presence of limestone can be considered as filler, although it can higher the value of effective water-to-cement ratio, lower the amount of products, leads to a higher porosity, thus increases free chloride content and decreases the amount of bound chloride (Sui et al. 2019).

Despite the importance of deconvolution of both chemical and physical binding chlorides for hardened paste performance, it is difficult to determine the amount of physically adsorbed chloride (Maraghechi et al. 2018). The focus should be on chemically bound chloride and free chloride changes. However, the amount of physically bound chloride to C-S-H still can be calculated through the differences between total chloride and other chlorides (Physical chloride and free chloride). Chemical binding chloride can be quantified by using XRD, TGA and other methods.

Carbonation is another reason cause of corrosion initiation in steel bars in reinforced-concrete structures(X. Y. Wang 2017). The service life of those structures is not only connected to the chloride corrosion but also closely related to carbonation in an atmospheric environment. Carbonation of concrete is an occurrence which involves the reaction of CO_2 with alkaline ions from the pore solution. Conventionally, carbonation reaction of concrete is considered an unfavorable event as it demeans the durability performances of cementitious materials.

In the case of OPC-based systems, most phases in hydrated cement paste can react with CO_2, to convert the calcium ions Ca^{2+} from cement paste to $CaCO_3$. Specifically, CH reacts with CO_2 to produce $CaCO_3$ and water (Šavija and Luković 2016; Tang, Ling, and Mo 2021). Other main binding component of cement, the calcium-silicate-hydrate (C-S-H), is believed to decalcify upon extended exposure to atmospheric CO_2, eventually becoming a silica gel and $CaCO_3$ in the process and losing its binding capability consequently (A. E. Morandeau and White 2015; A. Morandeau, Thiéry, and Dangla 2014). Besides, ettringite and monosulfate also can be carbonated to form $CaCO_3$, aluminum gels, water and gypsum (Šavija and Luković 2016). Meanwhile, carbonation also induces a neutralizing effect on the highly alkaline environment provided by clinker hydration, thereby increasing the vulnerability of embedded reinforced steel to corrosion (D. Zhang, Ghouleh, and Shao 2017). The carbonation reaction reduces the alkalinity of concrete and hence, making the reinforcement susceptible to corrosion. These changes can be considered passive because they occur spontaneously when cement paste reacts with CO_2. Therefore, they are commonly considered as deterioration.

Blast furnace slag (BFS) is one of the most widely used materials due to its positive effects on concrete are well known. For instance, slag-blended cements are recommended in aggressive environments such as the marine environment in coastal areas (Sanjuán et al. 2018). Although the slag can provide an adequate surface for the formation of nuclei of hydration products, cement-based

materials made of slag have a weak carbonation resistance, especially when short curing periods are applied. In fact, carbonation rate increases with increasing slag content in mortars. When AAS concrete was exposed to an atmosphere rich in CO_2, reduction in pH at the surface and crystallization of calcite and decalcified C-S-H can be observed. An increased porosity can be observed in the areas of calcite crystallization, and it is found I that AAS concrete had lower resistance to carbonation than that of OPC concrete (Bakharev, Sanjayan, and Cheng 2001). In addition, blended cements containing large replacements of OPC with BFS have been used. Slag-blended cement samples cured at high temperature have lower carbonation rates due to the fact that increased curing temperature promoted the hydration of slag forming a denser microstructure, which reduced the diffusion rate of CO_2 into the matrices, improving the durability of these pastes to carbonation (Borges et al. 2010). Moreover, the replacement of limestone in cement accelerates the carbonation rate. 15% addition rate of limestone can uptake 12% CO_2 based on dry cement mass in an accelerated carbonation process (Shao et al. 2014).

The carbonation reactions of cement-based materials occur in natural environment at a very slow rate due to the low CO_2 concentration in the atmosphere. Usually, accelerated carbonation schemes are used in the laboratory to investigate the effects of carbonation on concrete. The carbonation rates of accelerated carbonation tests are considerably higher than those of atmospheric condition. The higher carbonation rates are obtained by using higher CO_2 concentration and controlled environment (Ashraf 2016). Carbonation of hydrated paste reduces the pH of the pore solution to a low value of under 9, which is less than the depassivation threshold of reinforced steel (around 9.5) (Šavija and Luković 2016). Thus, if the front of low pH reaches the surface of reinforced steel, the protective oxide film on its surface breaks down. Corrosion then initiates, provided that moisture and oxygen are present. Apart from causing the pH drop, the most notable changes are changes in porosity, mechanical properties, and appearance of cracks, even the disintegration of the binding matrix (Ashraf 2016).

1.2 Purpose of this work

This research work attempts to study the hydration and microstructure behaviour of a new clinker-free binder containing BFS, calcite, calcium hydroxide and an expansive agent. The influence of water-to-powder ratio (W/P), calcite content and specific surface area of calcite of the clinker-free mixture on the hydration kinetics and products were also comprehensively investigated based on experiments involving selective dissolution, X-ray diffraction (XRD), Thermo gravimetric analysis (TGA) and Mercury intrusion porosimetry (MIP) analysis. Eventually, the thermodynamic framework proposed in our previous work (Yogarajah Elakneswaran et al. 2016; Krishnya, Yoda, and Elakneswaran 2021) has been amended to predict the hydration products and the porosity of clinker-free binder. The predictions were validated with the raw experimental results.

Also, the chloride transport of the new cement-free material is investigated by considering total chloride as free chloride in pore solution, chemically bound chloride in Afm phase and physically bound chloride in C-(A)-S-H. Each chloride changes as a function of immersion period are established through titration, ion chromatography analysis and X-ray diffraction (XRD) test.

Besides, a series of experiments were conducted with a view to investigate the carbonation characteristics of new cement-free binder. For this purpose, mortar specimens of this new composite with different type and amount of calcite were made to evaluate the changes between their hydration products before and after carbonation through tests of the carbonation depth measurement by indicator test, together with X-ray diffraction (XRD), Thermogravimetric analysis (TGA).

1.3 Significance of this research

The cement and concrete industries are seeking a new sustainable binder to replace the OPC, as the goal of net zero carbon dioxide emission to limit the global warming. Therefore, herein is a new cementless material consisting of (i) BFS which is the by-product of the iron and steel manufacturing industry, and (ii) calcite that can be taken from naturally available limestone or can be synthesized

by using carbonation reaction with hydrated lime slurry (i.e., the carbon dioxide stored in carbon captured storage wells can be effectively used to synthesize the calcite), for reducing the CO_2 gas emission. A considerable reduction in emitting the carbon dioxide gas during the manufacturing process of the material can be obtained by using the proposed new material as an alternative binder for OPC in the construction industry. The well-experimentally verified model proposed for the clinker-free material which incorporate the all the possible hydration products can facilitate the selection of construction materials and can be used for design purposes.

1.4 Structure of dissertation

Chapter 1 describes the background, purpose of this work and the significance of this research.

Chapter 2 shows literature reviews on various topics, including hydration, chloride penetration, and carbonation behaviours in OPC, slag-blend cement, limestone-cement and alkali-activated slag.

Chapter 3 presents the hydration and microstructure behaviour of the proposed clinker-free binder containing BFS, calcite, calcium hydroxide and expansive agent, as well as the prediction of hydration products and the porosity of clinker-free binder.

Chapter 4 presents the chloride resistance of this proposed cement-free binder by considering the chemical bound chloride, physically bound chloride and free chloride in the hardened paste.

Chapter 5 presents the carbonation behaviour of this proposed clinker-free binder through its phase changes.

Chapter 6 shows the characterization overview and conclusions of the new clinker-free binder, as well as the recommendations for future works.

CHAPTER 2

Literature review

2.1 Introduction

Understanding the kinetics of cementitious reactions intersects both academic and practical interests. In this part, progress in understanding hydration mechanisms of cementitious materials including Ordinary Portland Cement (OPC), slag-blended cement, limestone-blended cement and alkali-activated slag are reviewed. The current knowledge of cement clinker hydration is reviewed starting from the reaction mechanism of its initial phases including two calcium silicate phases, alite (C_3S) and belite (C_2S), and two calcium aluminate phases (aluminate (C_3A) and ferrite (C_4AF)). Also, the hydration of slag-blended cement, limestone-blended cement and alkali-activated slag are summarized in this part. The fundamental study of hydration therefore offers significant scientific challenges with regard to experimental techniques and multi-scale theoretical modelling methods. More knowledge of basic kinetic mechanisms of hydration is needed to provide a rational basis for mixture proportioning as well as the design and selection of chemical admixtures.

Reinforcement corrosion induced by chloride ions is one of the main factors causing the deterioration of reinforced concrete structures. When concrete is exposed to seawater or de-icing salts, chloride ions will penetrate the concrete and if critical chloride levels are reached at the steel reinforcement, corrosion may occur. Therefore, chloride penetration is one of the major problems that affect the durability of reinforced concrete structures. Although chloride ions in concrete do not directly cause severe damage to the concrete, they contribute to the corrosion of embedded steel bars in the structure. Besides, cement paste is known to react with atmospheric carbon dioxide. The carbonation of cement paste has long been recognized as one of the causes of reinforcement corrosion. On the other hand, carbonation causes significant chemo mechanical changes in the cement paste, most notably changes in strength, porosity, pore size distribution, and chemical composition. Furthermore, it can cause shrinkage and cracking of the cementitious matrix. For these two reasons, durability characterizations including chloride penetration and carbonation of Ordinary Portland Cement (OPC), slag-blended cement, limestone-blended cement and alkali-activated slag are also reviewed.

2.2 Hydration

Hydration of cementitious material involves a collection of coupled chemical processes, each of which occurs at a rate that is determined both by the nature of the process and by the state of the system at that instant. These processes fall into one of the following categories:

1. Dissolution/dissociation involves the detachment of molecular units from the surface of a solid in contact with water. A good comprehensive review of dissolution kinetics was performed by Dove et al (Bullard et al. 2011).

2. Diffusion refers to the transport of solution components through the pore volume of cement paste (Dove, Han, and De Yoreo 2005) or along the surfaces of solids in the adsorption layer .

3. Growth involves surface attachment, the incorporation of molecular units into the structure of a crystalline or amorphous solid within its self-adsorption layer (Bullard et al. 2011).

4. Nucleation initiates the precipitation of solids heterogeneously on solid surfaces or homogeneously in solution, when the bulk free energy driving force for forming the solid outweighs the energetic penalty of forming the new solid–liquid interface (Kashchiev and Van Rosmalen 2003).

5. Complexation, reactions between simple ions to result in ion complexes or the adsorption of molecular complexes on solid surfaces (Bullard et al. 2011).

6. Adsorption, the accumulation of ions or other molecular units at an interface, such as the surface of a solid particle in a liquid (Bullard et al. 2011).

These processes may operate in series, in parallel, or in some more complex combination. For example, even simple crystal growth from solution involves diffusion of solute to the proximity of an existing solid surface, adsorption of the solute onto the surface, complexation of several solute species into a molecular unit that can be incorporated into the crystal structure and, finally, attachment and equilibration of that molecular unit into the structure (Bullard et al. 2011).When in series, these steps are coupled in the sense that the products of one step are the reactants of the next step, and so on. Often, but not always, one step has a significantly lower rate than any of the other steps in the

sequence. In that case, all but the slowest step, the rate-controlling step, can reach equilibrium conditions and will determine the activities of the reactants and products of the rate-controlling step (Bullard et al. 2011). In this simple case where one step is rate-controlling, that step alone is responsible for the observed kinetic rate equation, the rate constant, and their temperature dependences. When the rates of two or more fundamental steps are comparable, then the rate equations and their dependence on system variables can be significantly more complicated and difficult to determine experimentally(Bullard et al. 2011).

2.2.1 Cement clinker hydration

The Ordinary Portland Cement (OPC) mainly consisted of ground clinker which is produced by sintering an ensemble of limestone with silica, alumina, and iron oxide-containing materials. This process results in a multi-phase solid consisting of round micron-sized calcium silicate particles of two different chemical compositions, alite (C_3S or $(CaO)_3(SiO_2)$) and belite (C_2S or $(CaO)_2(SiO_2)$), immersed in an interstitial matrix of aluminate (C_3A or $(CaO)_3(Al_2O_3)$) and ferrite (C_4AF or $(CaO)_4(Al_2O_3)$ (Fe_2O_3))(L. Ferrari et al. 2012). These four components, which represent the main cement phases, can be directly observed by microscopy on a polished clinker surface(H. F. W. Taylor 1997). When the clinker surface is brought in contact with an aqueous solution, amorphous and crystalline hydration products of different types according to the time of hydration are formed(Lucia Ferrari et al. 2012; Kreppelt et al. 2002). Different products are produced depending on the chinker composition and mixing conditions during the hydration process. Calcium silica hydrate (C-S-H), portlandite (CH), ettringite, monosulfate, hydrogarnet and hydrotalcite are constituent phases present in Ordinary Portland Cement.

The alite and belite comprise over 80 wt % of most Portland Cements. It is known that C_3S is the most important phase in cement for strength development during the first month, while C_2S reacts much more slowly, and contributes to the long-term strength of the cement. Both the silicate phases

react with water to form calcium hydroxide and a calcium-silicon-hydrated rigid gel (Bishop, Bott, and Barron 2003).

$$2(CaO)_3(SiO_2) + 7H_2O \rightarrow (CaO)_3(SiO_2)_2 \cdot 4H_2O + 3Ca(OH)_2$$

$$2(CaO)_3(SiO_2) + 5H_2O \rightarrow (CaO)_3(SiO_2)_2 \cdot 4H_2O + Ca(OH)_2$$

In cement chinkers, tricalcium aluminate (C_3A or $(CaO)_3(Al_2O_3)$) is also one of the main components. Although it is usually present in fairly low amounts (2–10 wt%), it has a significant effect on the setting of cement and the early-age heat release as a result of its very high reactivity(Joseph, Skibsted, and Cizer 2019).

In the absence of gypsum, OH-AFm (hydroxy-AFm or h-AFm) phases such as C_4AH_{13} and C_2AH_8 are formed. According to previous research (Baquerizo et al. 2015), C_4AH_{19} can form in place of C_4AH_{13} depending on relative humidity (RH). Nonetheless, these metastable h-AFm phases are subsequently transformed into the more stable C_3AH_6 (water garnet) via an endothermic reaction, releasing additional water into the system (Bishop, Bott, and Barron 2003; Joseph, Skibsted, and Cizer 2019; Kirchheim et al. 2009)

$$2(CaO)_3(Al_2O_3) + 21H_2O \rightarrow (CaO)_4(Al_2O_3) \cdot 13H_2O + (CaO)_2(Al_2O_3) \cdot 8H_2O$$

$$(CaO)_4(Al_2O_3) \cdot 13H_2O + (CaO)_2(Al_2O_3) \cdot 8H_2O \rightarrow 2(CaO)_3(Al_2O_3) \cdot 6H_2O + 9H_2O$$

Since C_3A has high reactivity and it does not develop strength (Bishop, Bott, and Barron 2003), gypsum ($CaSO_4 \cdot 2H_2O$) is added to slow the C_3A hydration. In the presence of gypsum, C_3A forms the needle-like mineral ettringite. The structure of ettringite consists of columns of calcium, aluminum, and oxygen surrounded by water and sulfate ions. If insufficient sulfate is present, then the ettringite will eventually react with excess C_3A and water to form the monosulfate. Reactions are shown below.

$$(CaO)_3(Al_2O_3) + 3CaSO_4 \cdot 2H_2O + 26H_2O \rightarrow (CaO)_3(Al_2O_3)(CaSO_4)_3 \cdot 32H_2O$$

$$2(CaO)_3(Al_2O_3) + (CaO)_3(Al_2O_3)(CaSO_4)_3 \cdot 32H_2O + 4H_2O$$
$$\rightarrow 3(CaO)(Al_2O_3)(CaSO_4) \cdot 12H_2O$$

Tetracalcium aluminoferrite (C_4AF) reacts much like C_3A, i.e., with the formation of an iron-substituted ettringite, in the presence of gypsum. However, the hydration of the ferrite phase is much slower than that of C_3A. In addition, if there is insufficient gypsum to convert all of the C_4AF to ettringite, then an iron-rich gel forms at the surface of the silicate particles, which is sonsidered to slow their hydration (Bishop, Bott, and Barron 2003).

$$2(CaO)_4(Al_2O_3)(Fe_2O_3) + (CaO)_3(Al_2O_3)(CaSO_4)_3 \cdot 32H_2O + 12H_2O$$
$$\rightarrow 3(CaO)(Al_2O_3)(CaSO_4) \cdot 12H_2O + 4Fe(OH)_3 + 2Ca(OH)_2$$

2.2.2 Slag-blended cement

Ground granulated blast furnace slag is produced when iron ore is reduced by coke in the blast furnace. The oxides of calcium, magnesium, aluminium and silicon are the main phases in BFS. Since the ground granulated blast furnace slag shows both cementitious behaviour and pozzolanic characteristics, it is used extensively as a cement replacement material (Kolani et al. 2012). However, the addition of slag gives both advantages and disadvantages compared to pure cement.

The advantages of slag-blended cement compared to clinker production include not only energy savings and reduced pollution, but also higher mechanical strength (Palacios et al. 2009) over a longer service life due to its finer pore structure reducing the carbon footprint of cement while potentially improving technical performance (Moon, Kim, and Choi 2006; Ogirigbo and Black 2016). As a result, it gives higher durability than Ordinary Portland Cement. Compared with OPC, slag-blended cements have a higher sulfate- and alkali-aggregate reaction resistance and a lower chloride diffusion rate (Kolani et al. 2012; Moon, Kim, and Choi 2006). However, slag-blended cement also shows poor early strength due to pure slag hydration at a lower rate (Kolani et al. 2012). And give lower resistance against carbonation than non-blended Portland Cement. Slag-blended cements also has lower heat of

hydration values than OPC and the reactions involved in their hydration are more complex (Escalante-Garcia and Sharp 2004).

The slag-blended cement hydration process is more complex than OPC due to the coexistence of clinker hydration and slag reaction. The fraction of reacted slag in blended cement which hydrated under various conditions of hydration has been reported by several researchers (Escalante et al. 2001b). The hydration of slag is activated by the alkali released by clinker hydration in blended cement. The reactivity of the blended cement decreases as the percentage of slag replacement increases, and it increases as the curing temperature increases, while the reactivity is reduced as the percentage of slag replacement is increased, and higher curing temperatures increased the reactivity of the slag (Escalante et al. 2001b).

The main hydration products of blast furnace cement include those products from both Portland cement and slag hydrations. Portlandite released due to Portland cement hydration could be consumed by the slag hydration reaction. As a result, ettringite, portlandite and a compound like hydrotalcite from the reaction of the magnesium containing in the slag are the common products in slag-blended cement system. The production of hydrotalcite and the reduction of portlandite are the most significant changes that occur when partial pure cement is replaced by slag (Castellano et al. 2016).

2.2.3 Limestone-blended cement

It is reported that a 3%-5% addition of limestone to Portland cement either increases the structural properties of the concrete or has no effect (Kevin and Kenneth 1991). However, some published results show a reduction in physical properties upon carbonate addition. Some of these changes, such as shrinkage upon drying, make the cement not suitable for construction applications (Kevin and Kenneth 1991). However, the use of limestone-blended cement seems to have many practical and economic area since limestone is an important material for cement manufacture (Kakali et al. 2000; Tsivilis et al. 2000; Vuk et al. 2001). Two effects can be considered when limestone is added to the cement during cement hydration. The competitive behavior of limestone cements is attributed to the

inert filler effect of the fine particles, as well as partial limestone reacts with calcium aluminate to form products (Kakali et al. 2000; Matschei, Lothenbach, and Glasser 2007).

Limestone addition can not only affect the mineralogical variant of the AFm phase(s), but also affect the amount of free calcium hydroxide as well as the balance between AFm and AFt phases, although C–S–H is unaffected for most compositions (Matschei, Lothenbach, and Glasser 2007). The mechanism proposed for the carbonate formation is the slow dissolution of calcium carbonate and its reaction with monosulfate or calcium aluminate hydrates produced by cement clinker to monocarboaluminate, which is more stable because of its greater insolubility (Kakali et al. 2000). It is difficult to observe the influence of limestone addition on pure C_3S because the main hydration product of C_3S is amorphous C-S-H. There is a significant difference between limestone addition and not for C_3A based the transformation of ettringite to monosulfate and the formation of carboaluminates. Pastes with limestone appear to contain lesser ettringite than in plain C_3A pastes, and the addition of limestone will delay the transformation of ettringite to monosulfate at an early age. Besides, monocarbonate hydrate is formed from the beginning of hydration. In other words, limestone suppresses the conversion of ettringite to monosulfate and favors the replacement of monosulfate by monocarbonate.

$$(CaO)_3(Al_2O_3) + \mathrm{CaC}O_3 + 11H_2\mathrm{O} \rightarrow (CaO)_3(Al_2O_3)(CaCO_3) \cdot 11H_2\mathrm{O}$$

For cement clinker, blending Portland Cement with limestone not only accelerates the initial hydration reaction but also to influences the hydrate assemblage of the hydrating cement pastes. The ettringite's transformation to monosulfate is delayed, while calcium aluminate monocarbonate is preferably formed instead of monosulfate even at early ages. In addition, the hydration of calcium silicates is accelerated (Kakali et al. 2000; Lothenbach et al. 2008).

2.2.4 AAS (Alkali-activated slag)

Alkali-activated slag (AAS) has attracted considerable attention since its first use as an alternative material to Portland Cement due to its superior properties and environmental impact such as fast development of strength, high resistance to chemical attack, low heat release rate and can release up to 80% less greenhouse gas emission (Amer et al. 2021; W. Chen and Brouwers 2007; Law et al. 2012). The usage of AAS promotes the reuse of slag and other waste materials and saves resources. Although slag is an active mineral material with potential hydraulicity, AAS exhibits larger autogenous and higher drying shrinkage compared to OPC (W. Chen and Brouwers 2007; Fu et al. 2021; Ye and Radlińska 2016) due to finer pore structure and lower stiffness. In addition, it requires widely available alkali activators like NaOH, Na_2CO_3, Na_2SiO_3 or Na_2SO_4 to react with the alumino-silicate source for producing cementitious materials (Amer et al. 2021). Generally, the shrinkage mechanism in AAS can be classified into autogenous shrinkage, drying shrinkage, and carbonation shrinkage. Autogenous shrinkage results from the macroscopic process of self-desiccation and chemical shrinkage (Awoyera and Adesina 2019; Melo Neto, Cincotto, and Repette 2008). While drying shrinkage occurs as a result of disjoining pressure and capillary suction (Scherer 2015). Besides, higher amount of mesopore coupled with higher capillary stress as a result of the pore distribution in AAS compared to OPC could also contribute greatly to its high shrinkage.

Different types of slag have almost identical chemical compositions, but their chemical components differ greatly. The composition of slag, as well as the type and dosage of the alkali activator would affect its activity and its hydration process because a variation in the composition of the slag can affect the activity of the slag hydration reaction and alter the rate of the hydration reaction and the alkali activators can affect the dissolution of slag and provide the ions required for specific reaction products (Fu et al. 2021). It is reported that a higher MgO content of the slag resulted in a faster reaction and higher compressive strength during the first few days after casting, and the main hydration products in hardened AAS pastes are C(-A)-S-H with a Ca/Si atomic ratio near 1 (Le Saoût et al. 2011), and a hydrotalcite-like phase (Haha et al. 2011; Le Saoût et al. 2011). Increasing the

MgO content of the slag from 8 to 13% increased the amount of hydrotalcite and lowered the Al uptake by C–S–H resulting in 9% higher volume of the hydrates (Haha et al. 2011). In the case of a higher content of Al_2O_3 of slag, decreased the Mg/Al ratio of hydrotalcite, increased the Al incorporation in the C(-A) S-H and led to the formation of strätlingite. Increasing the content of Al_2O_3 in the slag slowed down the early hydration and a lowered the compressive strength during the first few days (Haha et al. 2012). In addition, past studies have shown that the reaction degree of alkali-activated slag is approximately 60% after 91 days, which is generally lower than that of OPC (Le Saoût et al. 2011).

2.3 Durability

2.3.1 Chloride penetration

One of the major problems that affect the durability of reinforced concrete structures is chloride ingress. Although chloride ions in concrete do not directly cause severe damage to the concrete, they contribute to the corrosion of embedded steel bars in the structure. The changes in hydration phases in the interface between the steel bars and surrounding concrete is associated with large volume changes, like expansion or shrinkage, which may result in cracking, spalling, delamination etc. Once there is severe corrosion of steel bars, the physical properties, and load-carrying capacity of the structural members may be reduced due to the reduction of the cross-sectional area of the steel bars. Therefore, the study of chloride penetration in concrete has become an important aspect in the research for steel corrosion in reinforced concrete structures (Ababneh, Benboudjema, and Xi 2003). The chlorides not only give phase changes to the concrete binder, but also initiates pitting corrosion of the reinforcement when the chloride concentration at the reinforcement reaches a critical level. Corrosion leads to a decrease in structural performance. To reach the critical chloride level, chlorides have to ingress through the concrete cover towards the steel reinforcement. In concrete, Chloride ions exist either in the pore solution, chemically bound to the hydration products, or physically bound to the surface of the hydration products (Yuan et al. 2009). Chloride binding of cement-based material

is very complicated and influenced by many factors, such as chloride concentration, cement composition, hydroxyl concentration, cation of chloride salt, temperature, supplementary cementing materials, carbonation, sulfate ions and electrical field (Yuan et al. 2009). The chlorides can be bound in calcium chloroaluminate hydrates such as Friedel's salts or Kuzel's salts due to chemical reaction, or they can be adsorbed to the C–S–H by physical bound. Besides, they can be present in the pore solution as a free chloride shape. The only chlorides which are ''free'' to move are the chlorides in the pore solution. Hence, the ability of concrete to bond with chlorides might slow down the chloride ingress (Klaartje De Weerdt, Justnes, and Geiker 2014).

Different researchers had reported how chloride ions exist in cementitious materials. However, their reports are conflicted. Loser et al. (Loser et al. 2010) found that only a small fraction of the chloride ions are bound by cement hydrates and that the largest fraction of chloride is present in the pore solution. Some review articles (Yuan et al. 2009) have addressed that the main chloride binding originates from the tricalcium aluminate or ferrite phases through the formation of Friedel's salt and its iron-containing analogue. On the other hand, Tang and Nilsson (Luping and Nilsson 1993) suggest that the major binding is attributed to physical adsorption on the C-S-H. However, the adsorption of chlorides on the C-S-H varies with the Ca/Si ratio of the C-S-H and the pH value of the exposure solution (K. De Weerdt, Orsáková, and Geiker 2014). Experimental and modelling results (Friedmann, Amiri, and Aït-Mokhtar 2008) suggest that the chloride ions associated with the C-S-H are mainly present in the diffuse layer of the C-S-H surface, which is positively charged in the presence of high calcium concentrations.

2.3.1.1 Chloride ion interaction with cement clinker

Less studies were focused on C_3S and C_2S since their main hydration product is C-S-H gel, which dominates the physical binding of chloride. The adsorption of chloride ions to the C-S-H gel is the reason cause physical binding. Research (Yuan et al. 2009) reported that three types of interaction with C–S–H could exist: chlorides can either be present in a chemisorbed layer on the hydrated

calcium silicates, penetrate the C–S–H interlayer spaces, or be intimately bound in the C–S–H lattice. A higher content of C_3S and C_2S makes a higher physical binding of chloride. In addition, the binding capacity of C–S–H depends on its C/S ratio. Lower C/S ratios result in lower binding capacities. However, by adding chloride to pure alite paste, C–S–H only absorb a very small amount of chloride ions.

The chemical binding of chloride ions is dominated by C_3A and C_4AF, while the physical binding is dominated by C_3S and C_2S. It is studied (Suryavanshi, Scantlebury, and Lyon 1995) that higher C_3A content results in higher binding capacity. The chloride binding capacity increases significantly as the C_3A content increases due to the reactions between chloride ions and C_3A or C_4AF, resulting in the formation of Friedel's salt and its analogues (like Kuzel's salt).

$$(CaO)_3(Al_2O_3) + \mathrm{Ca}(OH)_2 + 2\mathrm{Cl}^- + 10H_2\mathrm{O} \rightarrow (CaO)_3(Al_2O_3)(CaCl_2) \cdot 10H_2\mathrm{O} + 2OH^-$$

$$(CaO)_3(Al_2O_3) + 0.5\mathrm{Ca}(OH)_2 + 0.5\mathrm{Ca}SO_4 + 2\mathrm{Cl}^- + 10H_2\mathrm{O}$$
$$\rightarrow (CaO)_3(Al_2O_3)(CaCl_2)_{0.5}(CaSO_4)_{0.5} \cdot 10H_2\mathrm{O}$$

The formation of Friedel's salt or Kuzel's salt forms by two separate mechanisms: adsorption and anion-exchange. In the adsorption mechanism, the formation of Friedel's salt or Kuzel's salt is due to the adsorption of bulk chloride ions present in the pore solution to the interlayer of the principal layer, the AFm structure to balance the charge. In the anion-exchange mechanism, a fraction of the chloride ions replace negatively charged ions present in the interlayers of the principal layer of the AFm hydrates, forming Friedel's salt or Kuzel's salt (Yuan et al. 2009).

2.3.1.2 Chloride in slag-blended cement

Partial replacement of cement with slag increases the chloride binding in case of a superior external chloride concentration. The increase in chloride binding due to the replacement of slag was also observed in the case of internal chloride. This may because that a high binding capacity of cement-slag paste may be due to the high alumina content in slag, resulting in the formation of more Friedel's

salt (Yuan et al. 2009). Influences of slag replacement level, w/b ratio and glass content on the paste resistance to chloride penetration have been reported in the past research. They are: at a given slag replacement level, regardless of the type of slag used, chloride conductivity and porosity increased with increasing w/b ratio implying that the chloride penetrability also increased. And At a given w/b ratio, regardless of the type of slag used, chloride conductivity and porosity decreased with increasing slag replacement level, giving improved chloride penetration resistance (Otieno, Beushausen, and Alexander 2014). In addition, a higher content of alumina in slag led to the formation of more Friedel's salt. The greater basicity led to a higher degree of hydration (formation of a larger amount of C-S-H phases), which resulted in the formation of a finer pore structure and increased chloride binding. These factors, in turn, resulted in shallower chloride penetration. However, an elevated curing temperature increased the hydration degree of slag, coarser the pore structure and results in an increase rate of chloride ingress and degree of chloride binding (Ogirigbo and Black 2017).

2.3.1.3 Chloride binding in limestone cement systems

Studies have shown that low levels of replacement of clinker with limestone improved the environment and economic benefits (Hawkins, Tennis, and Detwiler n.d.). However, the chloride binding condition needs to be confirmed under an influence of limestone addition when there is an external chloride. Similar to cement clinker, the chloride in limestone cement can be divided into 3 different shapes, which are physically bound chloride on C-S-H hydrates, chemically bound ions in AFm phases and free ions in pore solution.

The total chloride content in a paste sample can be measured by $AgNO_3$ titration. The results show a decrease in the total chloride content as a function of the increasing limestone replacement. The amount of total chloride decreased by around 35% when the limestone addition rate is 55% compared to OPC (Sui et al. 2019). As limestone content increases, free chloride in the pore solution increases. The amount of free chloride is almost 2.3 times in 55% limestone addition paste as it is in OPC paste due to the increase of porosity. A higher total porosity leads to a higher content of pore solution in

the structure and thus, leads to a higher amount of free chloride in the paste (Sui et al. 2019). Some different methods can be used to quantify the amount of chemically bound chlorides, such as XRD and TG. Although they give different results, both test methods give a decreased tendency when the addition rate of limestone gets higher. SEM-EDS testing of physically bound chlorides in C-S-H also indicates a decrease with the addition of limestone, since there is a filler effect for limestone additions. However, the decrease of chlorides on C–S–H was found not to be proportional to the replacement level of cement by limestone because there is an interaction between limestone and the hydration products. Also, it was found that the total amount of free chloride in the pore solution and physically bound chlorides in C-S-H are almost unaffected by the limestone addition rate. But a higher addition rate of limestone gives less clinker amount, which makes a lower amount of cement hydration product such as Afm, cause less chemically bound chloride in AFm phases. It is possible to cancel out the effects of limestone addition on free chloride and physically bound chloride, but fewer carriers for chemical reactions result in fewer chemically bound chloride. Therefore, limestone cement systems with a higher limestone addition rate have a lower total chloride (Sui et al. 2019).

2.3.1.4 Chloride binding in alkali-activated slag

As a type of alkali-activated material, the AAS have a good potential in chloride resistance. Its chloride behavior under the chloride environment is remarkable. Since the chemical composition of slag, type and concentration of activator, and even temperature and alkalinity could influence the phase assemblages of AAS, they also affect the chloride binding. However, the chloride binding capacity of AAS has been widely investigated and evaluated. Research reported that the binding chloride ion amount of AAS increases with a rising temperature as well as a rising pH. This may be due to the adsorption of ions on the gel surface is an endothermic process (Qiao et al. 2019). Besides, higher temperature moves OH^- faster, which gives it more changes to form Cl^- fixed sites (Y. Zhu et al. 2022). 0.7M and 3.4M NaOH immersion solution could rise the binding chloride around 0.23 wt% and 0.4 wt% at a pH of 14 (Ke et al. 2017; Jian Zhang, Shi, and Zhang 2019). Also, the influence of

internal chloride was studied. 0.10-0.12 wt% chloride is obtained with an amount of 0.64-0.76 wt% chloride binder after 28 days, and 0.6 wt% is obtained under a 1.5-2.0 wt% internal chloride binder after 56 days (Jun, Kim, and Kim 2020; Khan and Kayali 2018). These results mean the chloride binding capacity of AAS is slightly higher than it in OPC in general (Y. Zhu et al. 2022).

Another study found that the alkali activator type strongly influences chloride resistance. Because the main hydrate products of AAS are calcium silicate hydrate (C-S-H) and hydrotalcite. $Ca(OH)_2$ is not one of the hydration products of AAS (Y. Zhu et al. 2022). Pozzolanic materials react more with $Ca(OH)_2$, whether or not $Ca(OH)_2$ exists will make a huge difference to the chloride resistance. KOH and NaOH corrosion behavior was similar to Portland cement mortar, but $Ca(OH)_2$ activator increased corrosion resistance. As a result of the precipitation of $Ca(OH)_2$ in the matrix, AAS with the $Ca(OH)_2$ activator has a higher resistance to chloride-induced corrosion, but its binding capacity for chlorides was lower than for Portland cement paste. As a result of this reaction, $Ca(OH)_2$ could have physically formed $Ca(ClO)_2$ to remove free chlorides from the pore solution (Park, Ann, and Cho 2015).

2.3.2 Carbonation behaviour

2.3.2.1 Carbonation of cement paste

Cement paste is known to bind CO_2 from the atmosphere or environments with higher CO_2 concentration. The carbonation of cement paste has long been recognized as one of the causes of reinforcement corrosion. On the other hand, carbonation causes numerous chemomechanical changes in the cement paste, most notably changes in strength, porosity, pore size distribution, and chemistry. Furthermore, it can cause shrinkage and cracking of the cementitious matrix(Park, Ann, and Cho 2015). Carbonation is a common type of attack in cementitious materials. The process begins when CO_2 penetrates the cementitious matrix, dissolving in the pore solution to produce HCO_3^- and CO_3^{2-} ions, which react with Ca^{2+} from calcium hydroxide (CH), calcium silicate hydrate (C–S–H) and the

hydrated C_3A and C_4AF to precipitate as various forms of calcium carbonate ($CaCO_3$) silica gel and hydrated aluminium and iron oxides (Borges et al. 2010).

The carbonation of calcium hydroxide (CH) will follow the equation below. During the carbonation, mainly 3 steps are involved. The dissolution of CH, absorption of CO_2 and formation of carbonate ions and chemical reaction (García-González et al. 2006; Šavija and Luković 2016).

$$\mathrm{Ca}(OH)_2 + \mathrm{C}O_2 \rightarrow C\mathrm{aCO}_3 + H_2\mathrm{O}$$

The chemical reaction of CO_2 with CH begins immediately and results in the formation of calcium carbonate. In the early stage of carbonation, the diffusion of CO_2 through the already carbonated layer is the rate-controlling step for the carbonation of CH. Although CO_2 diffusivity is significantly higher in gas-filled pores compared to water-filled pores, the presence of water is required for the reaction between gaseous CO_2 and CH. The limiting step changes at a later stage of the carbonation process as the CH carbonation rate decreases due to the formation of a thin layer of calcium carbonate on the surface of the CH crystals. The type of $CaCO_3$ depends on kinetic and thermodynamic factors. If kinetic factors predominate, $CaCO_3$ will precipitate as aragonite or vaterite, both polymorphs eventually converting to calcite, the more stable shape. If thermodynamic factors prevail, $CaCO_3$ will precipitate as calcite. The calcite will be the final product (Šavija and Luković 2016).

Carbonation of C–S–H gel consists of the removal of calcium ions from the gel leading to the formation of an amorphous silica gel and various polymorphs of calcium carbonate (A. E. Morandeau and White 2015; A. Morandeau, Thiéry, and Dangla 2014). The chemical reaction between C-S-H and CO_2 results in the formation of calcium carbonate and amorphous silica gel and can be written as follows (A. E. Morandeau and White 2015; A. Morandeau, Thiéry, and Dangla 2014).

$$(CaO)_x(SiO_2)(H_2O) + \mathrm{x}C\mathrm{O}_2 \rightarrow x\mathrm{CaCO}_3 + (SiO_2) \cdot tH_2\mathrm{O} + (z-t)H_2\mathrm{O}$$

The type and degree of carbonation of C-S-H gels strongly depend on the initial Ca/Si ratio of the gel. It is reported that when C-S-H is carbonated, its Ca/Si ratio decreases and becomes highly porous,

approaching amorphous silica. During the carbonation reaction, the decomposition rate of C-S-H increases with the decrease of the Ca/Si ratio of C-S-H, while the amount of $CaCO_3$ formed by the carbonation of C-S-H decreases (Šavija and Luković 2016). The carbonation significantly reduces the porosity of the microstructure. When C-S-H is converted into CO_2, a decalcification occurs. Calcium ions are released in the porous media, leading to a C-S-H with a molar volume smaller than a non-carbonated C-S-H and to a smaller C/S. As for CH, this volume loss is compensated by $CaCO_3$ precipitation (A. Morandeau, Thiéry, and Dangla 2014).

Also, unreacted C_3S and C_2S are susceptible, both of them can react with CO_2, causing the formation of $CaCO_3$ and silica gel (J. Han et al. 2012; Peter et al. 2008).

$$(CaO)_3(SiO_2) + 3CO_2 + nH_2O \rightarrow (SiO_2) \cdot nH_2O + 3CaCO_3$$

$$(CaO)_2(SiO_2) + 2CO_2 + nH_2O \rightarrow (SiO_2) \cdot nH_2O + 2CaCO_3$$

Besides, hydration products like ettringite can be affected under a CO_2 environment (Šavija and Luković 2016).

$$(CaO)_3(Al_2O_3)(CaSO_4)_3 \cdot 32H_2O + 3CO_2$$
$$\rightarrow 3CaCO_3 + 3(CaSO_4 \cdot 2H_2O) + (Al_2O_3) \cdot xH_2O + (26 - x)H_2O$$

$$(CaO)_3(Al_2O_3)(CaCO_3) \cdot 11H_2O + 3CO_2 + 2OH^- \rightarrow 4CaCO_3 + 2Al(OH)_4^- + 8H_2O$$

The numerical value of x in the equation above is close to 3. It can be seen that the carbonation of ettringite forms gypsum and alumina gel.

Carbonation of all calcium-bearing phases contributes significantly to the formation of $CaCO_3$, and it is commonly reported that the total amount of $CaCO_3$ formed far exceeds that which could result from complete CH dissolution (Šavija and Luković 2016).

2.3.2.2 Carbonation of slag-blended cement

Although the blend of Portland cement with slag requires less energy for producing binders and improves durability somehow. It is also reported that the atmospheric carbonation of slag-blended cement rate is higher compared to OPC (Monkman and Shao 2010; Sanjuán et al. 2018). Some studies are carried out to evaluate the carbonation of OPC, as well as several supplementary cementitious materials under natural conditions (Htwe and Mon 2018; Lollini and Redaelli 2021). Regardless of water/binder ratios or curing times, pure OPC paste exhibited the lowest carbonation coefficient. The carbonation rate is getting lower with an increasing curing age from 1 to 28 days, which is due to more hydration product making the porosity of the paste finer, causing a lower gas penetration rate. However, porosity alone is not a reliable indicator of carbonation risk, since no correlation can be found between carbonation resistance and porosity (Younsi et al. 2013). But the ratio of the effective porosity (porosity accessible to gaseous CO_2) and the CH content provides an indicator to evaluate carbonation resistance more accurately than porosity or CH content. In addition, the carbonation rate increases as the replacement of cement by slag in the concrete increases. BFS addition paste has poor carbonation resistance, and while curing for longer periods (up to 3 months) increases the resistance, its performance remains low, especially at cement replacement levels of 70% and above (Gruyaert, Van Den Heede, and De Belie 2013). Compared to OPC paste, paste containing 70% slag carbonates twice as fast (Lollini and Redaelli 2021).

2.3.2.3 Carbonation of limestone-blended cement

When limestone is added to OPC, it influences the properties both in the hardened states, as well as the durability (Elgalhud, Dhir, and Ghataora 2017). It is reported that, the supplementary cementitious material addition promotes the carbonation process, including limestone (Htwe and Mon 2018; Lollini and Redaelli 2021). The combination of limestone with OPC leads to increase the carbonation (Elgalhud, Dhir, and Ghataora 2017). Cement paste with 15% limestone replacement makes the carbonation rate 1.5 times higher than it is in OPC paste, where 30% limestone replacement can

increase the rate of carbonation over 2 times (Lollini and Redaelli 2021). In other research, modeling of carbonation of Portland-limestone cement is carried out (X. Y. Wang 2017). This model evaluated the degree of hydration as a function of time using a kinetic hydration model considering mixing proportions, compound compositions and cement and limestone surfaces. A carbonation model is then developed based on calculations from the hydration model, such as carbonatable materials contents and porosities. The diffusivity of CO_2 and carbonation depth of limestone contained cement concrete are evaluated by considering concrete material properties and environmental conditions. As a result, with increasing water-to-binder ratios and limestone content or reductions in curing period, the carbonation depth of concrete increases. As limestone replacements can increase cement reaction degree, limestone replacements are associated with a decreasing carbonation resistance, which occurs due to the cement contents in mixing proportions (X. Y. Wang 2017).

2.3.2.4 Carbonation of alkali-activated slag

The carbonation mechanism is not the same in the OPC and AAS. Carbonation precipitation occurs much more intensely in OPC than in AAS when OPC is exposed to severe carbonation conditions since OPC contains a higher Ca content, including CH and C-S-H, which are susceptible to interaction with external CO_2. In AAS, carbonation occurs directly in the C-S-H gel since CH is not one of the hydration product (Palacios and Puertas 2006). Besides, the carbonation process is strongly affected by different activators, which gives a major difference in the pH of pore solution, while changes in slag composition, e.g. the MgO and Al_2O_3 contents mainly affect the mass fractions of hydration products and chemical properties. The pH of pore solution decreases as CO_2 uptake increases in the AAS. However, the presence of certain reaction products, such as hydroxylated hydrotalcite, hemi/monocarbonate, and M-S-H gels, can partially buffer the pH of pore solution while the CO_2 uptake increases, and the carbonation process proceeds.

Also, a model has been carried out to predict the CO_2 uptake performance during carbonation. The modelling results show that calcite, carbonated hydrotalcite and aluminosilicate gel with both Na^+

and Ca^{2+} as extra-framework charge balancing cations, are the main carbonation products predicted to form in AAS before the pH of pore solution dropped below 12.5. At extended degrees of carbonation, carbonated hydrotalcite can decompose to form the transitional phase M-S-H, which is eventually carbonated to huntite after the pH of pore solution dropped below 8.0.

Thermodynamic modelling of the carbonation process in the AAS systems can accurately simulate the phase evolution in the gel binders during CO_2 exposure, as well as the pore solution pH changes. This information is of great importance to predict the potential stability. The influence of different activators, or slags with different chemical compositions, on the carbonation process was simulated by the model developed (Ke et al. 2020). The modelling results indicate that sodium carbonate AAS can maintain higher pore solution pH at the same amount of CO_2 uptake compared with sodium silicate based AAS. When a slag precursor with higher MgO content is used, a higher amount of C-(N)-A-S-H and hydrotalcite are formed, contributing to a denser binder matrix which may show reduced permeability (Ke et al. 2020).

CHAPTER 3

Hydration characteristics

3.1 Introduction

Cementitious materials hydration is regarded as a simultaneous process including dissolution of clinkers and precipitation of hydration products. Portland cement is the most consumed building material worldwide. it has been used for over 200 years. The hydration behaviour of Ordinary Portland Cement (OPC) was well studied. In the presence of water, the OPC reacts rapidly. At the same time, various hydration products could be formed on the surface of cement particles to fill the pore structure and lead the matrix getting harden (Garrault-Gauffinet and Nonat 1999) . However, It is estimated that the annual production of ordinary cement exceeds 3 billion tonnes, releasing 5–7% of worldwide CO_2 emissions (Qi et al. 2019). By using mixed cement with some other materials instead of using pure cement, some of the CO_2 emissions can be cut off. Slag and limestone are the most common materials used in mixed cement. The hydration of slag-blended cement, limestone-blended cement and alkali activated slag have been reported by previous research. Although each of them has its own advantage, it still has some disadvantage in different aspect. For slag-blended cement, even it has a good physical performance in long-term, it has a poor early strength due to the reaction of slag in a low rate. In the case of limestone-blended cement, limestone does not have pozzolanic properties and consequently. It does not produce C-S-H and have a serious dry shrinkage. The reaction of alkali-activated slag strongly depends on the type of activator.

In this chapter, a new composite cementitious binder mainly containing slag and calcite is carried out. Since the hydration behaviour of a new composite cementitious binder containing of slag and calcite is not clear yet. In this part, the reaction degree of slag during hydration, its hydration products, as well as the effects of W/P, calcite addition rate and calcite fineness are investigated by combing the multiple methods including XRD, TG, MIP and selective dissolution. Also, a model based on PHREEQC is carried out to predict its hydration by inputting reactor component and composition, reactor component and composition, mixing proportions and curing conditions.

3.2 Materials and methods

3.2.1 Materials and sample preparation

In this study, blast furnace slag (BFS), portlandite (CH), and two different types of calcites [fine calcite (Cc-F) and coarse calcite (Cc-C)] obtained from a commercial supplier were used. In addition, an expansive agent (EX) was included to compensate the shrinkage caused by the reaction of slag. The chemical composition of BFS and EX determined by XRF and XRD method are tabulated in **Table 1** while the specific surface areas and density of the raw materials are given in **Table 2**.

Table 3 details the used mixing proportions of this study. Meaning of sample name is Calcite addition rate-Calcite type-water to powder ratio (for an example, Cc45-C-0.6 means 45% coarse calcite addition and the water to powder ratio is 0.6).

Initially, the raw materials were mixed for 1 minute in the dry mixer and the required water was added into the mixture, followed by mixing again for 1 minute at a low speed. Afterwards, the mixture attached to the surface of the container was scraped down and then mixed for another 1 minute at low speed and subsequently mixed for 1 minute at a high speed. For high water to powder ratio (w/p=0.6) systems, the mixture was stirred manually once an hour until the formation of bleeding stopped. Low water to powders ratio samples were stirred for one time after the initial mixing. The mixture was then cast into cylindrical moulds with dimension of ϕ 24.94 × 56 mm and kept in sealed-curing condition at 20 °C for 91 days.

Table 1 Chemical composition of BFS and EX

Component	BFS	EX
SiO_2	23.43	4.01
Al_2O_3	10.85	1.58
Fe_2O_3	0.50	1.46
CaO	51.7	69.51
MgO	4.11	0.61
SO_3	4.00	16.63
Na_2O	2.54	3.69
K_2O	0.62	0.45
P_2O_5	1.23	1.32
MnO	0.28	0.04
C_3S		30.1
C_2S		6.4
C_3A		6.9
Anhydrite	4.22	27.6
CaO_free		28.9

Table 2 Specific surface areas and density of each material

Material	Specific surface area* (cm^2/g)	Density (g/cm^3)
BFS	4,000	2.89
EX	3,450	3.15
Cc-C	4,840	2.70
Cc-F	52,400	2.67

Note: Cc-F is BET value and others are Blaine.

Table 3 Mixture proportions

Sample name	Water to powder ratio	Material mass (%)					Water reducing agent (%)
		BFS	EX	CH	Cc-C	Cc-F	
Cc45-F-0.6	0.6	46.4	4.18	4.42		45.0	
Cc45-C-0.6	0.6	46.4	4.18	4.42	45.0		
Cc70-F-0.6	0.6	25.3	2.30	2.40		70.0	
Cc45-F-0.305	0.305	46.4	4.18	4.42		45.0	0.9
Cc45-C-0.305	0.305	46.4	4.18	4.42	45.0		0.9
Cc70-F-0.36	0.36	25.3	2.30	2.40		70.0	1.5

Naming method: Cc (Calcite) 45 or 70 (Addition rate) - C or F (Calcite type, coarse or fine) - 0.6 or 0.36 or 0.305 (water to powder ratio)

3.2.2 Experimental procedure

The samples were ground and immersed in acetone for 24 h to stop the hydration after reaching the desired hydration period (1, 3, 7, 14, 28, and 91 days). Subsequently, the specimens were removed from the acetone by suction filtration using an aspirator and kept in an oven at 40 °C for 24 h. Finally, the ground samples powder with particle size less than 75 μm were used for selective dissolution experiments, X-ray diffraction (XRD) and thermo gravimetric analysis (TGA). The hydrated powder samples were analysed by XRD using a Rigaku X-ray generator with CuKα radiation, and the measurement conditions were a tube voltage of 40 kV, scanning range of 5°–70° 2θ, step size of 0.02° 2θ, and scan speed of 6.5°/min. Siroquant Version 4.0, manufactured by Sietronics, was adopted for quantitative Rietveld analysis. The TG-differential thermal analysis (DTA) was conducted using TG/ DTA7220 manufactured by HITACHI under an N_2 flow environment. The waiting time before the measurement for stabilising the apparatus was 50 minutes. The temperature was raised at a rate of 10 °C/min from 20 to 950 °C and was maintained for 60 min, followed by decreasing with a rate of 10 °C/min. Around 10 mg of the sample was weighed and used for measurements. The pore structure of the hardened matrix was investigated by Mercury intrusion porosimetry (MIP) analysis using Shimadzu Auto Pore IV 9500 (with the pressure range of 0.5-60000 psia). The specimen for MIP was

cut into a portion of about 3 mm cube, immersed in acetone for 24 hours, and then vacuum dried for 24 hours.

3.2.2.1 Selective dissolution

The selective dissolution method proposed in literature (Lumley et al. 1996; Villagrán-Zaccardi et al. 2018) was adopted to determine the reaction degree of slag. Initially, a mixture of 250 mL of triethanolamine (TEA) and 500 mL of distilled water was prepared, in which 173 mL of diethylamine (DEA) was rapidly added. The water was added to make the solution equivalent to 1000 mL. For the dissolution of each sample, 25 mL of the solution was diluted to 400 mL, and 0.25 ± 0.01 g (with a precision of 0.0001 g) of powder sample was spread onto the solution surface preventing from the formation of agglomeration. The mixture was stirred continuously at around 300 rpm and 20 °C for 60 min to achieve an effective dissolution of the sample. The insoluble residue was filtered under vacuum using a 47 mm diameter moistened membrane filter with a pore size of 0.5 μm. The residue was carefully washed for several times with distilled water until there was no left in the beaker. The filter with residue was then dried at 105 °C for 1.5 h and weighed with a precision of 0.0001g to determine the amount of the residue. The reaction degree of slag can be calculated according to the following equation (Eq. (1)).

$$\alpha_{slag} = 1 - \frac{m_{ir} \div [m \times (1 - f_{water})]}{f_{slag} \div \left(1 - f_{CH} \times \frac{M_{H_2O}}{M_{CH}}\right)} \quad (1)$$

where m_{ir} is the weight of insoluble residue after selective dissolution, m is the weight of sample before selective dissolution, f_{water} is the mass fraction of water before 450 °C in hydrated sample (measured by TGA), f_{slag} is the mass fraction of slag in initial dry binder, f_{CH} is the mass fraction of Portlandite in initial dry binder, M_{H2O} is the molar mass of water, and M_{CH} is the molar mass of portlandite.

3.3 Modelling approach

To predict hydrate assemblage as a function of hydration time for the slag-calcite mixture, the thermodynamic model developed in our previous studies (Yogarajah Elakneswaran et al. 2016; Krishnya, Yoda, and Elakneswaran 2021) was amended. The chemical composition and physical properties of each material, mixing proportions, and curing condition were inputted in the developed framework. The geochemical package PHREEQC was used for thermodynamic calculations along with the thermodynamic properties of cement hydrates collected from Cemdata18 (Lothenbach et al. 2019) and converted to PHREEQC format and PHREEQC default thermodynamic database (Parkhurst and Appelo 1999). The Details of converted data into a PHREEQC format are reported in earlier work [43]. It should be noted that the slag and components in EX such as C_3S, C_2S, and C_3A were herein considered as kinetic reactions whereas portlandite, calcite and other components in EX were assumed as thermodynamic equilibrium reaction.

3.4 Results and Discussion

3.4.1 Reaction degree of slag

Figure 1 shows the variation of reaction degree of slag with curing period for different W/P and calcite content determined by the selective dissolution. The effect of water to powder ratio (low W/P and high W/P), calcite addition (45% and 70%) and particle size of calcite (fine and coarse) on the reaction of slag are emphasised here. It can be seen that the slag reacts faster at the early stage and reaches low reaction rate after 28 days in all the cases. This could be attributable to two major factors: (i) remaining of the larger particles (the small particles react in the early age) and (ii) lack of water and space for the reaction (Paulini 1990). In each mix, the reaction degree of slag has reached between 35% and 45% after 91 days of reaction period. The similar range for the reaction degree was also reported by Escalante et al. (Escalante et al. 2001a) for 50% slag replacement in OPC with the W/P ratio of 0.35 and 0.5 at room temperature.

The reaction degree of slag increases with W/P ratio for a specific amount of calcite addition and reaction period as depicted in **Figure 1**. For example, the reaction degree of slag with 45 % of fine calcite addition and W/P of 0.305 (Cc45-F-0.305) is approximately 32 % after the 28 days of curing period, whereas it is about 38 % for W/P of 0.6. Similar tendency is observed even for coarse calcite samples (Cc45-C) and 70 % of fine calcite samples (Cc70-F). It can be attributed to the more available space to accommodate more products and sufficient water for reaction in high W/P ratio compared to low W/P ratio mixture (Escalante et al. 2001a; Lam, Wong, and Poon 2000). Besides, the results clearly demonstrate that increasing the filler content (calcite) in the slag-calcite system results in increasing the reaction degree of slag for a same W/P and specific surface area of the filler (see Cc45-F-0.6 and Cc70-F-06 or Cc45-F-0.305 and Cc70-F-0.36 in **Figure 1**). This is possibly due to the increase in effective water for the reaction of slag, consequently increasing the space for the growth of hydration products (Adu-Amankwah et al. 2017). For instance, additional 25% of calcite (Cc70-F) improves the reaction degree of slag by approximately 20% in both low and high W/P mixture compared to 45% of calcite addition (Cc45-F).

The effect of particle size of calcite on reaction degree of slag is also highlighted in **Figure 1** for low W/P and high W/P system. When the Blaine of calcite increases by 10 times, the reaction degree of slag shows approximately 15% increment in high W/P paste (**Figure 1** (A)). It is well known that the high specific surface area of fine calcite leads to increase the number of nucleation site, which results more reaction degree than coarse calcite (Knop, Peled, and Cohen 2014). However, the specific surface area (Blaine) of calcite does not affect significantly in low W/P mixture. Both fine and coarse calcite systems give similar slag reaction degree after 3 days of hydration period in W/P of 0.305 as depicted in **Figure 1**(B). Even though the high fineness of calcite increases the surface area for the reaction of slag, large specific surface area theatrically upsurges the solid surface area to be coated with water (Kwan and Chen 2013). As a result, the effective water for the reaction reduces with increasing the fineness of calcite, leads to the reduction of reaction rate in low W/P. But, due to the

excess amount of water in high W/P, the effect of particle size of calcite can be clearly seen in W/P ratio of 0.6.

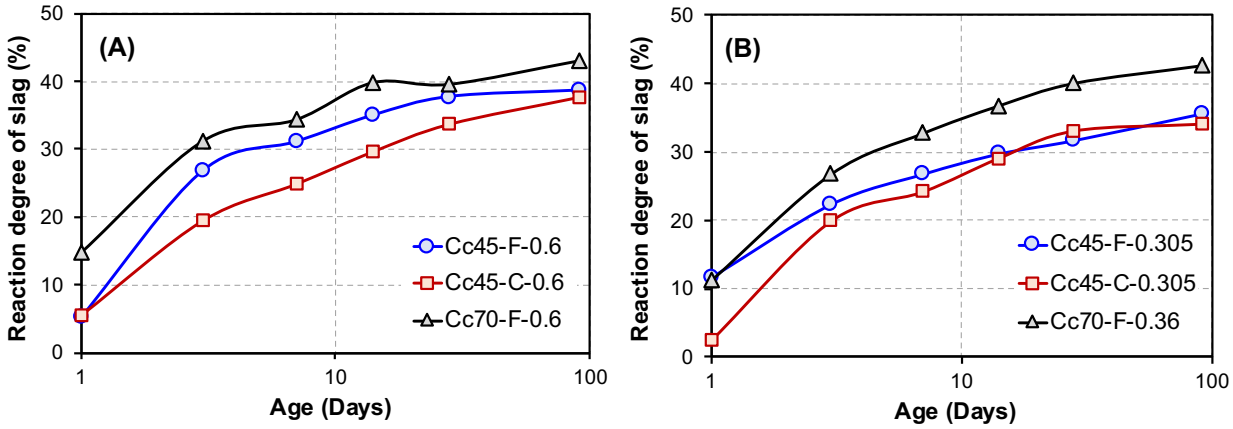

Figure 1 Reaction degree of slag for (A) high W/P and (B) low W/P paste

3.4.2 X-ray diffraction

The XRD patterns of representative mixture made with W/P ratio of 0.6 and 45 % fine calcite (Cc45-F-0.6) after the hydration periods of 1, 3, 7 and 14 days are illustrated in **Figure 2.** In the XRD patterns, the characteristic peaks of calcite, portlandite, ettringite and hemicarboaluminate are identified as crystalline phases in all the mixtures used in this work, i.e., different calcite content, specific surface area of calcite and W/P ratio. The peak of ettringite can be stably visible after 1 day of curing period for longer reaction period in addition to the unreacted portlandite and calcite. Since the destabilization of ettringite to monosulfate is inhibited by the presence of calcite, the carbonate phases and ettringite are more stable than monosulfate in the calcite-slag system which is detailed in Eq. (1) (Y. Han, Lin, and Wang 2021; Schöler et al. 2015).

$$\text{Monosulfate} + CaCO_3 + H_2O \rightarrow \text{Ettringite} + \text{Hemicarbonate/ Monocarbonate} \quad (1)$$

Where formula for monosulfate, ettringite, hemicarbonate and monocarbonate are

$3\mathrm{CaO}.\mathrm{Al}_2O_3.\mathrm{CaS}O_4.12H_2\mathrm{O}$, $3\mathrm{CaO}.\mathrm{Al}_2O_3.3\mathrm{CaS}O_4.32H_2\mathrm{O}$,

$3\mathrm{CaO}.\mathrm{Al}_2O_3.0.5\mathrm{CaC}O_3.0.5\mathrm{Ca}(OH)_2 11.5H_2\mathrm{O}$ and $3\mathrm{CaO}.\mathrm{Al}_2O_3.\mathrm{CaC}O_3.11H_2\mathrm{O}$ respectively.

The formation of hemicarboaluminate could also be observed after the curing for 3 days or a longer period, which is due to reaction of dissolved calcite, portlandite and aluminum oxide in the slag-calcite system (Hoshino, Yamada, and Hirao 2006; MacIej Zajac et al. 2014). The peak of hemicarboaluminate increases with hydration period in all slag-calcite system. On the other hand, the previous studies reported that in the presence of limestone or calcite, the formation of hemicarboaluminate increases up to 7 days, and then it is converted as monocarboaluminate in the cement and fly ash/ slag system (Deschner et al. 2012; Schöler et al. 2015; MacIej Zajac et al. 2014). The increasing tendency for the generation of hemicarboaluminate and monocarboaluminate with curing period in the OPC and OPC-slag mixture with the addition of calcite was observed by Hoshino et al (Hoshino, Yamada, and Hirao 2006). Nevertheless, the formation of monocarboaluminate or decreasing tendency of hemicarboaluminate is not observed in the cement free mixture i.e., slag-calcite-expansive agent-portlandite system. Due to the slow dissolution rate of calcite and the faster kinetic formation of hemicarboaluminate, the development of hemicarboaluminate can stably exist and increase even for longer curing period without forming the monocarboaluminate, although monocarboaluminate is thermodynamically more stable than hemicarboaluminate. Similar observation was also found for slag-calcite sample after 180 days hydration period (Jeong et al. 2017). It should be noted, yet, the monocarboaluminate was not found to be formed in the available previous studies. Owing to the high amount of slag (approximately 50% of the mixture) which gives high amount of aluminate, seems to be a favourable condition for the formation of hemicarboaluminate instead of monocarboaluminate (Avet and Scrivener 2018; Y. Han, Lin, and Wang 2021; Lin et al. 2021).

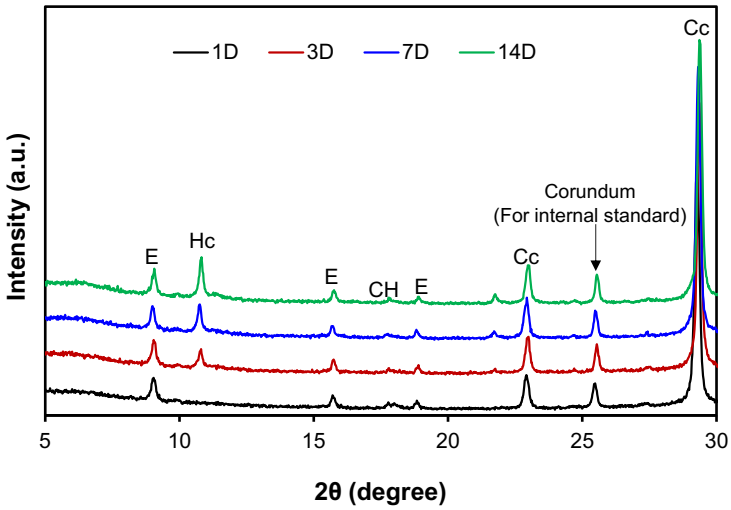

Figure 2 Observed XRD patterns of hydrated Cc45-F-0.6 paste with different curing age (E: Ettringite, Hc: Hemicarboaluminate, CH: Portlandite and Cc: Calcite)

3.4.3 Thermogravimetric analysis (TGA)

The percentage of weight loss along with differential thermal analysis against temperature at different curing ages for the representative sample of Cc45-C-0.6 obtained from thermogravimetric analysis is depicted in **Figure 3**. The considerable mass loss before 100 ºC is detected in all curing ages, which is mainly accredited to decomposition of ettringite and loss of bound water in C-S-H gel (Y. Wang et al. 2019; J. Yang et al. 2019). The sample after 3 days of hydration period or longer age reveals small peak in the temperature range between 120-140 ºC. As explained in Eq. (1), the peak of TG analysis for AFm phases i.e., monosulfate (approximately peak at 180 ºC) is herein shifted to lower temperature (approximately 120 ºC) due to the formation of carbonate phases in calcite-slag system. Based on the previous studies, this peak is confirmed due to the dehydration of hemicarboaluminate (Jeong et al. 2017; Schöler et al. 2015). Quite similar weight losses at approximately between 400-450 ºC were observed for all samples from the initial curing period (from 1 day to 91 day), indicating the occurrence of portlandite (Deschner et al. 2012; Jeong et al. 2017). This is because of the formation of portlandite during the hydration reaction and unreacted portlandite mixed with slag-calcite binder at the mixing time to activate the slag. Owing to the release of CO_2 from unreacted calcite, DTA curve illustrates a significant endothermic peak at nearly between 640-750 ºC as shown

in **Figure 3** and **Figure 4** (Deschner et al. 2012; J. Yang et al. 2019)**.** Overall, the results obtained from TGA are consistent with those of XRD patterns (see **Figure 2**). Therefore, the both analyses (XRD and TGA) confirm that ettringite and hemicarboaluminate are the main crystalline products in the slag-calcite mixture. The weight loss of crystalline phases during the thermal decomposition used for the quantification is shown in the **Table 4**.

Table 4 The weight loss of crystalline phases during the thermal decomposition

Phases	Formula	MW (g/mol)	H_2O loss (g/mol)	H_2O (wt.%)	CO_2 loss (g/mol)	CO_2 (wt.%)
Ettringite	$3CaO•Al_2O_3•3CaSO_4•32H_2O$	1,255	576	45.9		
Hc	$3CaO•Al_2O_3•0.5Ca(OH)_2 • 0.5CaCO_3•11.5H_2O$	564	207	36.7		
Portlandite	$Ca(OH)_2$	74	18	24.3		
Calcite	$CaCO_3$	100			44	44.0

Hc stands for hemicarboaluminate

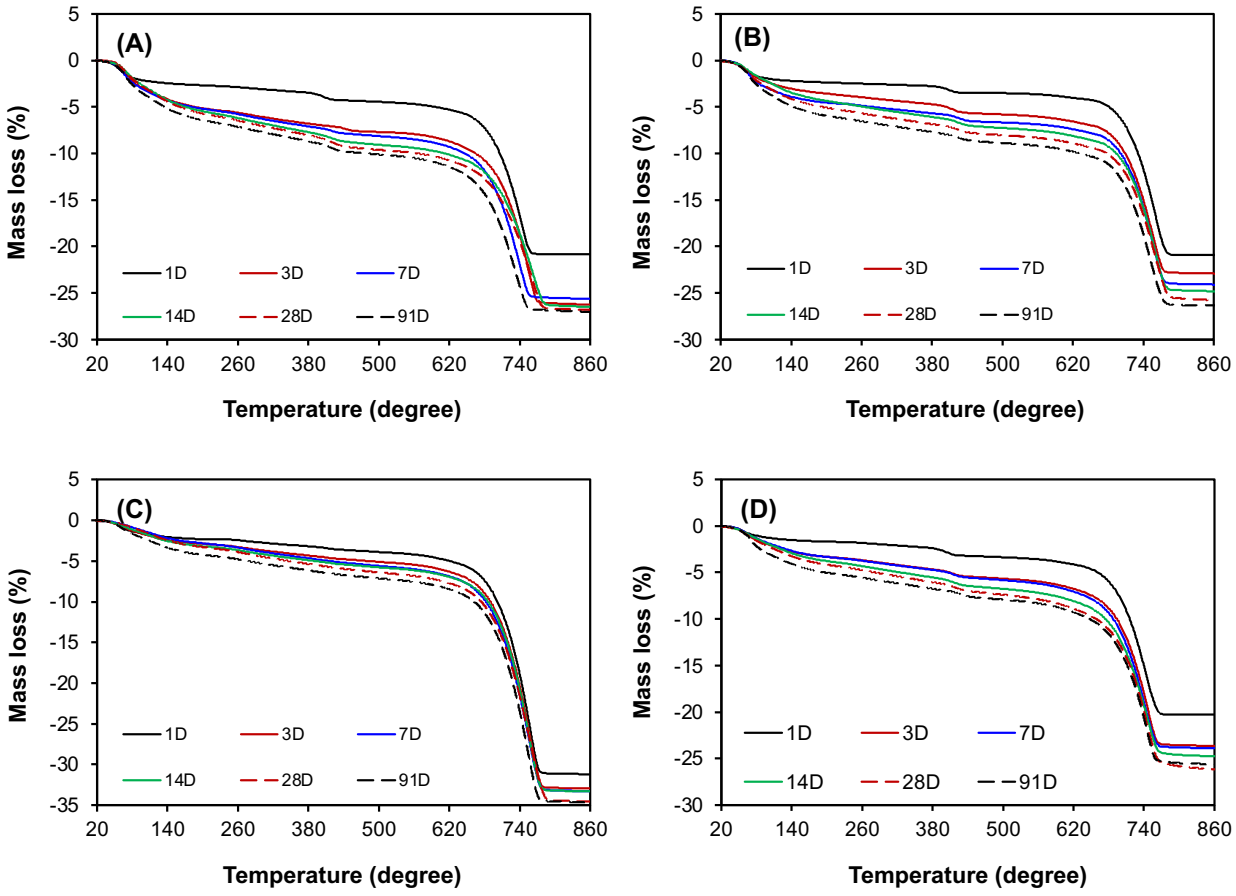

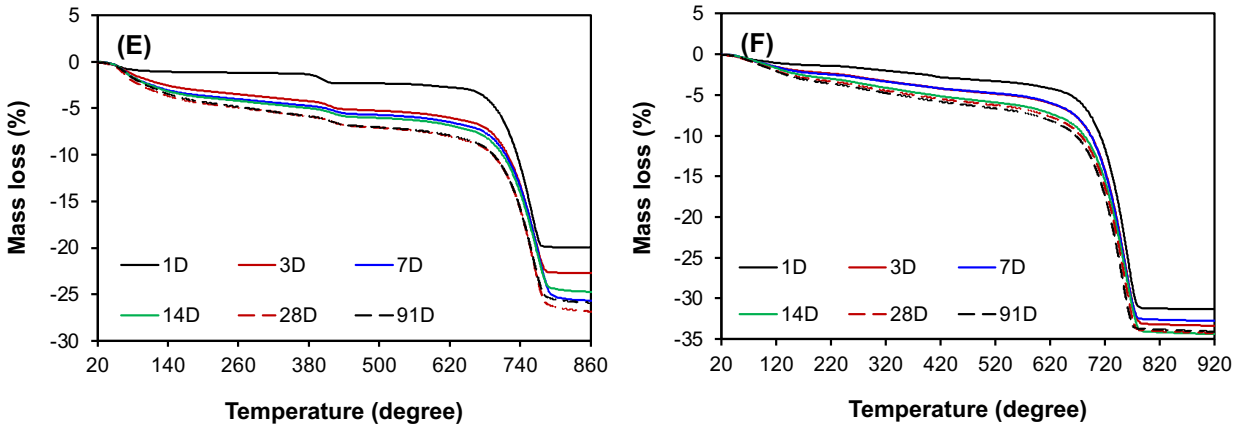

Figure 3 Mass loss of hydrated (A) Cc45-F-0.6 (B) Cc45-C-0.6 (C) Cc70-F-0.6 (D) Cc45-F-0.305 (E) Cc45-F-0.305 (F) Cc70-F-0.36 sample

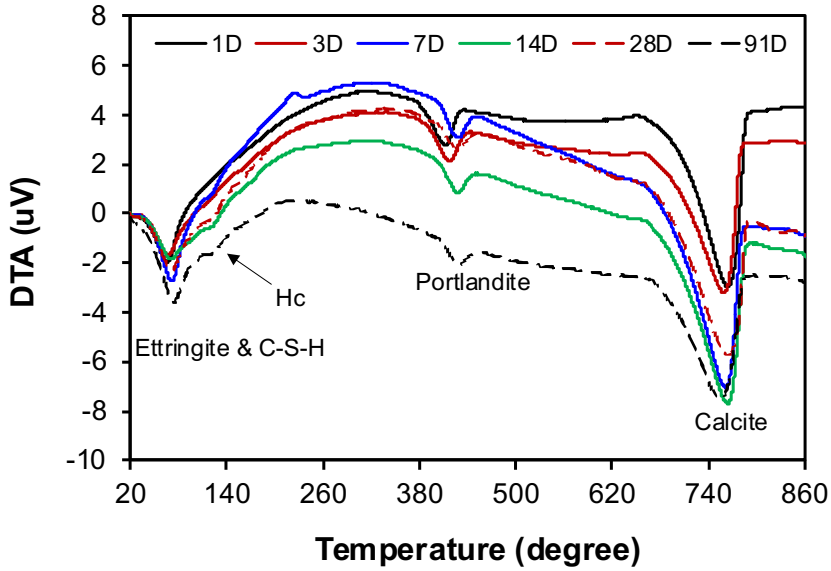

Figure 4 DTA results of hydrated Cc45-C-0.6 sample: (Hc: Hemicarboaluminate)

3.4.4 Thermodynamic model verification

The coupled hydration and thermodynamic model proposed in previous works (Yogarajah Elakneswaran et al. 2016; Krishnya, Yoda, and Elakneswaran 2021) was herein adopted and modified to predict the phases of ecofriendly cement paste i.e., cement free system (Slag and calcite). The predictability of the modified model is verified with the raw experimentals results including different W/P, calcite content and blaine of calcite. **Figure 5** and **Figure 6** present the comparison between

experimental results and predicted results of hydration products with curing age for high and low W/P paste respectively. The model results for C-S-H and hydotalcite are indicated as amorphous content in the predicted results (**Figure 5** and **Figure 6**). It can be seen that the predicted hydration products from the proposed model illustrate the similar tendency with experimental results for different W/P ratio, calcite content and its properties.

Decreasing tendency of calcite and slag are observed in all samples due to hydration reaction of dissolved raw materials. However, the calcite was not significantly dissolved as slag due to the low soluability of calcium carbonate (Jeong et al. 2017; Y. Wang et al. 2019). As a result, generally high amount of calcite replacement is used for the filler effect in the cementitious materials (MacIej Zajac et al. 2014). For instance, 45 % of calcite at the mixing time reduced to only 41 % after 91 days of hydration period for samples of 45 % calcite addition in both W/P ratio as shown in **Figure 5** and **Figure 6.** Previous studies also reported that only a small percentage of calcite reacts in the cement-slag or slag-calcite mixture after even longer hydration period (Adu-Amankwah et al. 2017; Jeong et al. 2017). The W/P ratio and specific surface area of calcite do not affect the dissolution rate of calcite i.e., approximately 5 % of calcite dissolves in both low and high W/P paste, and coarse and fine calcite content unlike the reaction rate of slag. As explained in section 3.1, hydration of slag has been modified by W/P ratio, calcite content and fines of calcite, and the slag content decreases with hydration period as clearly seen in **Figure 5** and **Figure 6**. On the contrary, the predicted results for the amorphous content upsurges with hydration period in all samples which imitates the tendency of the experimental results. This can be imputed to the formation of mainly C-S-H in the hydrated matrix resulting from the hydration reaction of slag. A noticeable increasing tendency of amorphous content is observed with W/P and blaine of calcite, and it shows the decreasing trend with calcite content for a specific curing age which is similar to the reaction degree of slag (section 3.1).

The precipitation of ettringite exhibits a rapid increment until about one day, and then it remains unchanged with curing period in all the conditions (refer **Figure 5** and **Figure 6**). This is because, ettringite forms until the depletion of gypsum ($CaSO_4.2H_2O$) i.e., formation of ettringite is correlated with the initial sulfate content as detailed in Eq. 2 (Avet and Scrivener 2018). Generally, the formed ettringite is converted as monosulfate in the absence of calcite or lime (see Eq. 3). On the other hand, the formation of monosulfate is terminated due to the presence of calcite and formed as carboaluminate phases as shown in Eq. 1. However, the monosulphate or carboaluminate phases start to form after the deplition of sulphate, i.e., after the complete formation of ettringite (Avet and Scrivener 2018; MacIej Zajac et al. 2014). As a result, the formation of hemicarboaluminate initiates approximately after 1 day of hydration period in the experimental results, which is exactly captured in the proposed model as well. The amount of portlandite is observed to remain constant throughout the curing period. Because portlandite eventhough contributes to the pozzolanic reaction of slag which leads to the reduction of portlandite, newly formed porlandite during the hydration reaction reimburses the portlandite reduction. Accordingly, the portlandite content obtained from the model and experimental results shows a constant value for specific condition from early age to 91 days of hydration period (see **Figure 5** and **Figure 6**).

$$(CaO)_3(Al_2O_3) + 3CaSO_4 \cdot 2H_2O + 26H_2O \rightarrow (CaO)_3(Al_2O_3)(CaSO_4)_3 \cdot 32H_2O \quad (2)$$

$$2(CaO)_3(Al_2O_3) + (CaO)_3(Al_2O_3)(CaSO_4)_3 \cdot 32H_2O + 4H_2O \rightarrow 3(CaO)(Al_2O_3)(CaSO_4) \cdot 12H_2O \quad (3)$$

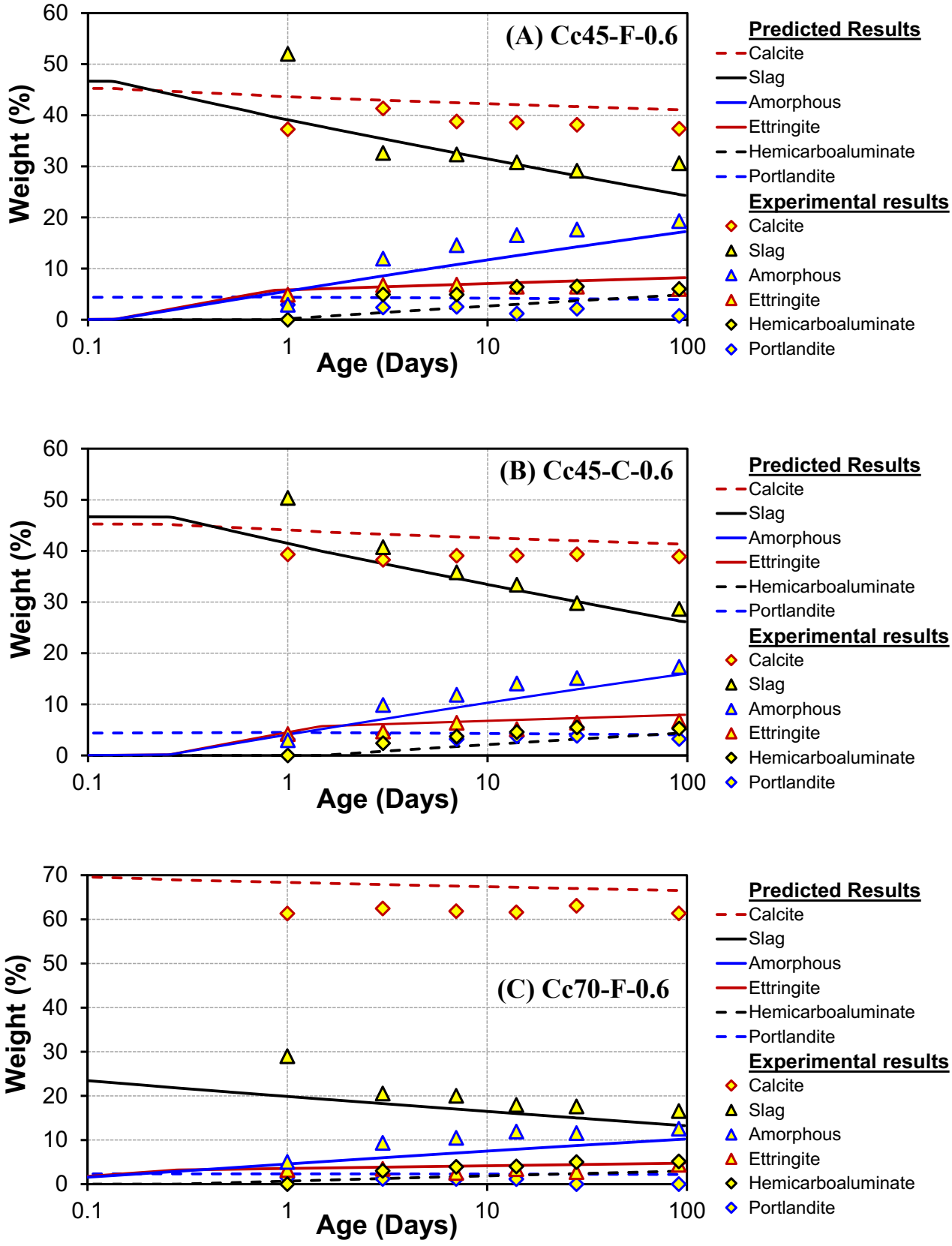

Figure 5 The comparison between predicted hydrates with the experimental results for the high W/P ratio samples

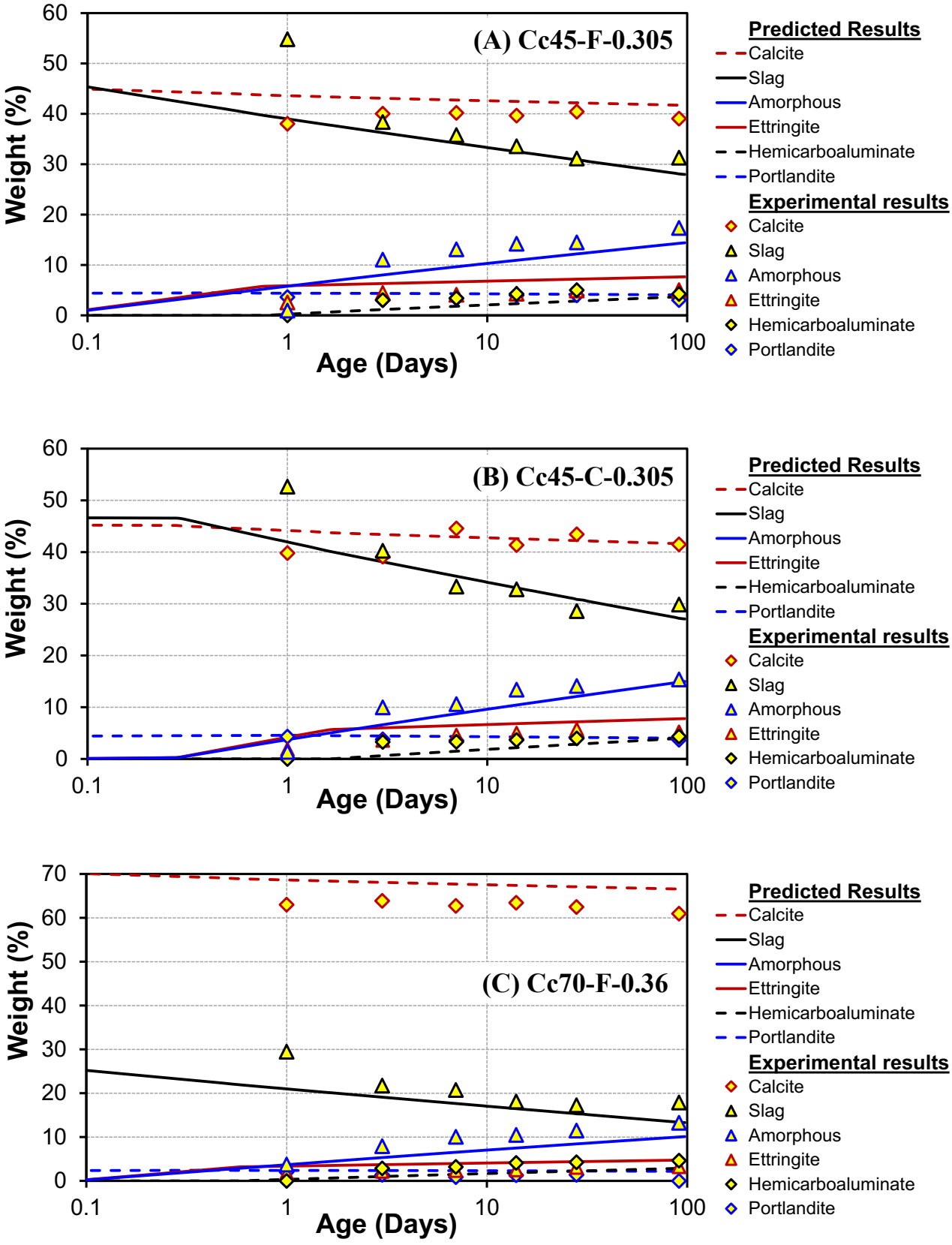

Figure 6 The comparison between predicted hydrates with the experimental results for the low W/P ratio samples

Following the successful verification of the amended model with experimental results of the hydrated matrix for slag-calcite system, the volume fraction of the hydrated matrix with curing age were predicted from the proposed model and it is depicted in **Figure 7** and **Figure 8** for high and low W/P ratio respectively. Here, C-S-H, ettringite, hemicarboalminate, hydrotalcite, portlandite and gypsum are considered as the hydration products of slag-calcite mixture. It has been verified in the previous studies that the C-S-H tends to form in two distinct structures such as low-density C-S-H (LD C-S-H) and high-density C-S-H (HD C-S-H) (Constantinides and Ulm 2004; Tennis and Jennings 2000). The LD C-S-H initiates to form the outer surface of the raw material at the initial stage of the reaction process, and with the progression of hydration reaction, the LD C-S-H fully covers the raw material. Afterwards, the new HD C-S-H forms within the space confined by the LD C-S-H due to the diffusion of ions through the previously formed LD C-S-H. These abovementioned two types of C-S-H are formed with different characteristics such as density and porosity. Therefore, in the proposed model, the formation of two types of C-S-H is realistically considered to simulate the actual hydration behaviour of the hydrated matrix. The Ca/Si ratio of C-S-H decreases with slag replacement ratio which can be attributed to low Ca content in slag and low reactivity of slag compared to that of OPC (F. Han and Zhang 2018; Y. Li, Qiao, and Ni 2020; Luan et al. 2012; Song et al. 2000). The Ca/Si for the slag replacement range of 0 % to 100 % is reported between 1.7 to 1.1 in the earlier studies (Luan et al. 2012; R. Taylor, Richardson, and Brydson 2010). However, in the presence of limestone or calcite, the formation of C-S-H exhibits higher Ca/Si ratio than the slag mixture due to the additional amount Ca from the dissolution of calcite or limestone (Adu-Amankwah et al. 2017; Rakhimova et al. 2016). Therefore, the Ca/Si for the cement free mixture (slag and calcite) is reliably considered as 1.5 which is higher than pure slag and lower than pure OPC mixture. The densities for LD and HD C-S-H for the Ca/Si ratio of 1.5 are taken as 1.4 g/cm^3 and 1.7 g/cm^3 with the gel porosity value of 0.36 and 0.26, respectively, based on the findings reported in our previous work for high volume fly ash binder (Krishnya et al. 2022). The reaction degree for each mixture obtained from the selective dissolution experiment (see section 3.1) is inputted in the proposed model to compute the

dissolution rate of slag with curing period, as reaction degree of slag may vary with chemical composition and the activation method (Altan and Erdoğan 2012; Giergiczny 2019). The shrinkage due to the molar volume difference between reactant and product referred as chemical shrinkage for slag is considered as 0.3 mL/g of reacted slag for the calculation of volume fraction of the hydrated matrix.

As illustrated in **Figure 7** and **Figure 8**, the unreacted slag and capillary porosity of the matrix decrease with curing period as the hydration reaction is taken place between the raw material and water which shows an upsurge in hydration products. For a specific W/P ratio, reaction products decrease with increasing the calcite content. Even though the slag reaction degree increases with calcite addition, slag content for the hydration reaction reduces, and also the reaction degree of calcite is very low. As a result, considerably low amount of hydrates form in 70% calcite mixture compared to 45% calcite system in both W/P pastes. When comparing the formation of LD and HD C-S-H in low and high W/P ratios, the volume fraction of LD C-S-H increases with W/P ratio. The formation tendency of HD C-S-H shows contrary behaviour to the LD C-S-H. Because the LD C-S-H forms in the space occupied by water during the early stage, and the HD C-S-H begins to develop in the constricted area at later stage more slowly (Jennings et al. 2005). The available space for the precipitation of LD C-S-H tends to increase with W/P ratio, leading to the more formation of LD C-S-H in high W/P paste compared to that of low W/P binder. The total volume reduction by chemical reaction (chemical shrinkage) increases with hydration period and decreases with increasing of W/P ratio and calcite content. With the increasing hydration period, slag reaction degree increases i.e., reacted amount of slag increases due to the hydration reaction, as a result, it upsurges the volume reduction due to the molar volume differences between the reactants and products. Moreover, the slag content of the total mixture (water, calcite and slag) decreases with W/P ratio and calcite content which leads to reduce the volume fraction of chemical shrinkage in high W/P and calcite paste.

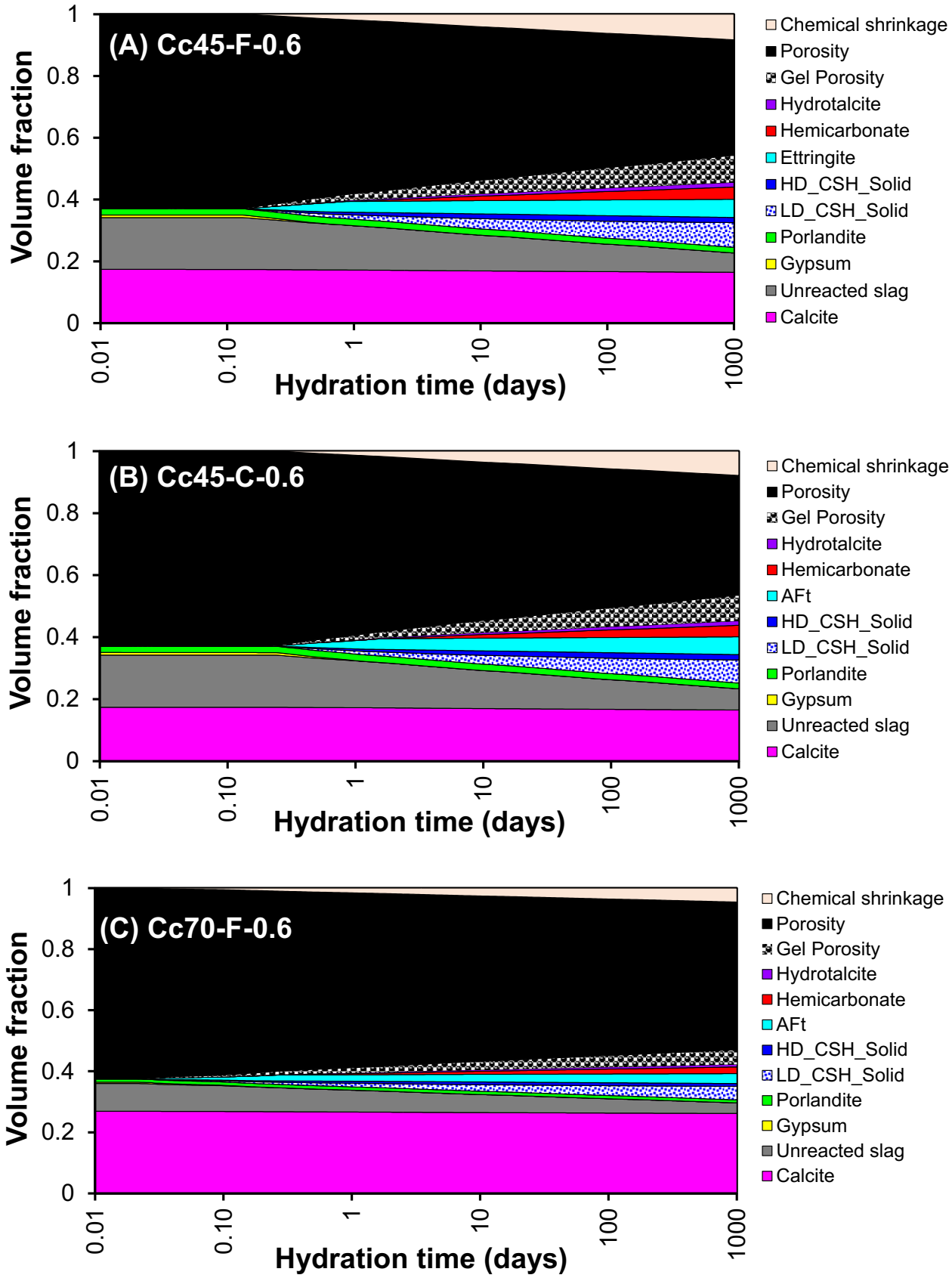

Figure 7 Mineral assemblage of hydrated slag-calcite system with hydration period for high W/P ratio

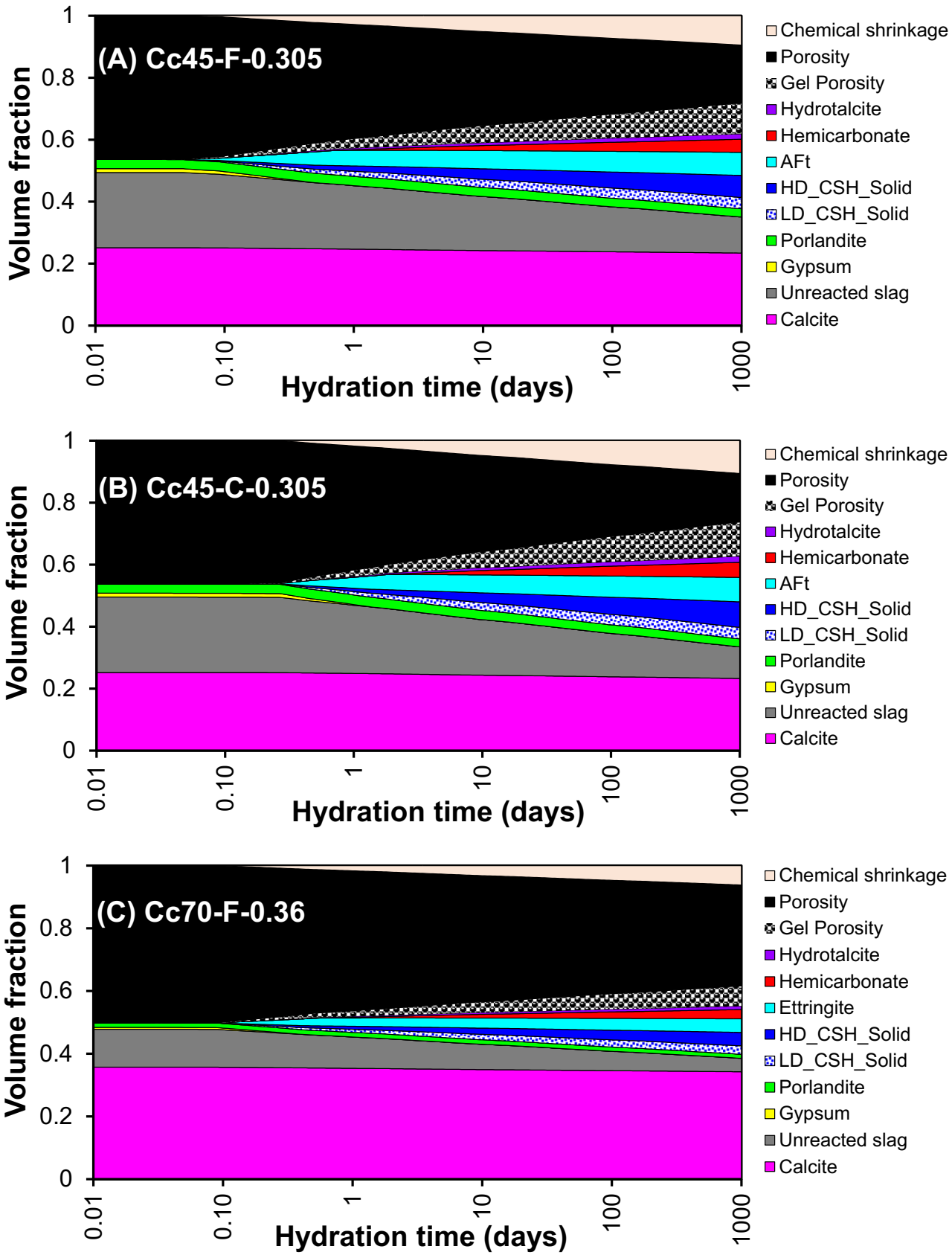

Figure 8 Mineral assemblage of hydrated slag-calcite system with hydration period for low W/P ratio

3.4.5 Porosity and pore structure

The experimental results of porosity by MIP method and the predicted results from the proposed model as a function of curing period for all systems are demonstrated in **Figure 9**. The capillary porosity obtained from the developed model corresponds to the difference between the initial volume fraction (water and raw material) and the volume fraction after the hydration reaction (unreacted material, hydration products and chemical shrinkage) at the desired curing period. The porosity measured by MIP covers the pore diameter ranging from 3 nm to hundreds of μm, which partially includes the C-S-H gel pores as the pore size less than 10 nm, is generally considered as gel pores inside the C-S-H matrix (Peng et al. 2012; Tariq et al. 2011). Therefore, the MIP results compared herein is the summation of predicted results of capillary porosity and gel porosity of the LD C-S-H matrix since the LD C-S-H consists of large pores than the HD C-S-H (Noguchi et al. 2021). As described in **Figure 9**, the predicted porosity shows an excellent agreement with the measured values for all the mixtures. It is evident that the computed results deviate only a maximum of 6 % compared to the experimental results.

The initial mixture porosity is high, and with the progression of hydration reaction, the pore space occupied by water is employed by hydration products. Thus, the porosity of the matrix reduces with hydration period (**Figure 9)** which is consistent with generally accepted concepts of hydration process. The composite having high amount of calcite (70 %) reveals more pore space than that of the mixture with 45 % of calcite for both high and low W/P binder. Similar phenomenon of the porosity is reported for the replacement percentage of limestone in numerous previous studies (Elgalhud, Dhir, and Ghataora 2016; Maciej Zajac et al. 2018). When increasing the calcite substitution percentage, the amount of unreacted material also increases in the mixture as the reactivity of the calcite is very low. As a result, the amount of hydration products to fill the pore space decreases due to the low amount of slag, leading to the more pore space in the 70 % calcite mixture. In high W/P binder, the porosity decreases with increasing specific surface area of the calcite. This should be mirrored by a significant

increase in the reaction degree of slag as shown in **Figure 1**. However, in the low W/P mixture, the effect of specific surface area of calcite can only be seen during the initial stage (up to 10 days) and afterwards, both calcite mixtures (Cc45-C-0.305 and Cc45-F-0.305) show almost similar porosity values which is exactly reflected in the slag reaction degree for low W/P paste (see **Figure 1**(B)). As mentioned earlier, the effective W/P ratio decreases with specific surface area of calcite in W/P of 0.305 due to the more surface area to be coated with water. As a result, the required water for the hydration reaction reduces, leading to almost similar reaction degree and porosity for 45 % of both fine and coarse calcite in low W/P binders in later age. Besides, the predicted and experimental results clearly demonstrate that increasing the W/P of the system displays in increasing porosity of the matrix, as high W/P paste has more water between unhydrated particles due to the high-water content.

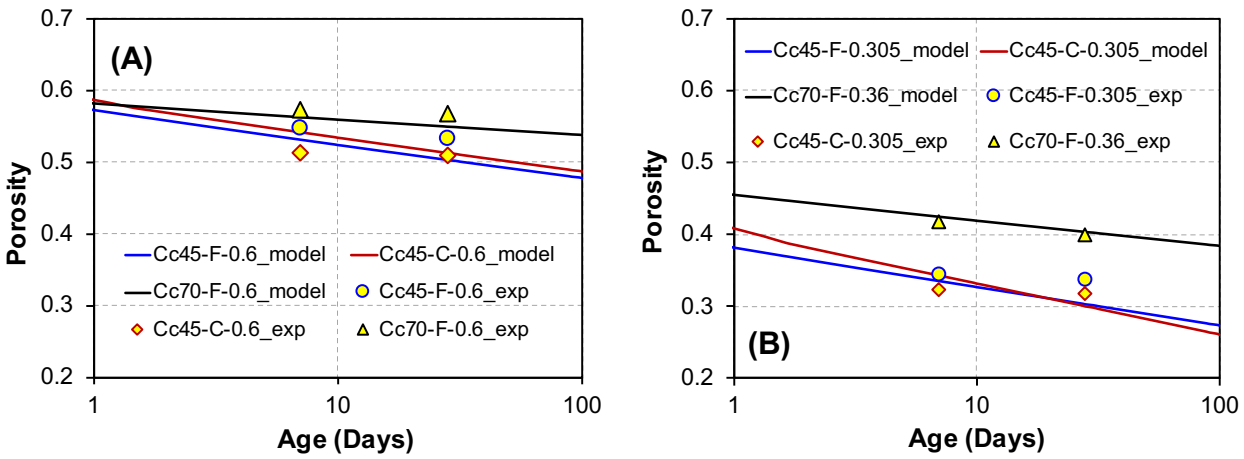

Figure 9 Comparison between experimental results and predicted results for the porosity of (A) High W/P samples; (B) Low W/P samples

The pore size distribution measured by MIP for different W/P, calcite content, specific surface area of calcite and curing period are presented in **Figure 10**. The composites with high W/P samples systematically have higher pore size distribution than the low W/P samples. For instance, the mixtures with W/P of 0.6 shows the pore diameter ranging from 4 nm to 1000 nm after 7 days of hydration period (**Figure 10** (A)), whereas it is only up to 100 nm for the binders with low W/P ratio ((**Figure 10** (C))). It is generally considered that the space between the unhydrated particles (pore space) is

controlled by the inter-granular spacing at the setting time (X. Chen and Wu 2013; Okpala 1989). Therefore, large pore diameters are generated in high W/P due to the high volume of the mixture. This inter-granular space is subdivided or reduced due to the formation of products during the hydration reaction, hence the pore size distribution has shifted to the left side, as pores are becoming finer with an increasing of hydration period as detailed in **Figure 10**. When increasing the calcite content, the pore space becomes larger which might be attributed to the poor pore space refinement in the high calcite content - due to the low amount of slag in the mixture and very low calcite reaction rate which leads to the reduced amount of hydration products. However, the samples Cc45-F-0.6 and Cc70-F-0.6 show almost similar pore size distribution after 7 days of curing period which may be an uncertainty in the experimental results. Moreover, fine calcite addition samples have large number of smaller pores compared to coarse calcite addition samples due to the filler effect of fine calcite particles in the large pores of the mixture.

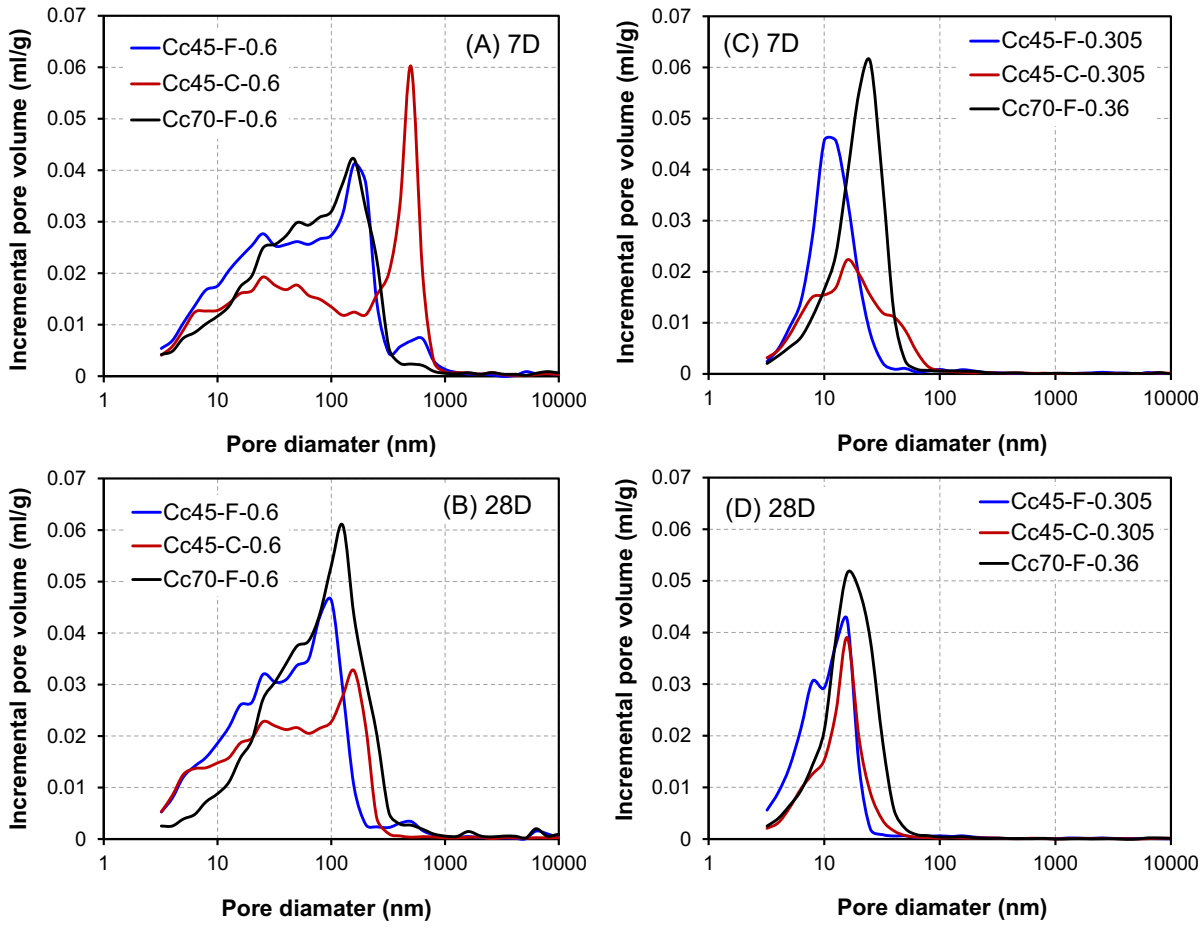

Figure 10 Pore size distribution of slag-calcite mixtures by MIP experiment as a function of pore diameter after curing for 7 and 28 days

3.5 Conclusions

The presented work revealed the effect of calcite content, fineness of calcite and W/P ratio on hydration behavior, hydrate phases and porosity in cement-free BFS system. The comprehensive investigation of the BFS-calcite mixture during the hydration reaction was undertaken with two different calcite contents (45% and 70 %), calcite fineness (coarse and fine) and W/P ratios (low and high) based on the numerous experimental techniques. The determined experimental results were used to check the predictability of the developed model in terms of hydration products and porosity as a function of curing period. The subsequent conclusions can be drawn based on the results:

1. The reaction degree of slag in the absence of cement was mainly enhanced by W/P ratio, calcite content and specific surface area of the calcite for a specific condition. However, the effect of fineness of filler on the hydration reaction was not considerably observed in the selective dissolution experimental analysis for low W/P binder, owing to the low amount of available water for the hydration reaction.
2. The characterization experimental analyses confirmed that the ettringite and hemicarboaluminate are the main crystalline hydration products of BFS-calcite hardened matrix, and the formation of monocarboalumate or destabilization of ettringite was not observed in any samples due to the presence of calcium carbonate.
3. It is notable that the predicted hydration products and porosity as a function of hydration period from the proposed model for the cementless binder showed excellent agreement with experimental results for all the binder compositions.
4. The porosity of the hardened matrix decreases with curing period and fineness of calcite as slag reaction degree increases with hydration time. The reaction rate is promoted by high specific surface area of the filler content. On the other hand, when increasing the calcite content and W/P ratio, it generates to increase the pore space of the matrix. Because, even though the reaction degree of slag increases with calcite content, the amount of the slag for

the reaction decreases, which leads to the increased amount of unreacted material with more pore spaces in the mixture.

CHAPTER 4

Carbonation

4.1 Introduction

Carbonation of cement-based material is one cause of corrosion initiation in steel rebar in reinforced concrete structures except chloride ingress. The CO_2 gas react with hydrated matrix followed by the diffusion of CO_2 gas via the pore network, this process is referred to as the carbonation. The service life of these structures in an atmospheric environment is closely related to carbonation. Almost all the cement-based structures need to tolerate a certain level of carbonation reaction during their lifetime owing to the existence of CO_2 gas in Earth's atmosphere. Carbonation is the result of the dissolution of natural CO_2 from the atmosphere (Friedmann, Amiri, and Aït-Mokhtar 2008). Most of the hydration products can be consumed by the reaction with CO_2 and transferred to carbonate phases like calcium carbonate. The precipitation of calcium carbonate could reduce the pH level of the material, making the surface became rough and large pits appeared, causing corrosion happened. Also, it can lead to the breakdown of steel passivity and thus present a risk of loss of rebar cross-section and spalling of structure cover owing to corrosion. Besides, carbonation of cement-based materials significantly affects the strength, porosity, pore size distribution and chemistry. Furthermore, it can cause shrinkage and cracking of the cementitious matrix. So, it is needed to investigate the carbonation behaviour caused by external environment.

Previous study reported that concretes made with Portland cement without additions showed the higher resistance to natural carbonation (Lollini and Redaelli 2021). In fact, due to a low reaction degree of slag in early age, slag-blended cement always give a higher carbonation rate and lower carbonation resistance compared to OPC (Sanjuán et al. 2018). In general, the carbonation of raw slag is not possible, while carbonation of AAS powdered paste involves reactions. The majority reaction within the first 28 days causes the gel decomposition and formation of different calcium carbonates in AAS (Nedeljković et al. 2018). Besides, instead of CH crystal in Portland cement, the main hydration product of AAS is calcium silicate hydrate. Even AAS binder shows high mechanical properties, low permeability and good resistance to chemical erosion, it still cause the carbonation resistance of AAS concrete is poor (He et al. 2018). Also, it is reported that although the addition of

limestone in cement can accelerates the carbonation rate, in the case of limestone-blended cement has a similar strength with Portland cement after carbonation, the accelerated carbonation curing of limestone with cement reduces carbon emissions since additional limestone can uptake more CO_2 (Shao et al. 2014).

However, the carbonation behaviour of this new composite cementitious binder is not clear, especially research about the change of hemicarbonaluminate under CO_2 environment is less. In order to understand the effects of carbonation on this new binder, it is important to understand the reactions of CO_2 with main phases in the binder and the factors which influence this process. The main aim of this chapter is to establish the potential resistance of this new composite cementitious binder to carbonation by focusing on the experimental study of the influence of calcite fineness, addition amount and carbonation period on carbonation process. What's more, under natural conditions (~0.04% CO_2) the carbonation process of cements and concretes normally takes place slowly. Therefore, most studies of the carbonation of cementitious materials are conducted under accelerated conditions. In this chapter, the carbonation behaviour of this new composite cementitious binder with different calcite addition rate, different type of calcite and curing period until 6 months under an environment of 5% CO_2 as well as 60% humidity conditions is observed. Apart from the experimental results, this part reviews the application of carbonation as a curing approach, with topics covering the reaction mechanism, process of implementation, and final product performance.

4.2 Experiments procedure

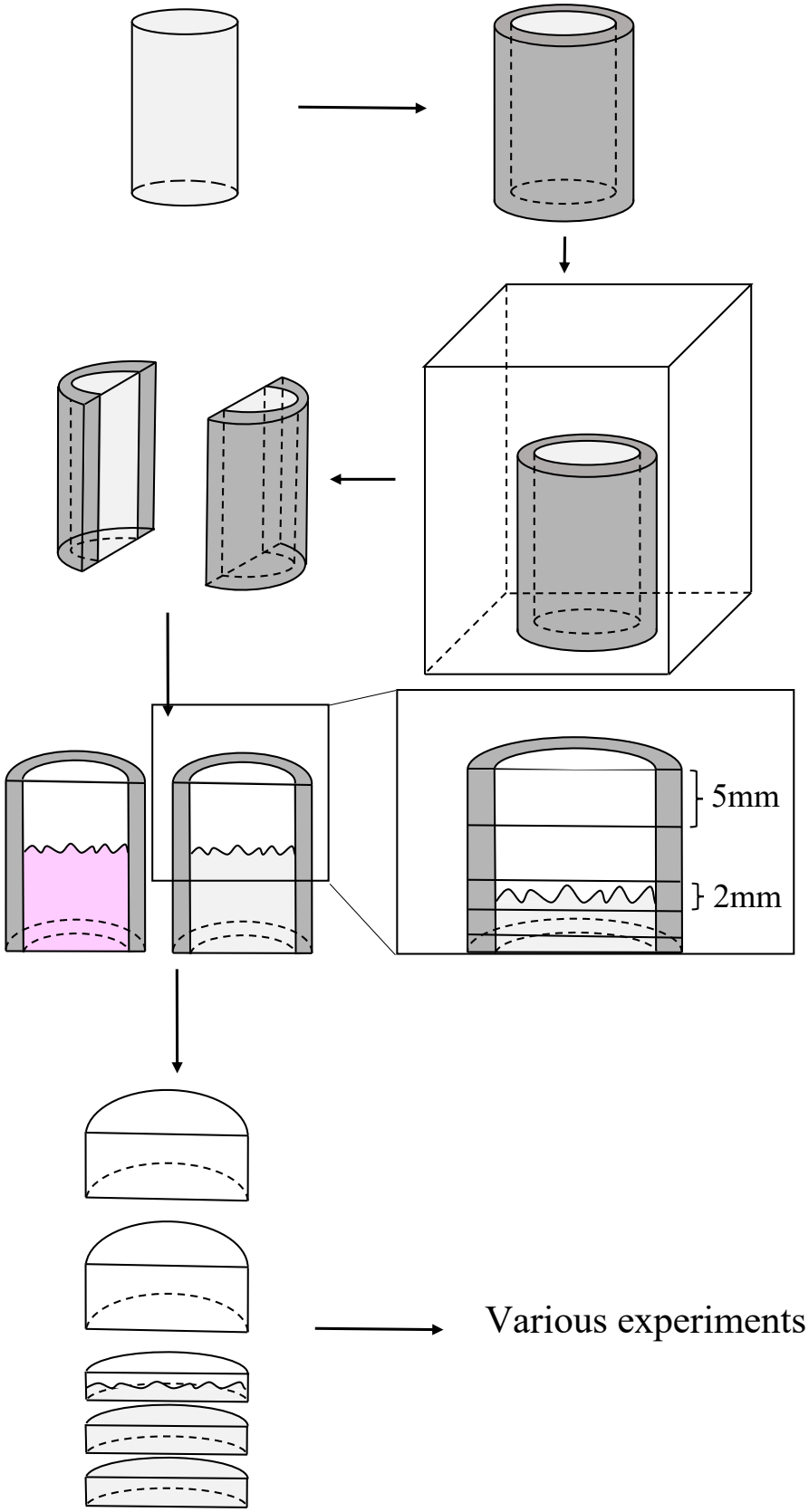

Figure 11 Experiment procedure for testing carbonation behaviour

The mix compositions are given in

Table 3. Cylinder samples (diameter 5 cm and height 10 cm) reached the predetermined curing period (28 days) were covered by epoxy resin except for the bottom of the circular surface which will face to exposure solution, only leaving the bottom surface exposed to a chamber (5% CO_2 and 60% humidity environment) to allow CO_2 to diffuse into the inner part of the sample. The prepared cylindrical specimen was exposed to accelerated carbonation for 2, 4 and 6 months. After the predetermined exposure period, take out the sample from the chamber, remove the surrounding resin. In order to determine the initial carbonation depth, the cylindrical specimens were spilt into two parts and the carbonation depth was determined by phenolphthalein test using one part. The carbonation depth was measured as the distance between the boundary of color change and sample edge for each side of the specimen first. Then the other part of cylindrical specimens was ground using a file at an interval of 5 mm depth from the exposed surface in the fully carbonated area and then the interval of 2 mm closed to the depth determined by phenolphthalein solution. The powder samples obtained from various depths below the exposed surface were used to determine the phase content in each layer and exact carbonation depth by XRD method and TG analysis to determine phase contents as a function of penetration depth. Experimental procedures are shown in **Figure 11**, where the sample preparation and exposure conditions during external chloride absorption are shown in **Table 5**.

Table 5 Sample preparation and conditions during carbonation

Parameter	**Description**
Calcite replacement ratio	45%, 70%
Proportion of water to binder	0.305, 0.36
Curing condition	Sealed curing for 28 days at 20 ºC
Carbonation environment	5% CO_2, 60% humidity
Carbonation period	2, 4 and 6 months

4.3 Results

4.3.1 Indicator test

Phenolphthalein is a pH indicator which is purple if the pH value is above 10 and colorless under 8.3 (A. Morandeau, Thiéry, and Dangla 2014). The specimens dedicated to the phenolphthalein test were split in half-cylinders. The treatment of the fractured specimens with phenolphthalein solution indicator leads recognizable color changes in the alkaline subarea. The sharp boundaries in the color transition from colorless to purple can be clearly achieved, which means the change of pH from neutralization to alkaline. Thus, the carbonation depth was accurately estimated.

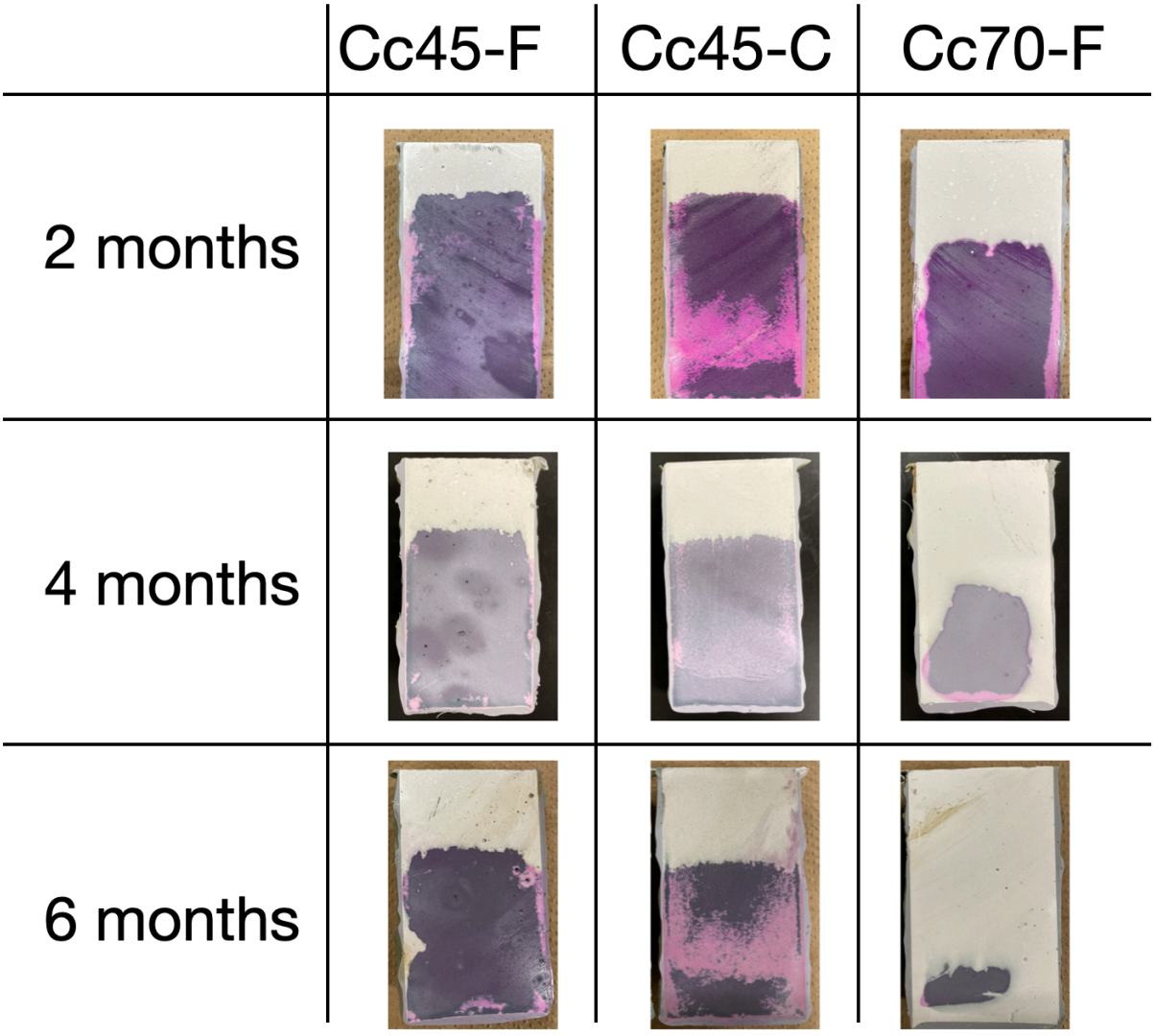

Figure 12 Samples treated with phenolphthalein indicator solution

The results from the phenolphthalein test show a good visual match in all case. The pictures of the specimens with calcite addition rate of 45% and 70% with different carbonation period are shown in **Figure 12**. The carbonation measurements were performed after 2, 4 and 6 months of accelerated carbonation treatment, where the approximately carbonation depth determined by phenolphthalein solution are shown in **Figure 13**. It is important to note that the phenolphthalein test does not really measure the carbonation depth but only its pH value. However, it still can give a reference about the approximately carbonation depth.

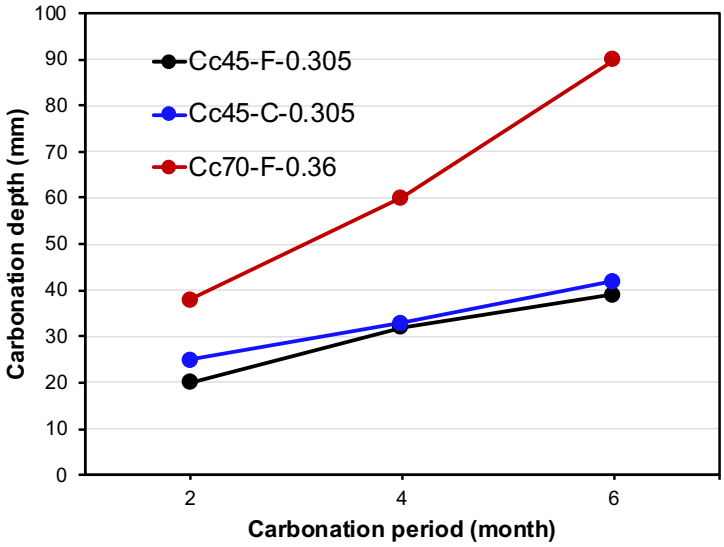

Figure 13 Carbonation depth as function of carbonation period in different mixtures

The carbonated depth for all mixtures gives an increase result as the carbonation period getting longer. In case of the coarse calcite addition samples (Cc45-C-0.305), the phenolphthalein test led to a slightly higher carbonation depth compared to fine calcite addition samples (Cc45-F-0.305). The differences in depth between these 2 mixtures are lower than 5 mm among all 3 different carbonation period. However, calcite addition rate gives a significant influence on carbonation behaviour. Higher fine calcite addition rate accelerates carbonation rate. Carbonation rate in 70% fine calcite addition samples shows an almost double rate as it in 45% fine calcite addition rate samples, which are around 40 mm depth after 2 months, 60 mm depth after 4 months and nearly full carbonated after a carbonation period of 6 months.

4.3.2 Phase assemblage

4.3.2.1 XRD

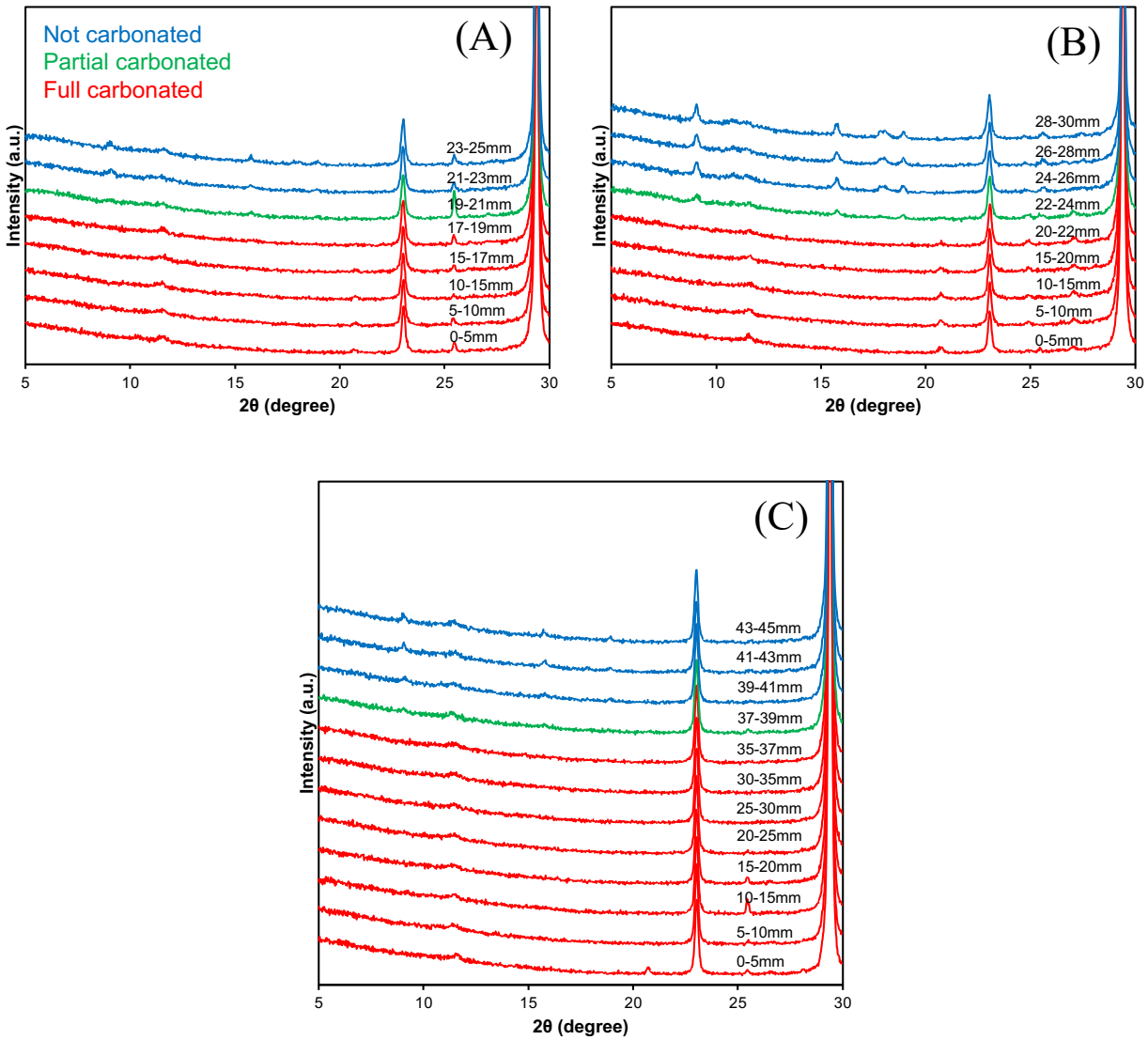

Figure 14 2 months XRD results for (A)Cc45-F-0.305 (B)Cc45-C-0.305 (C)Cc70-F-0.36 samples

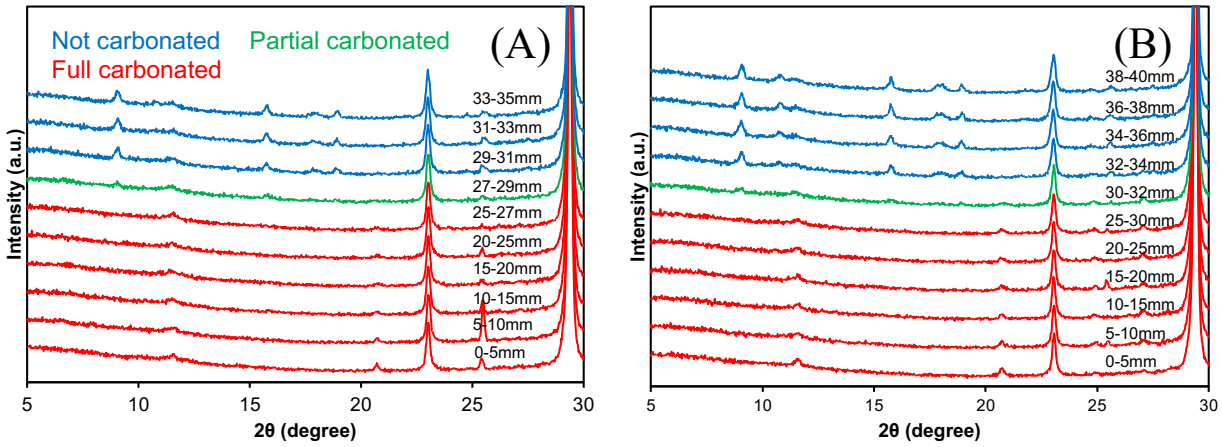

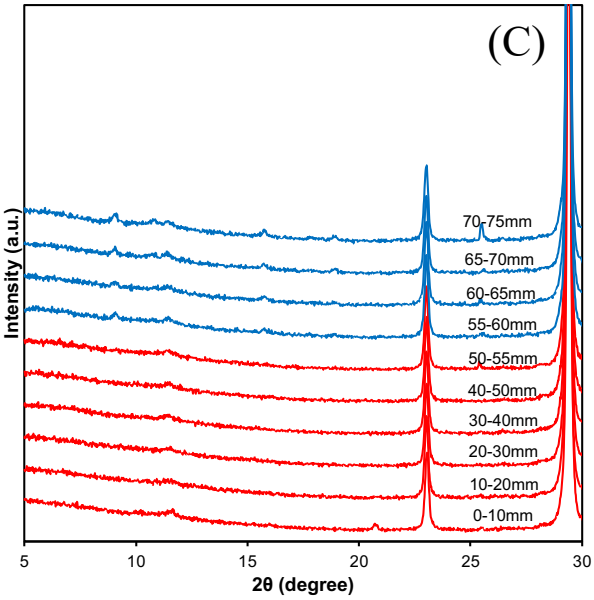

Figure 15 4 months XRD results for (A)Cc45-F-0.305 (B)Cc45-C-0.305 (C)Cc70-F-0.36 samples

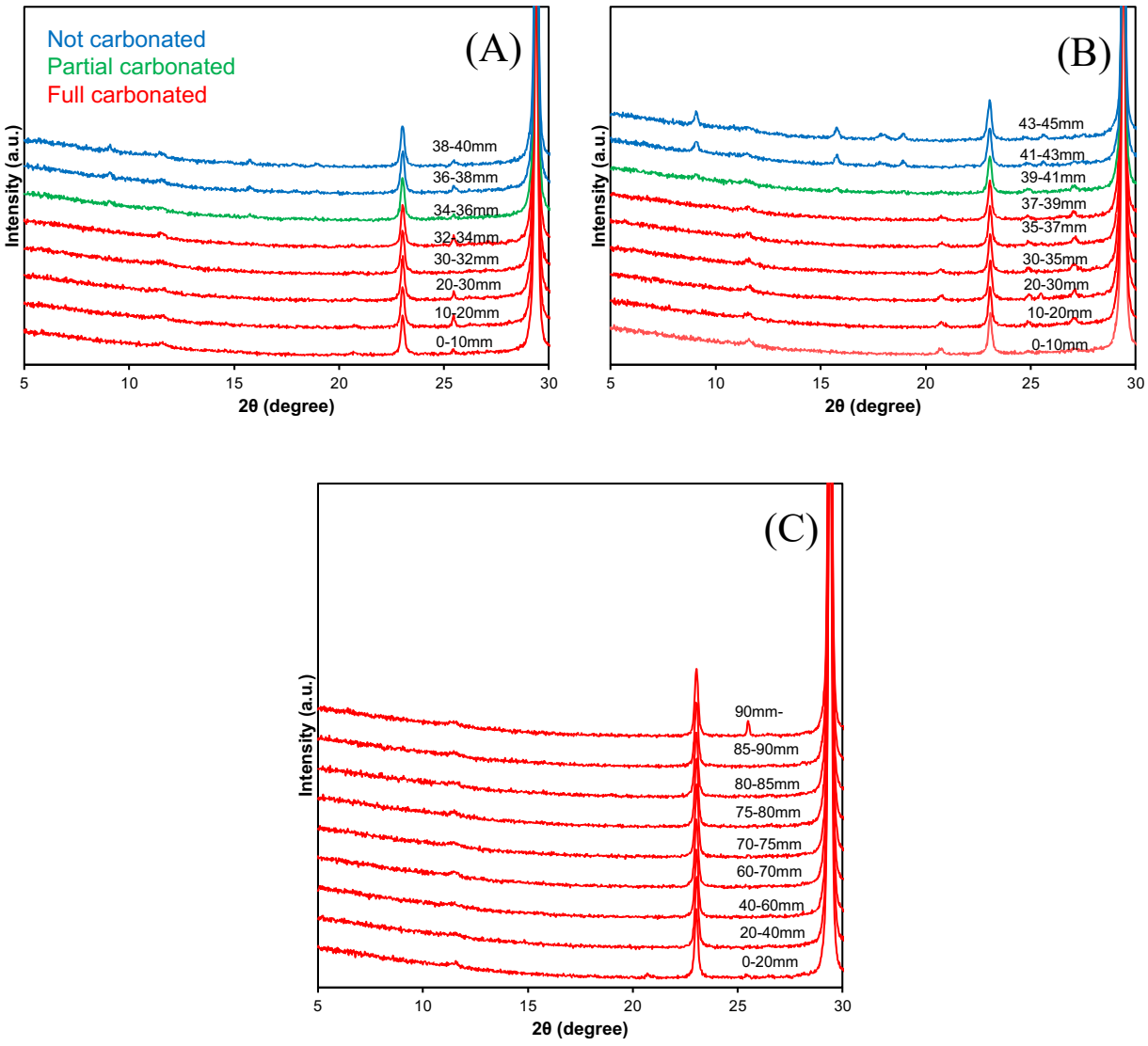

Figure 16 6 months XRD results for (A)Cc45-F-0.305 (B)Cc45-C-0.305 (C)Cc70-F-0.36 samples

Figure 14, **Figure 15** and **Figure 16** present the XRD patterns for continuous carbonated sample. For the colored part tested by phenolphthalein solution, XRD scans shows the presence of portlandite, ettringite and hemicarboaluminate as major crystalline hydrated phases in uncarbonated samples. No peaks corresponding to portlandite, ettringite and hemicarboaluminate were observed in colourless part tested by phenolphthalein solution, where is the carbonated part. The XRD patterns indicate ettringite, portlandite and hemicarboaluminate dissolution as their peaks were observed in the uncarbonated part while no peaks for these phases after carbonation. Besides, higher intensity for calcite indicate that calcium carbonate is one of the main products formed during carbonation. Also, partial carbonated samples were observed as the peaks of ettringite and portlandite are smaller compared to uncarbonated part which is marked in green colour. In addition, a small peak around 11.5 degree is observed in carbonated sample, this is due to the formation of gypsum caused by the carbonation of ettringite (Šavija and Luković 2016).

4.3.2.2 TGA

This method was used to determine the percentage of portlandite and calcite. Thermogravimetric (TG) curves of uncarbonated and carbonated samples are shown in **Figure 17**. The derivative of the mass loss during heating shows different peaks associated with the carbonation. It is very easy to detect the DTG (derivative thermogravimetry) peak related to the dehydration of portlandite around 400–500 °C, calcite (600–800 °C) decomposition can be easy to detect due to the CO_2 in calcite started to be expelled from the carbonate at approximately 600 °C. However, the mass loss in carbonated samples after 600 °C is higher than it in uncarbonated part. This is suggested that the precipitated calcite was more crystalline in CO_2 treated part than it of the uncarbonated samples. In addition, peak from 400–500 °C were observed in uncarbonated part while no curves in carbonated part, which indicate the portlandite reacted with CO_2 during carbonation as reported in previous research (García-González et al. 2006; Šavija and Luković 2016).

The temperature range from 30 to 300 °C is related to mass loss due to decomposition of C-S-H, AFt and AFm phase (Shah et al. 2018), but the quantification of C-S-H, Aft and AFm phases through TG method is difficult. However, it still can give some information about the carbonation behavior. The mass loss before 400 °C showed a signification difference between carbonated and uncarbonated samples, which is much lower in carbonated part compared to uncarbonated part. In XRD part, the curves for ettringite and hemicarboaluminate disappeared in carbonated part, and combine with the TG results, it can be deduced that both ettringite and hemicarboaluminate reacted with CO_2 and transferred to another phase. Also, a small curve around 120 °C can be observed in carbonated part, which confirm the carbonation of ettringite cause the formation of gypsum. The carbonation of ettringite gives an agreement with previous work (Šavija and Luković 2016). However, the report about carbonation of hemicarboaluminate is limited.

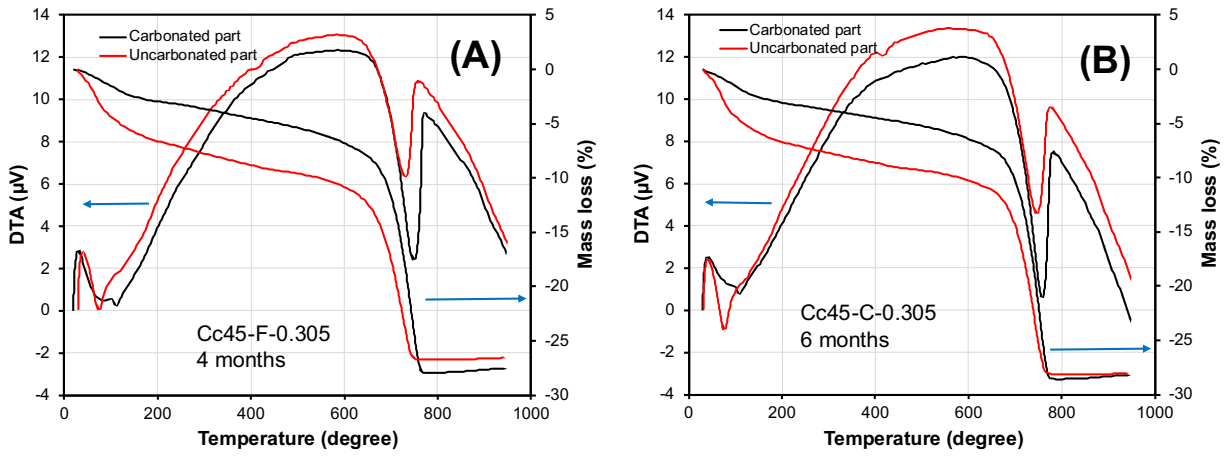

Figure 17 TG results in carbonated and uncarbonated samples

4.4 Discussion

4.4.1 Credibility of indicator test

Previous research (Phung et al. 2015) reported that the carbonation depth in samples with small amounts of limestone cannot determined by phenolphthalein solution test because portlandite can be observed through other test like XRD or TG, but the phenolphthalein test indicated a pH higher than

9. If it is assumed that under accelerated conditions in which the transport of CO_2 is faster than Ca ions, a calcite layer may form around the portlandite particles in a paste rich in portlandite before carbonation (Borges et al. 2010), then two main reasons can be considered cause this result, which are: portlandite particles are difficult to access for CO_2 due to the face that portlandite is covered by carbonation products and thus further carbonation is prevented, and the pH of the pore solution is no longer buffered by portlandite. However, in this clinker-free binder, only a few portlandite was added as a reactant and portlandite is not a major product during hydration. The amount of portlandite is limited among whole reaction. Also, there is enough Ca ions since calcite is added from the beginning. As a result, the carbonation depth determined by phenolphthalein solution test almost showed a same result compared to XRD and TG test. Therefore, it is possible to determine the carbonation depth through phenolphthalein indicator test in this clinker-free composite.

4.4.2 Phases distribution

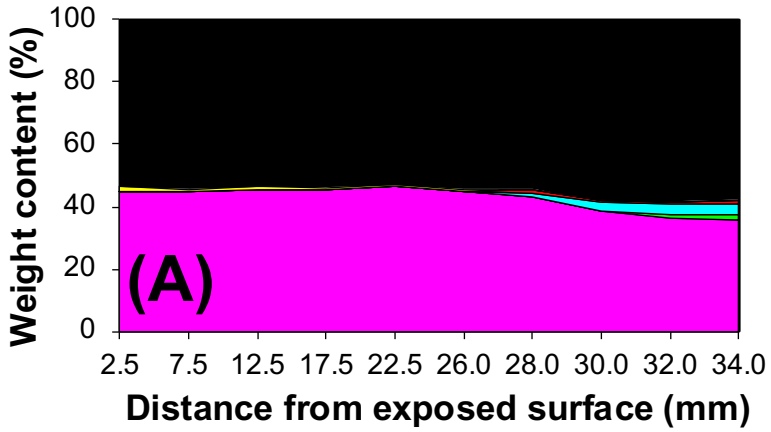

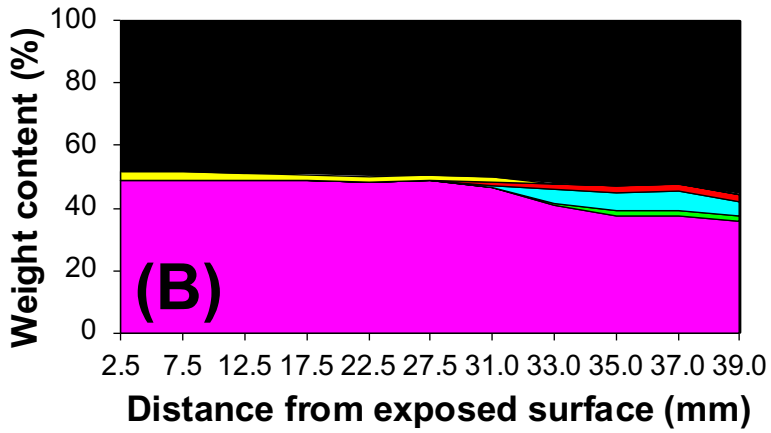

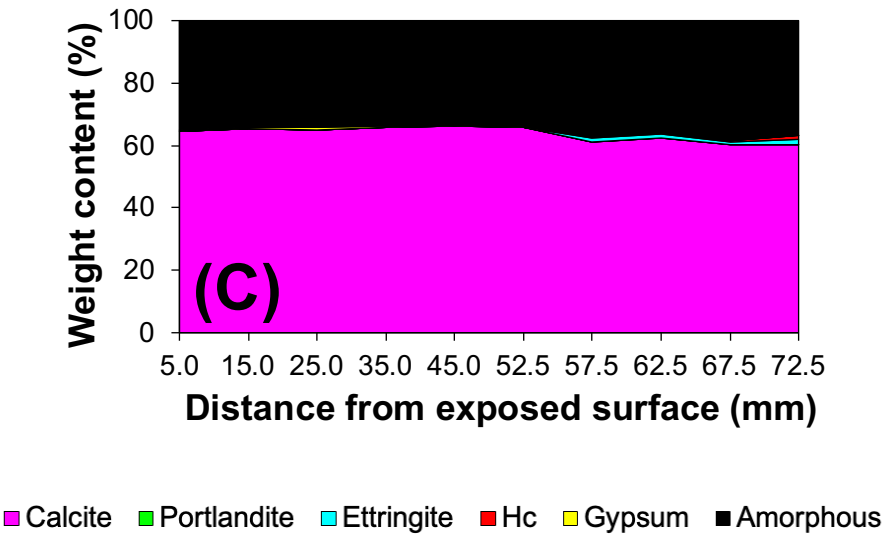

Figure 18 Distribution of phases in (A)Cc45-F-0.305; (B)Cc45-C-0.305; (C)Cc70-F-0.36 after 4 months of carbonation

The volume fraction of the carbonated binder as a function of distance from the exposed surface is depicted in **Figure 18** for Cc45-F-0.305, Cc45-C-0.305 and Cc70-F-0.36 respectively. Here, C-S-H, un-reacted slag, and other non-crystalline products were considered as amorphous. The weight content of calcite increases in the surface part as the carbonation is taken place between the hydration products and CO_2 which shows a drop in some hydration products. For a specific calcite addition rate, the differences in the carbonation depth between two different types of calcites (coarse and fine calcite) are less than 5 mm, which means the specific surface area of calcite did not affect carbonation behaviour significantly. However, considerably low amount of raw materials form in 70% calcite mixture compared to 45% calcite system, higher calcite addition rate faster the carbonation reaction. As a result, carbonation depth in 70% calcite addition samples have an almost double value (around 60 mm) than it in 45% calcite addition samples (around 30 mm).

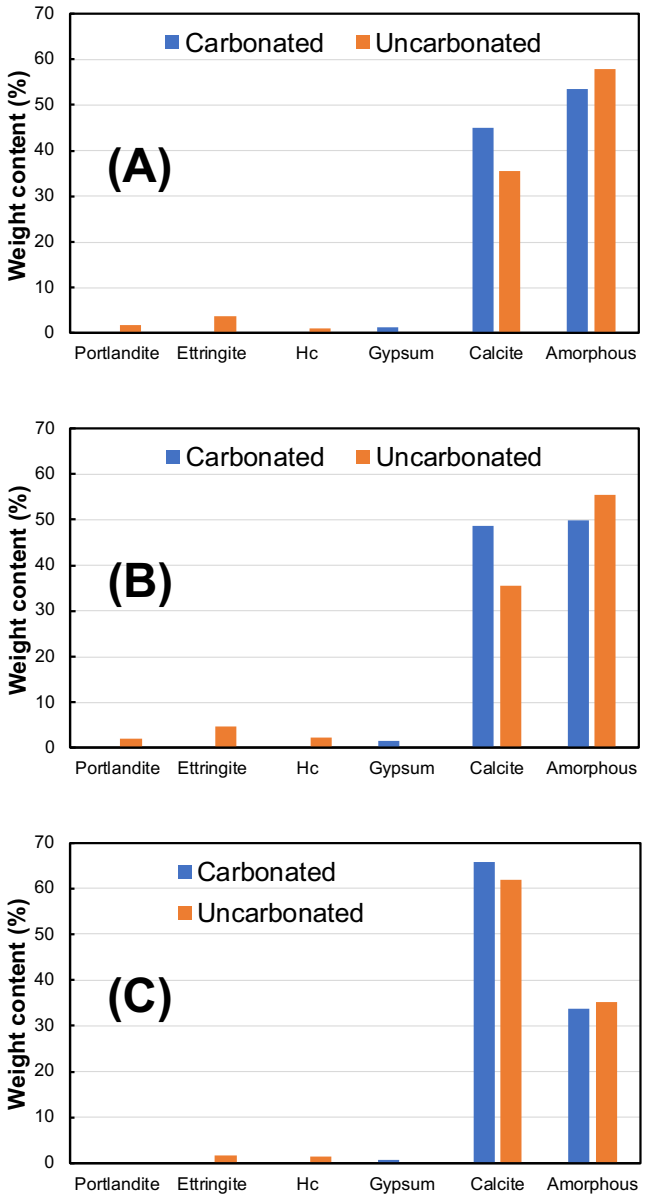

Figure 19 Comparisons of (A) Cc45-F-0.305, (B) Cc45-C-0.305, and (C) Cc70-F-0.36 before and after carbonation

Based on XRD and TG result, phase changes for each depth can be quantified. The comparisons between before carbonation and after carbonation are shown in **Figure 19**. The carbonation of hydration products additionally produce calcite, which can be seen close to the exposure surface from all cases. It is well known that unreacted portlandite can react with CO_2, causing the formation of calcite and water (Šavija and Luković 2016; Tang, Ling, and Mo 2021). Also, the total amount of amorphous content in carbonated samples was lower as compared to uncarbonated samples indicating carbonation of certain amorphous phase like C-S-H. In fact, C–S–H gel also can react with CO_2,

forming an amorphous silica gel and various polymorphs of calcium carbonate (A. E. Morandeau and White 2015; A. Morandeau, Thiéry, and Dangla 2014). In addition to the carbonation of portlandite and C-S-H, ettringite and hemicarboaluminate also reacted with CO_2 and produced calcite close to the surface from both XRD and TG test. The formation of gypsum was observed due to carbonation of ettringite (Šavija and Luković 2016; Tang, Ling, and Mo 2021).

4.4.3 Reaction mechanism

Since portlandite is one of the substances in this cement-free composite, the carbonation of portlandite occurred under CO_2 environment. Unreacted portlandite can react with CO_2 by following the equation below, causing the formation of calcite as reported in previous research (Šavija and Luković 2016; Tang, Ling, and Mo 2021).

$$\mathrm{Ca}(OH)_2 + \mathrm{C}O_2 \rightarrow C\mathrm{aCO}_3 + H_2\mathrm{O}$$

Also, both XRD and TG results showed that ettringite was affected under by CO_2, and transfer to other phase. Researcher (Šavija and Luković 2016; Tang, Ling, and Mo 2021) found the carbonation of ettringite consume it and could form calcite, and at the same time, gypsum is formed by the following reaction formular.

$$(CaO)_3(Al_2O_3)(CaSO_4)_3 \cdot 32H_2\mathrm{O} + 3\mathrm{C}O_2 \rightarrow 3\mathrm{CaC}O_3 + 3(CaSO_4 \cdot 2H_2O) + (Al_2O_3) \cdot xH_2\mathrm{O} + (26 - x)H_2\mathrm{O}$$

The formation of gypsum can be confirmed through both XRD and TG results. The XRD results showed the presence of ettringite in uncarbonated part and showed the presence of gypsum in carbonated part. Furthermore, the DTA (differential thermal analysis) curve around 120 to 140˚C also confirmed the production of gypsum, which showed an excellent agreement with the reaction formular mentioned above.

For hemicarboaluminate, less research was reported about its carbonation behaviour. However, its structure and formular is similar to other Afm phases like ettringite and monocarboaluminate. Previous study (Šavija and Luković 2016) showed that both ettringite and monocarboaluminate have the potential to react with CO_2, leading carbonation phenomenon. Therefore, it can be deducted that hemicarbonaluminate also transferred into calcite in carbonation as following reaction.

$$(CaO)_3(Al_2O_3)(Ca(OH)_2)_{0.5}(CaCO_3)_{0.5} \cdot 11.5H_2O + 3.5CO_2$$
$$\rightarrow 4CaCO_3 + (Al_2O_3) \cdot xH_2O + (12 - x)H_2O$$

Less amount of amorphous after carbonation in all samples gives a consistency to previous research (A. E. Morandeau and White 2015; A. Morandeau, Thiéry, and Dangla 2014), which may led by the carbonation of C-S-H. The carbonation of C–S–H gel consists of the removal of calcium ions from the gel leading to the formation of an amorphous silica gel and various polymorphs of calcium carbonate. The chemical reaction between C-S-H and CO_2 results in the formation of calcium carbonate and amorphous silica gel and can be written as follows.

$$(CaO)_x(SiO_2)(H_2O) + \mathrm{xC}O_2 \rightarrow x\mathrm{CaC}O_3 + (SiO_2) \cdot tH_2\mathrm{O} + (z - t)H_2\mathrm{O}$$

As a result, all phases besides unhydrated slag and calcite can be influenced under CO_2 environment, and their reaction mechanism are summarised above. Both the carbonation of hydrated crystalline part (Ettringite, hemicarboaluminate and portlandite) and amorphous part (C-S-H) causing the formation of calcite, as well as some other gel phases. All these reaction mechanisms agree with experiment results.

4.4.4 Influence of calcite

The carbonation mechanism of ettringite and portlandite are shown in chapter 2. The carbonation of both ettringite and portlandite cause the formation of calcium carbonate. In addition, the carbonation of ettringite cause a formation of gypsum. However, the type of calcite, as well as the addition rate

of calcite give an influence on carbonation behaviour. The transport of CO_2 in coarse calcite addition sample could be faster than it in fine calcite addition sample, which means lower fineness of calcite increases the carbonation depth in the case of same carbonation period. However, the carbonation depth difference between fine and coarse calcite addition samples didn't increase even with a longer carbonation period. The difference between them is less than 5 mm through whole carbonation. Two reasons can be considered from this result: both of them have a closed carbonation rate after a certain time, and a faster carbonation behaviour in initial period caused by lower fineness of calcite. Pervious reported (A. Morandeau, Thiéry, and Dangla 2014) that pore size and pore distribution have a significant influence in continuous carbonation. In this clinker-free case, although the porosity in both fine and coarse addition samples gives a closed value, the pore distribution is different. Much smaller pores filled by pore solution initially in higher fineness calcite sample, preventing CO_2 gas get to the pathway. However, since the porosity is similar, they have an almost same potential to reaction with the hydration products after saturation. As a result, higher fineness of calcite shallower carbonation compared to lower fineness one. Besides, higher calcite addition rate causes a high porosity of sample, leading a faster carbonation rate. Also, the total amount of amorphous content in carbonated samples was lower as compared to uncarbonated samples indicating carbonation of amorphous phases like C-S-H.

4.5 conclusion

In this part, the main effects of accelerated carbonation on different mixture of clink-free material are carried out. Since the phenolphthalein test alone is not an adequate indictor for carbonation rate despite of its common use, both XRD and TG measurement are used to learn its exact carbonation condition. In summary, the following points have been highlighted:

1. The XRD analyses confirmed the disappearance of hemicaboaluminate, ettringite, and portlandite peaks which shows all main crystalline phases carbonated during accelerated

carbonation. In addition, a higher amount of calcite in both XRD and TG results indicated calcium carbonation is one of the main products during carbonation.

2. After the carbonation period of first 2 months, the higher fineness of calcite showed a lower carbonation rate. However, it didn't show a significant effect in carbonation rate after a carbonation period of 2 months, which is probably due to there being much smaller pores in fine calcite addition samples and the porosity of 2 different type of calcite addition samples being closed to each other.
3. The effect of addition rate of calcite during carbonation was considerably observed from all three different tests. Higher calcite content increases the porosity and decreases the hydration products, thus increasing the carbonation rate. As the carbonation is progressed with time. The BFS-calcite hardened matrix could not resist carbonation.

CHAPTER 5

Chloride transport

5.1 Introduction

Assessing the durability performance of both new and existing structures remains one of the most significant challenges, particularly while considering the long-term life of the structure. This is turn dictated by the capability of the cementitious materials structures for a larger extent to resist numerous deterioration processes such as transportation of ions, gas and moisture. Among varying processes, chloride ingression is one of the most serious degradation processes in reinforced structure.

Reinforced concrete is a commonly used construction material for infrastructure exposed to sea water or deicing salts, such as harbors, tunnels and bridges (Machner et al. 2022). Once the chloride gets into the cementitious matrix, chloride-induced corrosion of the steel reinforcement happened, which is one of the main degradation mechanisms and one of the major forms of environmental attack for these reinforced concrete structures (Machner et al. 2022; X. Shi et al. 2012). Due to small radii and high activity, chloride ions can easily enter into the pore solution of concrete and reach the reinforcement surface, leading to the damage of passive film and pitting corrosion of the reinforcement and subsequently cracking and spalling of concrete (Cai et al. 2022). Chloride diffusion of cementitious materials is a complicated process, which is mainly influenced by both internal factors, including pore structure and the hydration products which are determined by the type of reactor, water to powder ratio, curing condition, as well as external factors, like the concentration of the exposure solution and the exposure period.

Physical adsorption and chemical reactions (Loser et al. 2010) are the main routes whereby chloride combines into the cementitious materials when there is a superior chloride ion concentration gradient external. The former two types of chloride ions are often both referred to as bound chlorides. Chemical binding refers the reaction of chloride ions with AFm phases. Some studies (Jones et al. 2003; Loser et al. 2010; Klaartje De Weerdt, Justnes, and Geiker 2014) have reported the formation of Friedel's salt from the hydrated products due to the penetration of chloride ions into cement pastes and concretes. Generally speaking, the sulfate in the Afm phase could be replaced by chloride, and it

causes the dissolution of the Afm phase and the formation of Friedel’s salt or Kuzel's salt. Physical binding of chloride ions is by the surface of C-S-H as it is the main hydration products in cementitious materials and having a high specific surface area. Even the bound chloride like Friedel’s salt or adsorbed chloride by C-S-H almost has no effect on the corrosion of steel bars directly, the free chloride in the pore solution causes the reinforcement corrosion. The free chloride ions destroy the passive film cover on the rebar leads to the initiation of corrosion.

However, in this slag-calcite system, in addition to the Afm phase, the formation of another phase, hemicarboaluminate is confirmed. Therefore, it is necessary to evaluate the long-term performance of hydrated slag-calcite material against external chloride gradient and the stability of each hydrated phase and its phase change. Especially the changes in the hemicarboaluminate phase under different chloride diffusion conditions are not understood well due to limited study.

The objective of this part is to investigate the chloride binding and diffusion mechanisms of external chloride based on the hydration behavior of this new cement-free slag-calcite established before. The chloride binding capacity of this new composite cementitious binder incorporating various calcite, the phase transformation during chloride exposure, and the relationship between chloride binding capacity and mixture of binder were investigated to uncover the chloride binding mechanisms of this new composite cementitious binder. Besides, the chloride diffusion profiles of this new composite cementitious binder are measured, and some assumptions are applied to investigate how chloride binding affects the chloride diffusion. Also, the stability of all products formed during the hydration period is evaluated when the hydration products are exposed to sodium chloride solution. The quantification of each phase in this system during the hydration period and after chloride penetration is determined by powder X-ray diffraction (XRD), titration and ion chromatography. Based on the chloride profiles, the chloride resistance of this cement-free material is evaluated.

5.1.1 Chemical chloride binding in AFm

When chloride ion from environmental solutions penetrates the cementitious matrix, some of them are captured by the hydration products. This is called chloride binding (Yuan et al. 2009). Friedel's salt ($3CaO{\cdot}Al_2O_3{\cdot}CaCl_2{\cdot}10H_2O$) and Kuzel's salt ($3CaO{\cdot}Al_2O_3{\cdot}0.5CaSO_4{\cdot}0.5CaCl_2{\cdot}11H_2O$) are two common chloride containing AFm phases. However, Kuzel's salt is not stable in the presence of even small amounts of carbonate (Balonis et al. 2010). Since calcite is added in this cement-free system, instead of Kuzel's salt, the formation of Friedel's salt is expected. Also, the quantification of Friedel's salt can be determined by XRD method.

5.1.2 Physical chloride binding in C-S-H

In addition to chemical binding in AFm phases, chlorides can also be bound physically by accumulating in the diffuse layer of the C-S-H as explained by the electric double layer theory (Machner et al. 2022; Yuan et al. 2009). Some searcher (Ramachandran 1971) distinguished three types of interaction with C-S-H, which occur in a chemisorbed layer on hydrated calcium silicates, in the C-S-H interlayer spaces, and in the C–S–H lattice. However, other searchers (Luping and Nilsson 1993) suggested that most of the bound chloride is physically bound to ion exchange sites of C–S–H gel. They also suggested that a significant degree of reversibility exists and, thus, reducing the pore solution chloride concentration could result in desorption of bound chlorides. Besides, other research (Yuan et al. 2009) reported that physical binding only accounts for a very small fraction of the total chloride ion bound by cement. Until now, there is no method can quantify the physical bound chloride amount in C-S-H accurately. In this research, total chloride content, chemical bound chloride amount in Friedel's salt and water-soluble chloride (consider as free chloride) content were quantified, then physical bound chloride amount can be calculated through the different of the 3 values above.

5.1.3 Free chloride in pore solution (Water-soluble chloride)

Among 3 different shape chloride (Chemical bound chloride, physical bound chloride and free chloride), free chloride can be considered as the most dangerous because of its capacity to diffuse towards the steel bars (Barberon et al. 2005). The amount of free chloride ions in the pore solution was evaluated by using the water-soluble chloride content in this research. Research (Mohammed and Hamada 2003) has reported that there is a linear relationships between free chloride and total chloride contents under a long-term exposure tests for various cements, such as ordinary portland cement, high early strength portland cement, moderate heat portland cement, calcium aluminate cement, slag cements, and fly ash cement. To determine how far the free chloride in pore solution have penetrated into the cementitious binder, chloride ingress profiles are obtained. These profiles give the free chloride content in the binder as a function of depth below the exposed surface.

5.2 Experiments procedure

The mix compositions are given in

Table 3. Cylinder samples (diameter 5 cm and height 10 cm) reached the predetermined curing period (28 days) were covered by epoxy resin except for the bottom of the circular surface which will face to exposure solution, only leaving the bottom surface exposed to a solution (500mL 0.5M NaCl solution) to allow ions diffuse into the inner part of the sample. After an immersion period of 3, 6 and 12 months, take out the sample from the solution, remove the surrounding resin, and ground it using a file from the exposed surface in every 2 mm depth. The powder samples obtained from various depths below the exposed surface were used to determine the phase content in each layer by XRD method, to determine their total chloride content by potentiometric titration, and to determine their chemical bound chloride by Rietveld analysis, also, to determine their free chloride content through ion chromatography. Experimental procedures are shown in **Figure 20**, where the sample preparation and exposed conditions during external chloride adsorption are shown in **Table 6**.

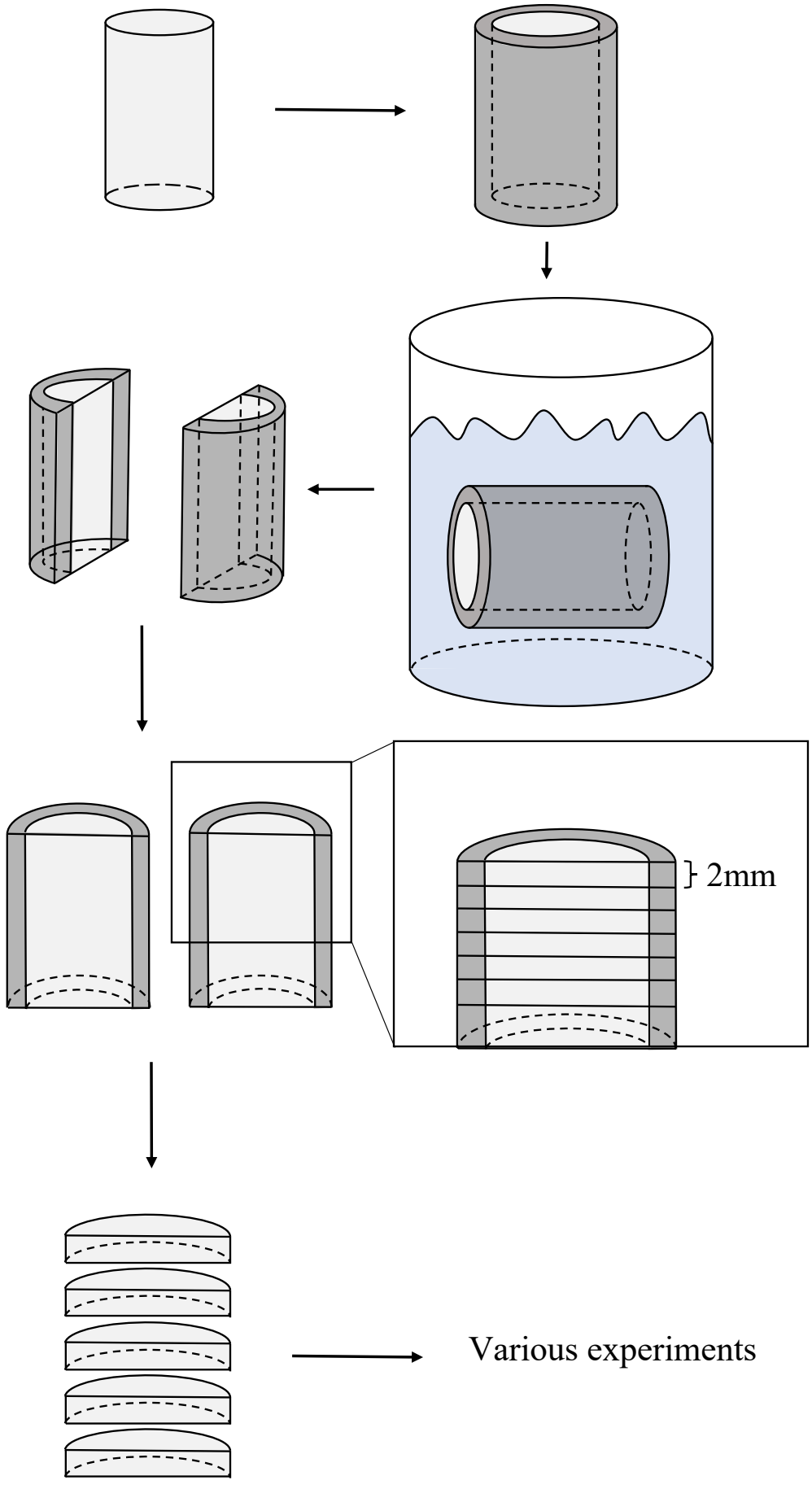

Figure 20 Experiment outline for testing chloride transport

Table 6 Sample preparation and exposure conditions for external chloride adsorption

Parameter	**Description**
Calcite replacement ratio	45%, 70%
Proportion of water to binder	0.305, 0.36
Curing condition	Sealed curing for 28 days at 20 ºC
Exposure solution	500 mmol/L NaCl
Exposure period	3, 6 and 12 months
Exposure solution volume	500mL

5.2.1 Chemical bound chloride

The collected powder was used for XRD measurement to quantify mineralogical composition, as well as coupled with Rietveld analysis to quantify the phase assemblage of paste samples after exposure to NaCl solutions for different periods. For Friedel's salt (F's), we assume the ideal chemical composition $3CaO{\cdot}Al_2O_3{\cdot}CaCl_2{\cdot}10H_2O$ with a molar mass of 561 g/mol. Under this assumption, chemically bound chloride can be quantified as the follow equation.

$$Chemical\ bound\ Cl(\%) = \frac{2M(Cl)}{M(F's)} \cdot wt(F's)$$

Where M(Cl) is the molar mass of chlorine (35.5 g/mol), M(F's) is the molar mass of Friedel's salt (561 g/mol), wt(F's) is the weight percentage of Friedel's salt calculated by XRD-Rietveld analysis.

5.2.2 Water-soluble chloride

Around 0.5 ± 0.01 g of the powder was weighed after drying at 105℃ for 30 mins to limit the impact of free water on the determination of the water-soluble chloride content. The dried powder was put into 100 mL bottle within 50 mL water. Then heating the bottle by water bathing around 80℃ for 5 minutes. After that, left the bottle at room temperature for 24 hours. the immersed samples were filtered through a filter and filled into 50 mL centrifuge tubes then diluted for 10 times for testing ion

chromatography. The results of the water-soluble chloride content could be calculated with the following equation.

$$\text{Water soluble Cl}(\%) = \frac{10 \cdot \text{c}(\text{Cl}) \cdot \text{V}_{\text{sample}}}{10^6 \cdot \text{m}_{\text{sample}}} \cdot 100\%$$

Where 10 is the dilution time for solution containing the sample, c(Cl) is the concentration of water-soluble chloride tested by ion chromatography. V_{sample} is volume of the solution (50 mL in this experiment), m_{sample} is the mass of the sample immersed.

5.2.3 Total chloride

For the determination of the total chloride content, 0.25 ± 0.01g of each profile ground powder sample was weighed and dried for 30 mins in an aerated oven at 105 degrees. After cooling the samples to room temperature in a desiccator, they were weighed again and were dissolved in 50 mL HNO_3 solution (65%, diluted from 3 mL) until the solution is clear. After that, the mixtures were titrated against a 0.01 mol/L $AgNO_3$ solution with a AUT-501 machine. The results of the total chloride content can be calculated with the following equation.

$$\text{Cl}(\%) = \frac{\text{V}_{\text{AgNO}_3} \cdot \text{c}_{\text{AgNO}_3} \cdot \text{M}(\text{Cl})}{\text{m}_{\text{sample}}} \cdot 100\%$$

where V_{AgNO3} is the volume of silver nitrate added at the inflection point of the titration, c_{AgNO3} is the concentration of the silver nitrate solution (0.01 mol/L), M(Cl) is the molar mass of chlorine (35.5 g/mol), and m_{sample} is the mass of the dissolved samples after drying at 105 degrees.

5.3 Results

5.3.1 Phase assemblage

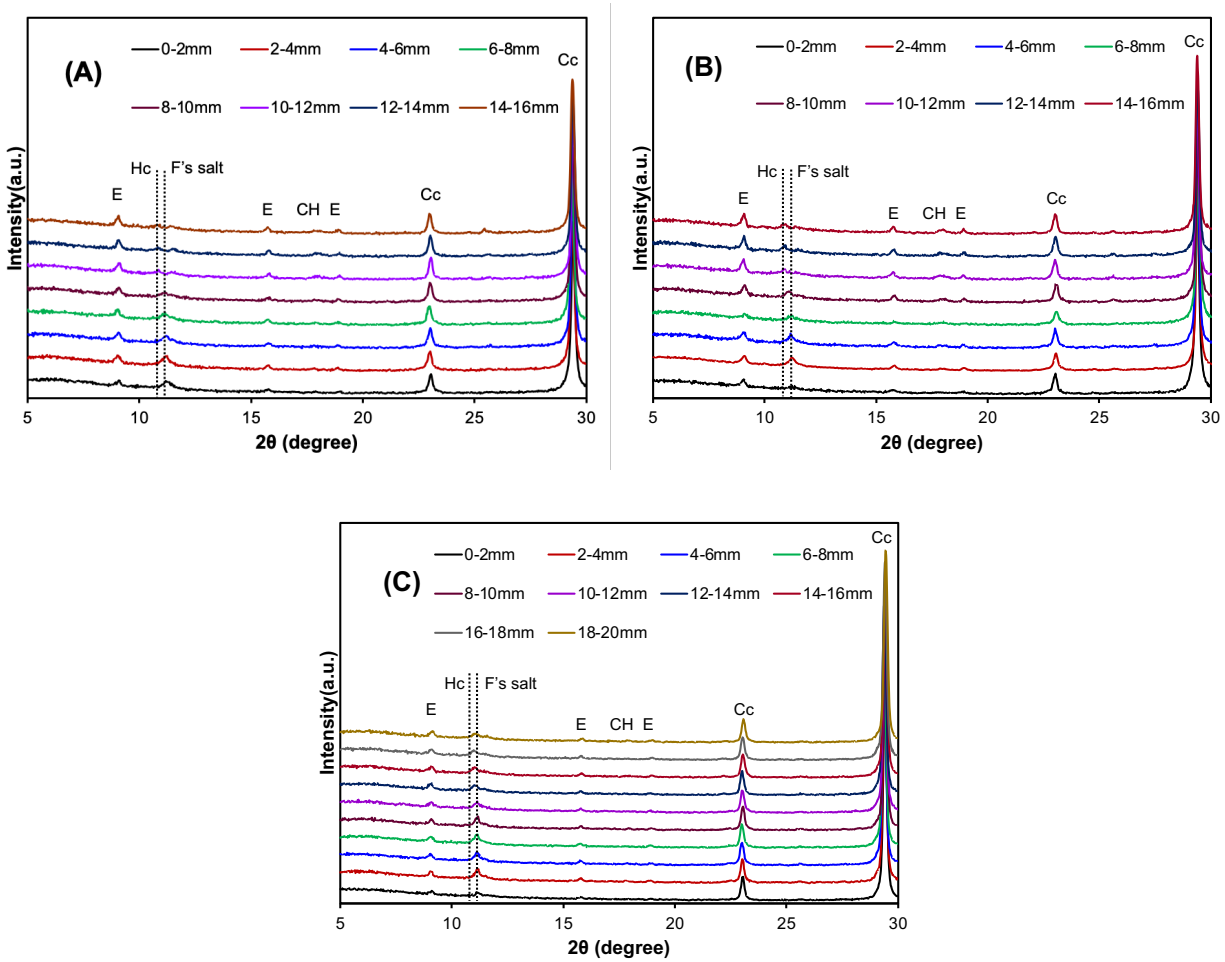

Figure 21 3 months XRD results for (A)Cc45-F-0.305 (B)Cc45-C-0.305 (C)Cc70-F-0.36

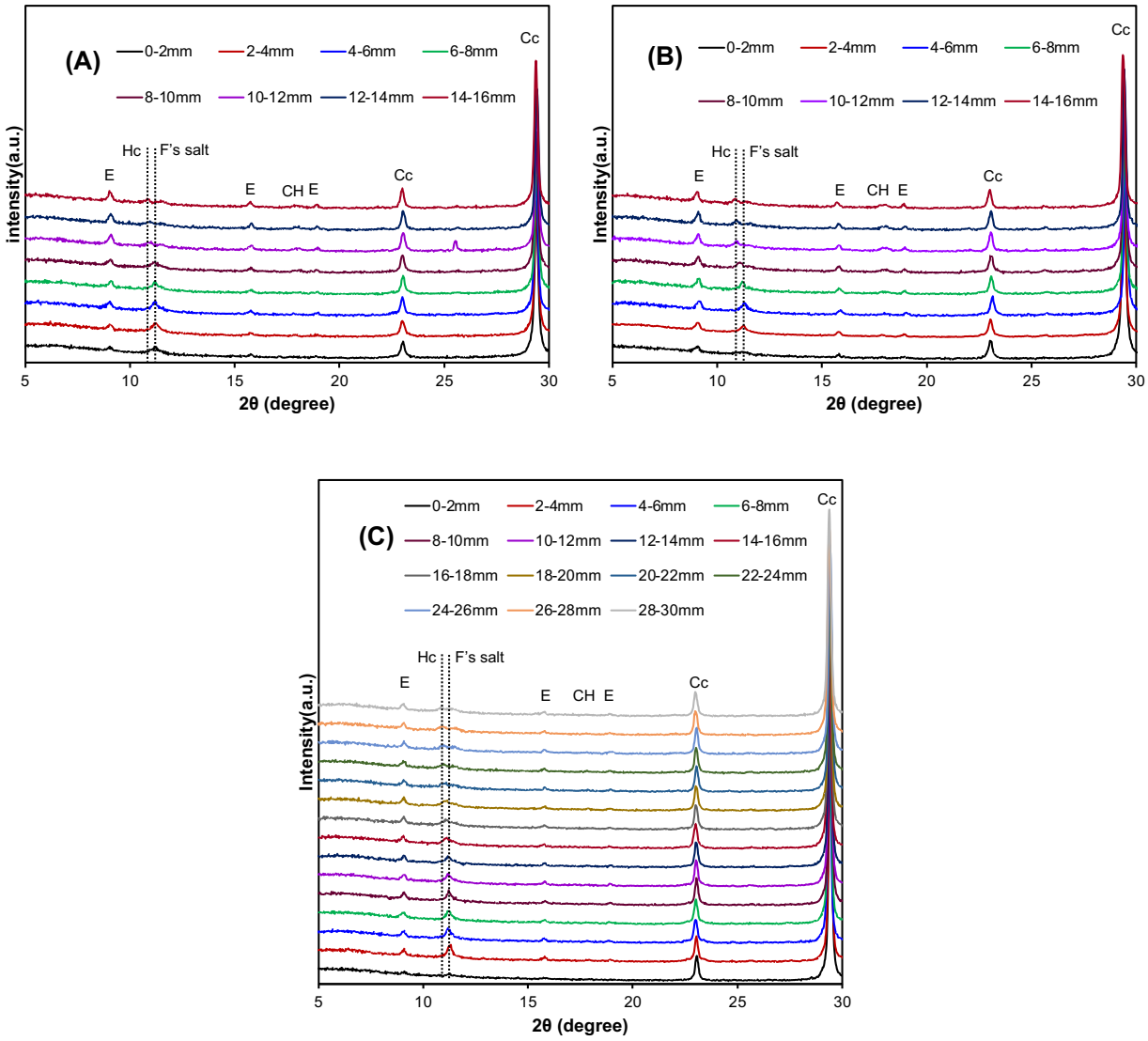

Figure 22 6 months XRD results for (A)Cc45-F-0.305 (B)Cc45-C-0.305 (C)Cc70-F-0.36

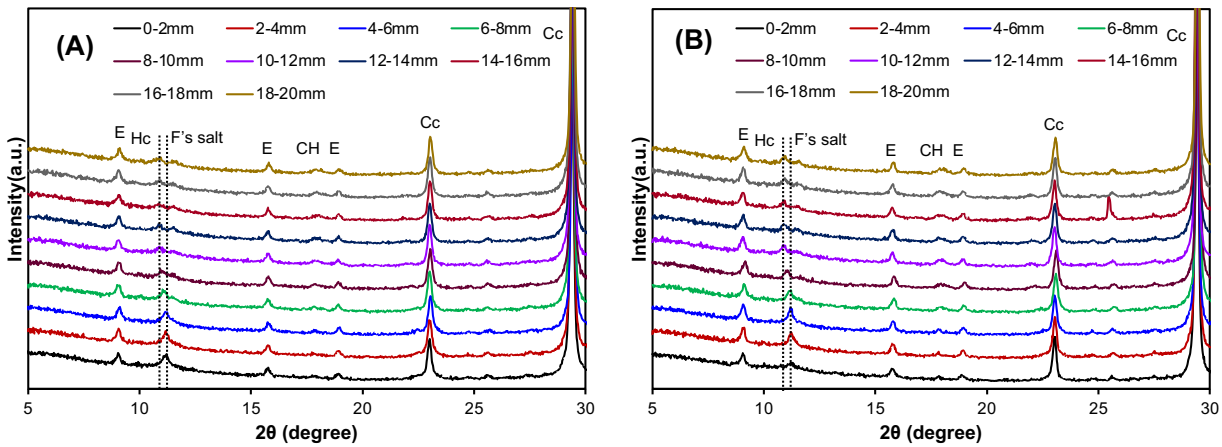

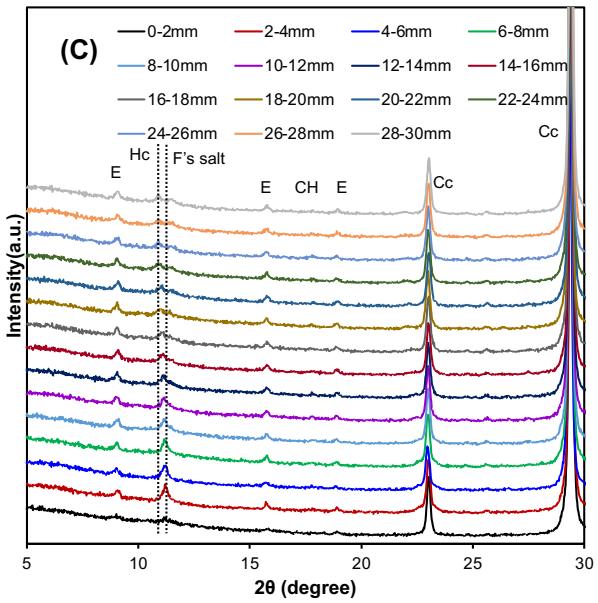

Figure 23 12 months XRD results for (A)Cc45-F-0.305 (B)Cc45-C-0.305 (C)Cc70-F-0.36

The XRD patterns for representative specimens after 3, 6 and 12 months of exposure to NaCl solutions (after a hydration period of 28 days) are shown in **Figure 21**, **Figure 22** and **Figure 23**. In the XRD patterns, as reported in hydration part, ettringite and hemicarboaluminate are main hydration crystalline products, where calcite is the main filler and the consumed portlandite is balanced with formed portlandite. The peaks of calcite and ettringite are identified as crystalline phases in all the mixtures no matter the distance from the exposed surface. However, the peaks of ettringite and portlandite closed to exposed surface are smaller than those in the hydration results, which mean the dissolution of ettringite and portlandite during the immersion. As reported in previous research (K. De Weerdt, Lothenbach, and Geiker 2019), the decrease of the portlandite and ettringite is caused by leaching. The degree of leaching was independent of the solution concentration but increased with the immersion period.

Besides, the peak around 10.8° shifted to 11.2° near the surface. It is commonly believed that the Friedel's salts are formed in this slag-calcite binder as a result of phase transformation of existing AFm-type phases upon chloride exposure since the Kuzel's salt is not stable in the presence of even small amounts of carbonate (Balonis et al. 2010). The reaction formular can be deduced as follow.

$$(CaO)_3(Al_2O_3)(CaCO_3)_{0.5}(Ca(OH)_2)_{0.5} \cdot 11.5H_2O + 2Cl^-$$
$$\rightarrow (CaO)_3(Al_2O_3)(CaCl_2) \cdot 10H_2O + 0.5CO_3^{2-} + OH^- + 1.5H_2O$$

Also, the dissolution of Friedel's salt closed to exposed surface (0-2 mm) can be observed from the XRD results, due to Friedel's salt can be directly release to external solution by leaching.

Besides, for a certain composition, even there is a higher concentration of chloride in external solution compared to cementitious matrix, a longer exposure period didn't make more chloride penetrate into the central part to form more Friedel's salt. For 45% calcite addition rate samples (both fine and coarse calcite addition samples), the formation of Friedel's salt can be confirmed around 10 mm after 3 months immersion. Once the distance from the surface is deeper than 10 mm, instead of the peak of Friedel's salt (11.2°), the peak of hemicarboaluminate (10.8°), which is the original hydration product. However, for 6 months and 12 months immersed samples, similar results are observed from the XRD peaks. There is no Friedel's salt peak deeper than 10 mm.

The addition rate of calcite gives a significant effect on the chloride transport process. The formation of Friedel's salt in 45% calcite addition samples is around 10 mm, while the peak of Friedel's salt for 70% calcite addition rate samples can be seen around 16 mm. Also, the influence of immersion period can hardly be seen from the XRD results due to the peak of Friedel's salt can be seen around 16 mm from the exposed surface among all 3-, 6- and 12-months immersed samples.

5.3.2 Water soluble chloride

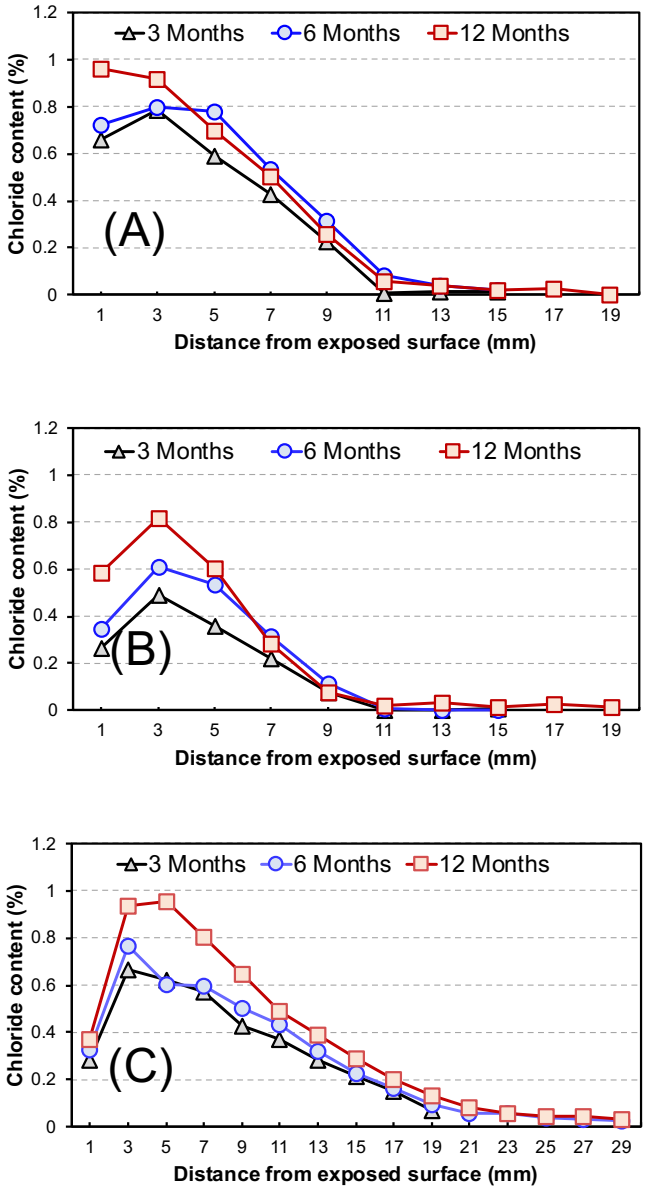

Figure 24 Water-soluble chloride content for (A)Cc45-F-0.305 (B)Cc45-C-0.305 (C)Cc70-F-0.36 samples

Figure 24 shows the water-soluble chloride content changes of the specimens from 3 months to 12 months immersion period as a function of depth from the exposed surface determined by ion chromatography. Over time the water-soluble chloride profiles start to show a reduction in the content at the surface (0–2 mm section) compared to the chloride content deeper in (deeper than 2 mm). This has a great agreement with the previous research, which is due to the convection of chloride. A convection zone happens for the chloride on specimens' surface. Chloride ion distribution in

specimen strongly depended on the way chloride ions penetrate into the samples. Actually, chloride ion penetration is a complex process not only connect with water pressure, capillary action, but also influenced by many other transportation mechanisms (Liu et al. 2020). Under a solution environment, when specimen is saturated, chloride ions are transferred into the specimen mainly by dissolution. This migration of chloride ions is mainly attributed to capillary suction and dispersion effects. Chloride aerosols deposited on the specimen's surface are absorbed by capillary suction. Then due to there is a superior chloride concentration gradient from the solution, free chloride ions are dispersed into the specimen. As water evaporates from specimen's pore, the chloride ions left in the pores accumulate to a peak concentration through a series of drying and wetting cycles. This leads to the convection of chloride ion migration under a solution environment (Liu et al. 2020).

The amount of water-soluble chloride gradually approached to zero at the depths more than 12 mm in the case of 45% calcite addition rate. The curves for depths of <12 mm indicted that the free chloride deposition of samples increases with the immersion period after every several months. The maximum free chloride amount in samples after 12 months' immersion gives an around 50% to 60% higher content compared to that of 3 months' immersion. However, its transition depth almost had no change even the period of exposure increased. In addition, the ingress depth depended on the mixture used. The penetration depth for the 70% calcite content samples (approximately 20–22 mm) was almost double that for the 45% calcite content samples. This result indicated that chloride content in pore solution is improved with the addition of calcite. Besides, free chloride behavior of the samples with different type calcite addition gives a different result. Firstly, convection of chloride closed to exposed surface in fine calcite addition samples gives a less impact compared to coarse calcite addition samples. Secondly, the maximum amount of free chloride in fine calcite addition samples is higher than that in coarse calcite addition samples, which means a higher fineness of calcite in pore solution.

5.3.3 Total chloride

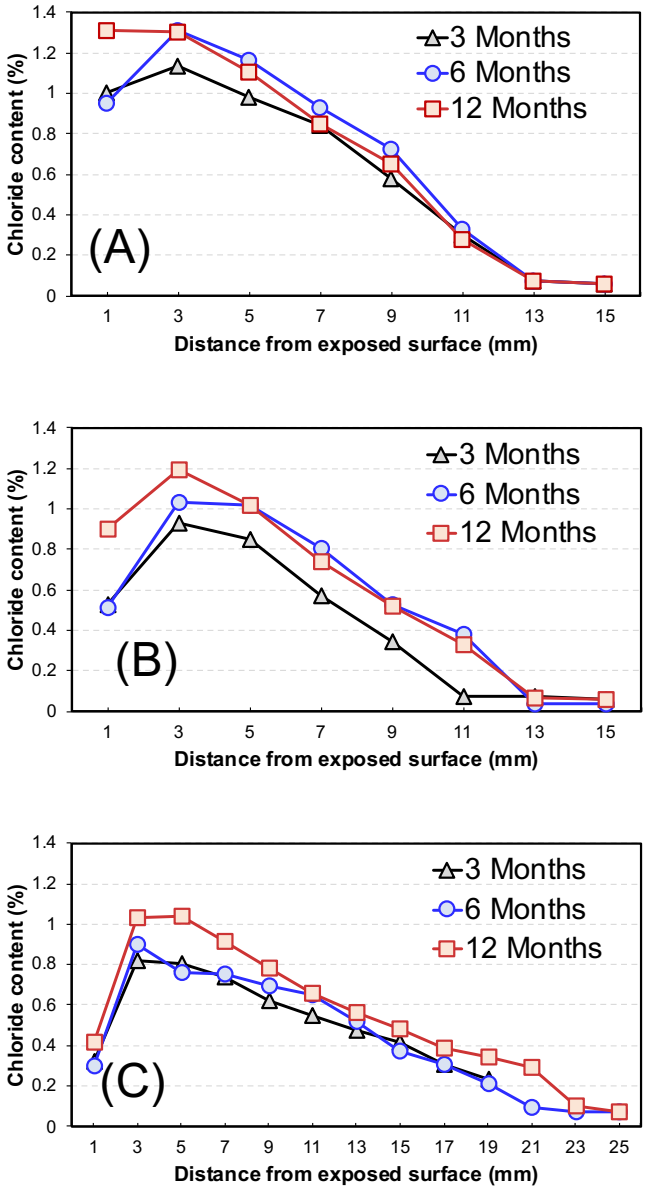

Figure 25 Total chloride content for (A)Cc45-F-0.305 (B)Cc45-C-0.305 (C)Cc70-F-0.36 samples

Figure 25 shows the total chloride content of the specimens exposed to the NaCl solution for 3, 6 and 12 months as a function of depth below the exposed surface. Similar to the results of water-soluble chloride, the total chloride content increased in specimens over time from 3 months to 12 months of exposure period. During these 12 months, the total chloride profile of all different specimens shows typical peaking behaviour, in that the outermost section (0-2 mm) shows a lower total chloride content than the section slightly deeper (after 2 mm) in due to the dissolution of the specimens. This peaking

behaviour is commonly observed in total chloride profiles after long-term exposure to chloride-containing solutions or sea water with previous research due to the convection of chloride (Liu et al. 2020; K. De Weerdt, Lothenbach, and Geiker 2019; Klaartje De Weerdt et al. 2016).

Chlorides have penetrated into all specimens, however, the total chloride content and the chloride ingress depth depended on the exposure time due to the different type and addition rate of the calcite. The specimens with fine calcite addition exposed to the NaCl solution show a higher maximum total chloride content compared to the specimens with coarse calcite addition in the case of the same addition rate (45% calcite addition rate). Also, a higher calcite addition rate decreases the total chloride content and increases the ingress depth. Besides, a longer immersion period increases the total chloride content, but didn't influence the ingress depth significantly. Moreover, the depth of total chloride is deeper than that of free chloride, which indicates other chloride in binder matrix. And the influence of calcite fineness has a same tendency with it in free chloride, which a higher fineness of calcite increases the amount of total chloride.

5.4 discussion

To understand the chloride penetration exposed to NaCl solutions at different conditions (period, calcite type and calcite addition rate), it is necessary to figure out the how chloride changes. Different methods were employed to identify the different chloride species in this binder systems after exposure to NaCl solutions. The total chloride content was directly measured by titration, where water-soluble chloride is considered as free chloride and quantified by ion chromatography and chemically bound chloride was quantified through XRD-Rietveld analysis. The total chloride content includes chloride ions which are chemically bound in Friedel's salt, chloride ions which are physically adsorbed in the diffuse layer of the calcium-silicate-hydrate (C-S-H) phase, as well as free chloride ions present in the pore solution. The relationship among different chloride is shown as the follow equation.

Total chloride = Free chloride + Chemical bound chloride +Physical absorb chloride

Where free chloride is considered as water-soluble chloride, chemical bound chloride can be calculated from the content of Friedel's salt and total chloride can be measured by titration.

Figure 26 shows a summary of measured total chloride profiles, the calculated contribution of chemical bound chlorides in Friedel's salt, as well as the water-soluble chloride considered as free chloride after an immersion period of 12 months.

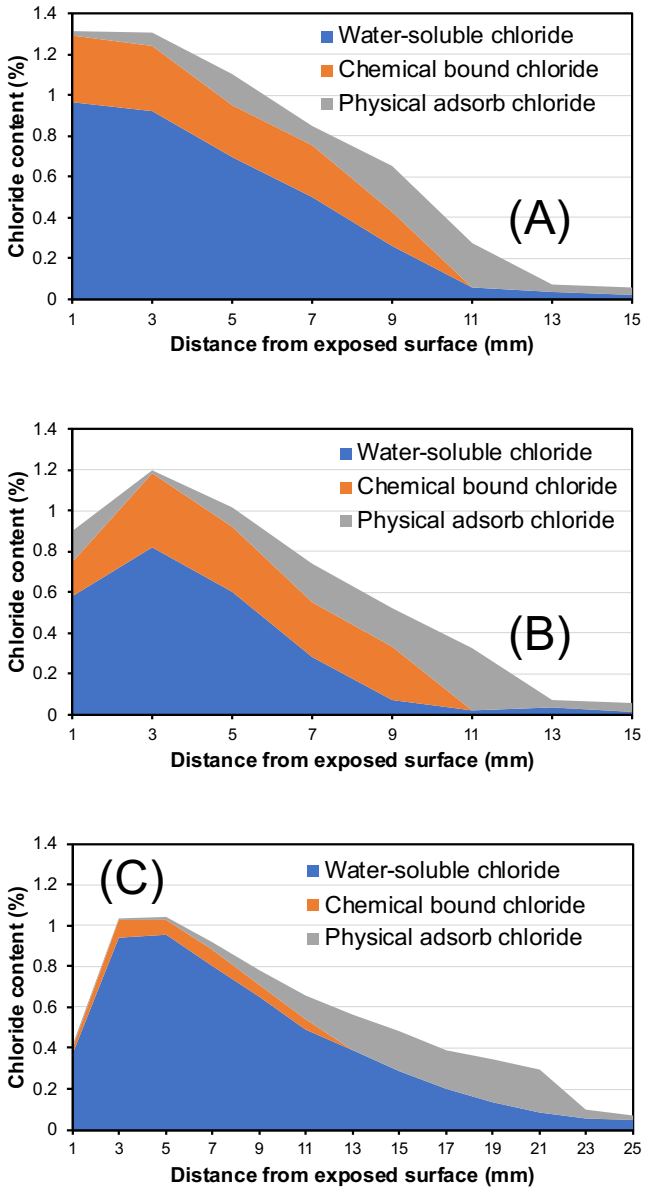

Figure 26 Chloride profiles after 12 months' immersion for (A)Cc45-F-0.305 (B)Cc45-C-0.305 (C)Cc70-F-0.36

5.4.1 Surface chloride

In all cases, not only the chloride content in outermost section (0-2 mm) shows a lower amount than the section deeper (after 2 mm) in free chloride, but also a similar tendency happened in total chloride. In fact, chloride ions are transferred mainly through diffusion due to the concentration gradient in the beginning. When the concentration of chloride reach a certain level, a small convection zone close to surface happened which due to accumulated chloride in a narrow region (Liu et al. 2020). Basically, the length of the convection zone is generally found in 3 mm, after this region, the chloride concentration is decreased with depth. However, not only the free chloride in pore solution has a reduction near to surface, but also other chlorides show a drop close to surface.

The physical adsorption of chloride also controls the total content of chloride in the sample. The main hydration product of cementitious materials, C–S–H, is made up of silicates and consists of silanol surface groups. The surface groups contain all the reactive sites available for release or adsorption of protons and also for adsorption of cations and anions. Calcium ions behave as the potential determining ions on the C–S–H surface and lead to a charge reversal. In this case, the surface charges of the C–S–H particles are neutralized by the calcium ions which lose some of their hydrated water molecules and form ionic bonds with silanol sites through the inner-sphere complexation reaction (Y. Elakneswaran et al. 2010).

$$\equiv SiOH + Ca^{2+} \Leftrightarrow \equiv SiOCa^{+} + H^{+}$$

Actually, the changes in calcium concentration directly lead to changes in adsorption of chloride due to chloride can adsorb on silanol sites where calcium is adsorbed ($SiOCa^{+}$) through the following reaction.

$$\equiv SiOCa^{+} + Cl^{-} \Leftrightarrow \equiv SiOCaCl$$

Since the calcium ions in C-S-H near the sample surface release to the external solution during immersion, less amount of $SiOCa^{+}$ is produced, causing a lower ability to bind chloride ions, giving a lower value of physically bound chloride content. Besides, the chloride in Friedel's salt also release to the immersion solution close to surface, owning less amount of chemically bound chloride. As a

result, all 3 different types of chloride, including free chloride in pore solution, chemically bound chloride and physically bound chloride give a reduction around the surface, making total chloride also shows a reduction in the surface.

5.4.2 Influence of immersion period

From **Figure 24** and **Figure 25**, the amount of total chloride and free chloride increase with the immersion period. However, the content of chemical bound chloride and physical chloride did not show a huge difference among the immersion. These results can be deduced by the following point: restricted amount of C-S-H to absorb chloride and limited amount of hemicarboaluminate to form Friedel's salt. Since the reaction degree of slag is around 45% and a low addition rate of slag in all samples, the products to adsorb and react with chloride ions is less than the condition with common cement. On the other hand, the content of free chloride increases after every several months' immersion. The amount of free chloride after an exposed period of 12 months is 1.5 to 1.6 times as it of 3 months. This may be due to the unsaturation of chloride in pore solution. Although the chemical bound chloride in Friedel's salt and the physical absorb chloride almost had no change during immersion, the increase of free chloride causes the increase of total chloride.

Also, the immersion period didn't influence the ingress depth significantly. First, it is reported that the corrosion resistance of AAS is strongly dependent on the activator, the $Ca(OH)_2$ activator could increase the corrosion resistance. This may attributed to precipitation of $Ca(OH)_2$ in the matrix, which can react with chlorides to physically form $Ca(ClO)_2$ to remove free chlorides from the pore solution, making the binding capacity of chlorides lower than common cement paste. Also, the fineness of AAS influence the resistance to ionic transport (Park, Ann, and Cho 2015). Although the slag used in this research doesn't have a high fineness, the addition of portlandite and slag can give a similar effect with the AAS react with $Ca(OH)_2$ activator since the calcite is considered as a filler, and also the fine calcite may fill up the void in binder, the modification of the pore structure may reduce the openness to external ions and molecules.

Secondly, an Electrical Double Layer (EDL) forms at the solution interface because of the surface charge. The EDL plays an important role in cementitious materials. The interaction between the ingress of ionic species and cement hydrates is influenced by the physical and chemical properties of the pore systems. It is reported that EDL can influence the ionic diffusion (Y. Elakneswaran et al. 2010). In fact, during NaCl solution immersion, diffusing chloride ions are much more affected by the surface charge than sodium ions. Since the size of chloride cluster is around 2-3 nm in the pore solution, as well as the EDL will work in a range around 3.6 nm (Y. Elakneswaran et al. 2010). Two EDL can be overlapped if the pore size under 10 nm as shown in **Figure 27**.

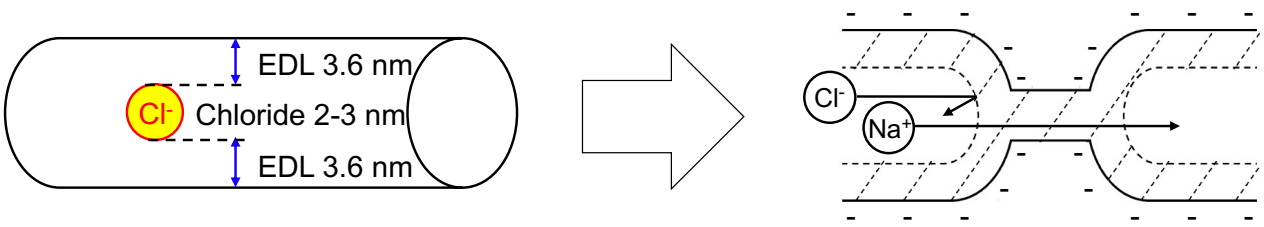

Figure 27 Overlapped EDL

The overlapping of EDL strongly effects the ionic transport. The transport of ions through cementitious materials is described at a microscopic scale with a pore modeled by two infinitely large flat plates. The theory of the EDL shows that the overlapping between the diffuse layers occurring in the pore is important as the pore diameter will be small and the pore walls will be strongly charged, and the fluxes of counterions will be respectively increased and attenuated in such pores (Friedmann, Amiri, and Aït-Mokhtar 2008). As a result, the penetration of the porous network by chloride ions gets harder affected by the overlapping of the diffuse layers until chloride ion cannot enter the samples as shown in **Figure 27**.

5.4.3 Influence of calcite

The fineness of added calcite didn't show a significant effect on both chemical bound chloride and physical absorb chloride content, which is due to a similar reaction degree of slag in both fine and coarse calcite addition binders after a hydration period of 28 days, cause an almost same content of hydrated hemicarboaluminate and C-S-H, show nearly identical potential in chemical and physical absorb ability. As a result, the amount of formed Friedel's salt and the chloride content adsorbed by C-S-H in two different fineness calcite addition samples give a similar tendency. However, in the case of free chloride, it shows a different result. The free chloride in fine calcite addition samples gives a high content, where in coarse calcite addition sample shows a lower amount. Although the fineness of calcite hardly influences the porosity, much smaller pore was generated during hydration, cause a relatively higher amount in free chloride content.

Free chloride content increases with the calcite addition rate. This is due to the increase of porosity. A higher total porosity leads to a higher content of pore solution in the structure and consequently leads a higher free chloride amount in the samples (Sui et al. 2019). Generally speaking, hydrates can fill large size pore in binder matrix and thus reduce porosity, narrow pore diameter and block the connectivity of the pores. All these reasons could slow the diffusion and migration of chloride ions. However, when increasing the calcite content, the pore space becomes larger, this might be attributed to the chloride ingress during immersion. On one hand, a higher porosity makes more convection happened closed to the surface during exposure. As a result, the amount of both free chloride and total chloride with 70% calcite addition rate are lower than that with 45% calcite addition rate samples closed to the surface. On the other hand, a lower amount of slag in the mixture and very low calcite reaction rate also leads a lower amount of hydration products, which means less amount of hemicarboaluminate to form Friedel's salt, cause a less amount of chemical bound chloride, as well as less C-S-H produced to physical absorb chloride ions. Hence, although the content of free chloride in pore solution with 70% calcite addition rate is higher than that with 45% calcite addition rate samples, less chemical bound chloride and physical absorb chloride make the total chloride content

in high calcite content samples less than it in low calcite content samples. Among 3 mixtures, the bound chloride amount is much lower than the amount of free chloride and total chloride in 70% calcite content samples.

Also, a higher calcite content increases the chloride ingress depth. This is highly agreed with the electrical double layer overlap theory, the overlapping between the diffuse layers occurring in the pore and the pore walls will be strongly charged (Friedmann, Amiri, and Aït-Mokhtar 2008). Since there are smaller pore in lower calcite content samples, the charge of overlapping layers is stronger than that with high calcite content. As a result, the ingress depth of chloride in higher calcite content samples is much deeper.

5.5 Conclusion

This part has shown that chloride binding capacity of this new type of slag-calcite binders. The chloride behaviour in binders is influenced by the fineness and the type of calcite. In summary, the following points have been highlighted:

1. The XRD analyses confirmed the disappear of hemicaboaluminate peak and the formation of Friedel's salt peak show the hemicaboaluminate transfer into Friedel's salt during immersion.
2. During NaCl solution immersion, the amount of free chloride, as well as total chloride was enhanced by immersion period. However, it didn't show a significant effect of the penetration depth no matter the calcite addition rate is. Thus, the new composite cementitious binder resists the chloride in contrast to carbonation.
3. The effect of fineness of filler on the during immersion was not considerably observed in the chemically and physically bound chloride due to a similar reaction degree of slag in both fine and coarse calcite addition binders. But it influences the free chloride content due to the different pore distribution.

4. A higher calcite content increases the chloride ingress depth due to the increase of porosity. Higher total porosity leads to a higher content of free chloride in pore solution in the structure.

CHAPTER 6

Conclusion and Future work

6.1 Introduction

This dissertation presents the hydration and durability characteristics of a new composite cementitious binder containing of slag and calcite to reduce the emission of CO_2. The objective of this research is to develop its hydration behavior, as well as its durability under chloride and CO_2 environment, and make sure the influence of calcite, including fineness and addition rate. Based on the results for its microstructural and durability, a considerable reduction in emitting the CO_2 gas during the manufacturing process of the material can be obtained by using the proposed new material as an alternative binder for OPC in the construction industry.

This research consists of the following part: (1) a previous study in cementitious materials, including pure cement, slag-blended cement, limestone-blended cement and alkali-activated slag, which is described in chapter 2. (2) investing the hydration characteristics in this new clinker-free materials and the prediction of its hydration products and porosity based on model as reported in chapter 3. (3) analysis of its carbonation behaviour under an accelerated carbonation in chapter 4. And (4) analysis of its chloride resistance according to its phase changes after different immersion periods in chapter 5.

6.2 Summary of conclusions

6.2.1 Hydration behaviour of proposed composite

In this part, the hydration behaviour of a new composite cementitious binder containing of slag and calcite is carried out. X-ray diffraction (XRD), thermo gravimetric analysis (TGA), mercury intrusion porosimetry (MIP) and selective dissolution were used to determine its reaction degree and hydration products. Also, The coupled hydration and thermodynamic model proposed in previous works (Yogarajah Elakneswaran et al. 2016; Krishnya, Yoda, and Elakneswaran 2021) was adapted to predict the phases of this clinker-free mixture. As a result, W/P ratio, calcite content and specific surface area of the calcite for a specific condition can enhance the reaction degree of slag. The

development of hemicarboaluminate can occur stably for a long curing period without the formation of monocarboaluminate and other hydration products such as ettringite, portlandite, and C-S-H. Although monocarboaluminate is thermodynamically more stable than hemicarboaluminate, the predicted model gives a good agreement with the experimental results in predicted hydration products and porosity as a function of hydration period. Even the reaction rate of slag can be promoted by high specific surface area of the filler content, it also leads to the increased amount of unreacted material with more pore space in the mixture.

6.2.2 Carbonation behavior of proposed composite

In this part, the main effects of accelerated carbonation on different mixture of clink-free material are carried out. In contrast to chloride penetration, the carbonation is progressed with time. In summary, hemicaboaluminate and ettringite, as well as portlandite disappeared and calcite was formed during carbonation. The carbonation of C–S–H gel was indicated by less amount of amorphous after carbonation. Both fineness and addition rate of calcite influence its carbonation behaviour by influence the pore distribution and porosity. After six months, full carbonation was observed in 70% fine calcite addition samples (Cc70-F-0.36). The ettringite and hemicarboaluminate were also carbonated and formed additional calcite, and gypsum was produced due to the carbonation of ettringite. However, the carbonation rate of this proposed mixture is much higher than it of OPC, which indicates that this proposed clink-free is not suitable for high CO_2 environment due to the hardened matrix could not resist carbonation.

6.2.3 Chloride resistance of proposed composite

In this chapter, cylinder samples (diameter 5 cm and height 10 cm) reached the predetermined curing period (28 days) were covered by epoxy resin except for the bottom of the circular surface which will face to exposure solution, only leaving the bottom surface exposed to a solution (500mL 0.5M NaCl solution) to allow ions diffuse into the inside part of the sample. After a certain period of immersion,

total chloride, physically bound chloride and free chloride were determined by different experiments. The transformation from hemicarboaluminate to Friedel's salt is the main chemical reaction during immersion was confirmed by XRD analyses. Free chloride in pore solution, as well as total chloride were enhanced by immersion period. Calcite content and fineness also enhance free and total chloride content. A higher calcite content increases the chloride penetration depth due to the increment of porosity, but the immersion period does not change the chloride penetration depth due to there are a lot of small pores <10 nm in this new composite. The electrical double layer overlapped. Thus, the BFS-calcite hardened matrix resisted chloride ingress after a certain period.

6.3 Suggestions for future work

Even the proposed model for predicting the hydration behaviour of this new composite showed an excellent agreement with experimental results regarding the hydration products, although the production of hemicarboaluminate was unexpected, as well as its generation period and its porosity (Chapter 3). But less research about himicarboalumianre was reported. Therefore, more research about hemicarboaluminate should be focused about its stability. Besides, further models need to be established to predict its chloride transport and carbonation behaviour. The carbonation is progressed with time, making it easy to predict using previously reported methods. However, the phenomenon of this slag-calcite hardened matrix resists chloride after a certain period and the transformation between of hemicarboalumiante into Friedel's salt making more factors should be attention to predict its chloride binding capacity.

Also, the presumption of overlapped electrical double layer (Y. Elakneswaran et al. 2010) for this new composite need to be confirmed by different experiments. If a smaller pore size can enhance the chloride resistance, whether the addition of other high specific surface filler can bring a similar effect or making the harden binder have a higher resistance from other attack (like sulfate attack) should be investigated.

Finally, this dissertation provides an overview of the hydration behaviour and durability of slag–calcite hardened materials to give less CO_2 emissions in the manufacturing of cement. More methods should be developed as an effective way to avoid release of CO_2 by overcoming economical and technical challenges.

References

Ababneh, Ayman, Farid Benboudjema, and Yunping Xi. 2003. "Chloride Penetration in Nonsaturated Concrete." *Journal of Materials in Civil Engineering* 15(2): 183–91.

Adu-Amankwah, Samuel et al. 2017. "Influence of Limestone on the Hydration of Ternary Slag Cements." *Cement and Concrete Research* 100: 96–109.

Altan, Ekin, and Sinan T. Erdoğan. 2012. "Alkali Activation of a Slag at Ambient and Elevated Temperatures." *Cement and Concrete Composites* 34(2): 131–39.

Amer, Ismail et al. 2021. "A Review on Alkali-Activated Slag Concrete." *Ain Shams Engineering Journal* 12(2): 1475–99. https://doi.org/10.1016/j.asej.2020.12.003.

Ashraf, Warda. 2016. "Carbonation of Cement-Based Materials: Challenges and Opportunities." *Construction and Building Materials* 120: 558–70. http://dx.doi.org/10.1016/j.conbuildmat.2016.05.080.

Avet, François, and Karen Scrivener. 2018. "Investigation of the Calcined Kaolinite Content on the Hydration of Limestone Calcined Clay Cement (LC3)." *Cement and Concrete Research* 107: 124–35.

Awoyera, Paul, and Adeyemi Adesina. 2019. "A Critical Review on Application of Alkali Activated Slag as a Sustainable Composite Binder." *Case Studies in Construction Materials* 11: e00268. https://doi.org/10.1016/j.cscm.2019.e00268.

Bakharev, T., J. G. Sanjayan, and Y. B. Cheng. 2001. "Resistance of Alkali-Activated Slag Concrete to Carbonation." *Cement and Concrete Research* 31(9): 1277–83.

———. 2002. "Sulfate Attack on Alkali-Activated Slag Concrete." *Cement and Concrete Research* 32(2): 211–16.

———. 2003. "Resistance of Alkali-Activated Slag Concrete to Acid Attack." *Cement and Concrete Research* 33(10): 1607–11.

Balonis, Magdalena, Barbara Lothenbach, Gwenn Le Saout, and Fredrik P. Glasser. 2010. “Impact of Chloride on the Mineralogy of Hydrated Portland Cement Systems.” *Cement and Concrete Research* 40(7): 1009–22. http://dx.doi.org/10.1016/j.cemconres.2010.03.002.

Baquerizo, Luis G. et al. 2015. “Hydration States of AFm Cement Phases.” *Cement and Concrete Research* 73: 143–57. http://dx.doi.org/10.1016/j.cemconres.2015.02.011.

Barberon, Fabien et al. 2005. “Interactions between Chloride and Cement-Paste Materials.” *Magnetic Resonance Imaging* 23(2 SPEC. ISS.): 267–72.

Benhelal, Emad, Gholamreza Zahedi, and Haslenda Hashim. 2012. “A Novel Design for Green and Economical Cement Manufacturing.” *Journal of Cleaner Production* 22(1): 60–66.

Bishop, Maximilienne, Simon G. Bott, and Andrew R. Barron. 2003. “A New Mechanism for Cement Hydration Inhibition: Solid-State Chemistry of Calcium Nitrilotris(Methylene)Triphosphonate.” *Chemistry of Materials* 15(16): 3074–88.

Borges, Paulo H.R. et al. 2010. “Carbonation of CH and C-S-H in Composite Cement Pastes Containing High Amounts of BFS.” *Cement and Concrete Research* 40(2): 284–92.

Briki, Yosra, Maciej Zajac, Mohsen Ben Haha, and Karen Scrivener. 2021. “Factors Affecting the Reactivity of Slag at Early and Late Ages.” *Cement and Concrete Research* 150(September): 106604.

Brough, A. R., and A. Atkinson. 2002. “Sodium Silicate-Based, Alkali-Activated Slag Mortars: Part I. Strength, Hydration and Microstructure.” *Cement and Concrete Research* 32(6): 865–79.

Bullard, Jeffrey W. et al. 2011. “Mechanisms of Cement Hydration.” *Cement and Concrete Research* 41(12): 1208–23. http://dx.doi.org/10.1016/j.cemconres.2010.09.011.

Cadavid-Giraldo, Nora, Mario C. Velez-Gallego, and Alexandre Restrepo-Boland. 2020. “Carbon Emissions Reduction and Financial Effects of a Cap and Tax System on an Operating Supply Chain in the Cement Sector.” *Journal of Cleaner Production* 275.

Cai, Weixi et al. 2022. “Chloride Binding Behavior of Synthesized Reaction Products in Alkali-Activated Slag.” *Composites Part B: Engineering* 238(March): 109919. https://doi.org/10.1016/j.compositesb.2022.109919.

Caré, Sabine. 2008. “Effect of Temperature on Porosity and on Chloride Diffusion in Cement Pastes.” *Construction and Building Materials* 22(7): 1560–73.

Castellano, C. C., V. L. Bonavetti, H. A. Donza, and E. F. Irassar. 2016. “The Effect of w/b and Temperature on the Hydration and Strength of Blastfurnace Slag Cements.” *Construction and Building Materials* 111: 679–88. http://dx.doi.org/10.1016/j.conbuildmat.2015.11.001.

Cheah, Chee Ban, Leng Ee Tan, and Mahyuddin Ramli. 2021. “Recent Advances in Slag-Based Binder and Chemical Activators Derived from Industrial by-Products – A Review.” *Construction and Building Materials* 272: 121657.

Chen, How Ji et al. 2012. “Effect of Curing Environments on Strength, Porosity and Chloride Ingress Resistance of Blast Furnace Slag Cement Concretes: A Construction Site Study.” *Construction and Building Materials* 35: 1063–70.

Chen, W., and H. J.H. Brouwers. 2007. “The Hydration of Slag, Part 1: Reaction Models for Alkali-Activated Slag.” *Journal of Materials Science* 42(2): 428–43.

Chen, Xudong, and Shenxin Wu. 2013. “Influence of Water-to-Cement Ratio and Curing Period on Pore Structure of Cement Mortar.” *Construction and Building Materials* 38: 804–12.

Coffetti, D. et al. 2022. “Pathways towards Sustainable Concrete.” *Cement and Concrete Research* 154: 106718.

Constantinides, Georgios, and Franz-Josef Ulm. 2004. “The Effect of Two Types of C-S-H on the Elasticity of Cement-Based Materials: Results from Nanoindentation and Micromechanical Modeling.” *Cement and Concrete Research* 34(1): 67–80.

Dai, Xiaodi et al. 2021. “Effect of Ca(OH)2 Addition on the Engineering Properties of Sodium Sulfate Activated Slag.” *Materials 2021, Vol. 14, Page 4266* 14(15): 4266.

Deir, Elisabeth, Berhan S. Gebregziabiher, and Sulapha Peethamparan. 2014. “Influence of Starting Material on the Early Age Hydration Kinetics, Microstructure and Composition of Binding Gel in Alkali Activated Binder Systems.” *Cement and Concrete Composites* 48: 108–17.

Deschner, Florian et al. 2012. “Hydration of Portland Cement with High Replacement by Siliceous Fly Ash.” *Cement and Concrete Research* 42(10): 1389–1400.

Dove, Patricia M., Nizhou Han, and James J. De Yoreo. 2005. “Mechanisms of Classical Crystal Growth Theory Explain Quartz and Silicate Dissolution Behavior.” *Proceedings of the National Academy of Sciences of the United States of America* 102(43): 15357–62.

Elakneswaran, Y. et al. 2010. “Ion-Cement Hydrate Interactions Govern Multi-Ionic Transport Model for Cementitious Materials.” *Cement and Concrete Research* 40(12): 1756–65. http://dx.doi.org/10.1016/j.cemconres.2010.08.019.

Elakneswaran, Yogarajah et al. 2016. “Hydration Study of Slag-Blended Cement Based on Thermodynamic Considerations.” *Construction and Building Materials* 124: 615–25. http://dx.doi.org/10.1016/j.conbuildmat.2016.07.138.

Elgalhud, Abdurrahman A., Ravindra K. Dhir, and Gurmel Ghataora. 2016. “Limestone Addition Effects on Concrete Porosity.” *Cement and Concrete Composites* 72: 222–34.

Elgalhud, Abdurrahman A., Ravindra K. Dhir, and Gurmel S. Ghataora. 2017. “Carbonation Resistance of Concrete: Limestone Addition Effect.” *Magazine of Concrete Research* 69(2): 84–106.

Escalante-Garcia, J. I., and J. H. Sharp. 2004. “The Chemical Composition and Microstructure of Hydration Products in Blended Cements.” *Cement and Concrete Composites* 26(8): 967–76.

Escalante, J. I. et al. 2001a. “Reactivity of Blast-Furnace Slag in Portland Cement Blends Hydrated under Different Conditions.” *Cement and Concrete Research* 31(10): 1403–9.

———. 2001b. “Reactivity of Blast-Furnace Slag in Portland Cement Blends Hydrated under Different Conditions.” *Cement and Concrete Research* 31(10): 1403–9.

Ferrari, L., J. Kaufmann, F. Winnefeld, and J. Plank. 2012. “Reaction of Clinker Surfaces Investigated with Atomic Force Microscopy.” *Construction and Building Materials* 35: 92–96. http://dx.doi.org/10.1016/j.conbuildmat.2012.02.089.

Ferrari, Lucia et al. 2012. “Characterization of Polycarboxylate-Ether Based Superplasticizer on Cement Clinker Surfaces.” *Journal of the American Ceramic Society* 95(7): 2189–95.

Friedmann, H., O. Amiri, and A. Aït-Mokhtar. 2008. “Physical Modeling of the Electrical Double Layer Effects on Multispecies Ions Transport in Cement-Based Materials.” *Cement and Concrete Research* 38(12): 1394–1400. http://dx.doi.org/10.1016/j.cemconres.2008.06.003.

Fu, Qiang et al. 2021. “Hydration Characteristics and Microstructure of Alkali-Activated Slag Concrete: A Review.” *Engineering*. https://doi.org/10.1016/j.eng.2021.07.026.

García-González, Carlos A. et al. 2006. “Modification of Composition and Microstructure of Portland Cement Pastes as a Result of Natural and Supercritical Carbonation Procedures.” *Industrial and Engineering Chemistry Research* 45(14): 4985–92.

Garrault-Gauffinet, S., and A. Nonat. 1999. “Experimental Investigation of Calcium Silicate Hydrate (C-S-H) Nucleation.” *Journal of Crystal Growth* 200(3): 565–74.

Gebregziabiher, Berhan S., Robert Thomas, and Sulapha Peethamparan. 2015. “Very Early-Age Reaction Kinetics and Microstructural Development in Alkali-Activated Slag.” *Cement and Concrete Composites* 55: 91–102.

Giergiczny, Zbigniew. 2019. “Fly Ash and Slag.” *Cement and Concrete Research* 124: 105826.

Gruyaert, Elke, Philip Van Den Heede, and Nele De Belie. 2013. “Carbonation of Slag Concrete: Effect of the Cement Replacement Level and Curing on the Carbonation Coefficient - Effect of Carbonation on the Pore Structure.” *Cement and Concrete Composites* 35(1): 39–48. http://dx.doi.org/10.1016/j.cemconcomp.2012.08.024.

Gunasekara, Chamila et al. 2020. “Effect of Nano-Silica Addition into High Volume Fly Ash–Hydrated Lime Blended Concrete.” *Construction and Building Materials* 253: 119205.

Haha, M. Ben, B. Lothenbach, G. Le Saout, and F. Winnefeld. 2011. “Influence of Slag Chemistry on the Hydration of Alkali-Activated Blast-Furnace Slag - Part I: Effect of MgO.” *Cement and Concrete Research* 41(9): 955–63. http://dx.doi.org/10.1016/j.cemconres.2011.05.002.

———. 2012. “Influence of Slag Chemistry on the Hydration of Alkali-Activated Blast-Furnace Slag - Part II: Effect of Al2O3.” *Cement and Concrete Research* 42(1): 74–83. http://dx.doi.org/10.1016/j.cemconres.2011.08.005.

Han, Fanghui, and Zengqi Zhang. 2018. “Properties of 5-Year-Old Concrete Containing Steel Slag Powder.” *Powder Technology* 334: 27–35.

Han, JianDe et al. 2012. “Application of Nanoindentation to Investigate Chemomechanical Properties Change of Cement Paste in the Carbonation Reaction.” *Science China Technological Sciences* 55(3): 616–22. https://doi.org/10.1007/s11431-011-4571-1.

Han, Yi, Runsheng Lin, and Xiao Yong Wang. 2021. “Performance and Sustainability of Quaternary Composite Paste Comprising Limestone, Calcined Hwangtoh Clay, and Granulated Blast Furnace Slag.” *Journal of Building Engineering* 43: 102655.

Hawkins, Peter, Paul Tennis, and Rachel Detwiler. *The Use of Limestone in Portland Cement : A State-of-the-Art Review*.

He, Juan et al. 2018. “Study on Improvement of Carbonation Resistance of Alkali-Activated Slag Concrete.” *Construction and Building Materials* 176: 60–67.

———. 2021. “Influence of Hydrated Lime on Mechanical and Shrinkage Properties of Alkali-Activated Slag Cement.” *Construction and Building Materials* 289: 123201.

Hoshino, Seiichi, Kazuo Yamada, and Hiroshi Hirao. 2006. “XRD/Rietveld Analysis of the Hydration and Strength Development of Slag and Limestone Blended Cement.” *Journal of Advanced Concrete Technology* 4(3): 357–67.

Htwe, Khin Su Su, and Yu Pyae Pyo Mon. 2018. “Effect of Natural Pozzolan on Carbonation and Chloride Penetration in Sustainable Concrete.” *International Journal on Advanced Science, Engineering and Information Technology* 8(4): 1049–54.

Irassar, E. F. 2009. “Sulfate Attack on Cementitious Materials Containing Limestone Filler - A Review.” *Cement and Concrete Research* 39(3): 241–54.

Jennings, H. et al. 2005. “Nanostructure of CSH Gel in Cement Paste as a Function of Curing Conditions and Relative Humidity.” *Creep, shrinkage and durability of concrete and concrete structures. Proceeding of Concreep* 7(November): 19–37.

Jeong, Yeonung, Woo Sung Yum, Juhyuk Moon, and Jae Eun Oh. 2017. “Utilization of Precipitated CaCO3 from Carbon Sequestration of Industrially Emitted CO2 in Cementless CaO-Activated Blast-Furnace Slag Binder System.” *Journal of Cleaner Production* 166: 649–59.

Jones, M. R. et al. 2003. “Studies Using 27Al MAS NMR of AFm and AFt Phases and the Formation of Friedel’s Salt.” *Cement and Concrete Research* 33(2): 177–82.

Joseph, Shiju, Jørgen Skibsted, and Özlem Cizer. 2019. “A Quantitative Study of the C3A Hydration.” *Cement and Concrete Research* 115(June 2018): 145–59. https://doi.org/10.1016/j.cemconres.2018.10.017.

Juenger, Maria C.G., Ruben Snellings, and Susan A. Bernal. 2019. “Supplementary Cementitious Materials: New Sources, Characterization, and Performance Insights.” *Cement and Concrete Research* 122: 257–73.

Jun, Yubin, Taewan Kim, and Jae Hong Kim. 2020. “Chloride-Bearing Characteristics of Alkali-Activated Slag Mixed with Seawater: Effect of Different Salinity Levels.” *Cement and Concrete Composites* 112(April): 103680. https://doi.org/10.1016/j.cemconcomp.2020.103680.

Kakali, G., S. Tsivilis, E. Aggeli, and M. Bati. 2000. “Hydration Products of C3A, C3S and Portland Cement in the Presence of CaCO3.” *Cement and Concrete Research* 30(7): 1073–77.

Kashani, Alireza, John L. Provis, Greg G. Qiao, and Jannie S.J. Van Deventer. 2014. “The Interrelationship between Surface Chemistry and Rheology in Alkali Activated Slag Paste.” *Construction and Building Materials* 65: 583–91.

Kashchiev, D., and G. M. Van Rosmalen. 2003. “Review: Nucleation in Solutions Revisited.” *Crystal Research and Technology* 38(7–8): 555–74.

Ke, Xinyuan, Susan A. Bernal, Oday H. Hussein, and John L. Provis. 2017. “Chloride Binding and Mobility in Sodium Carbonate-Activated Slag Pastes and Mortars.” *Materials and Structures/Materiaux et Constructions* 50(6): 1–13. https://doi.org/10.1617/s11527-017-1121-8.

Ke, Xinyuan, Susan A. Bernal, John L. Provis, and Barbara Lothenbach. 2020. “Thermodynamic Modelling of Phase Evolution in Alkali-Activated Slag Cements Exposed to Carbon Dioxide.” *Cement and Concrete Research* 136(January): 106158. https://doi.org/10.1016/j.cemconres.2020.106158.

Kevin, DI, and ED Kenneth. 1991. “A Review of Limestone Additions to Portland Cement and Concrete.” *Cement and Concrete Composites* 13: 165–70.

Khan, M S H, and O Kayali. 2018. “Chloride Binding Ability and the Onset Corrosion Threat on Alkali-Activated GGBFS and Binary Blend Pastes.” *European Journal of Environmental and Civil Engineering* 22(8): 1023–39. https://doi.org/10.1080/19648189.2016.1230522.

Kirchheim, A. P. et al. 2009. “Analysis of Cubic and Orthorhombic C3A Hydration in Presence of Gypsum and Lime.” *Journal of Materials Science* 44(8): 2038–45.

Knop, Yaniv, Alva Peled, and Ronen Cohen. 2014. “Influences of Limestone Particle Size Distributions and Contents on Blended Cement Properties.” *Construction and Building Materials* 71: 26–34.

Kolani, B. et al. 2012. “Hydration of Slag-Blended Cements.” *Cement and Concrete Composites* 34(9): 1009–18. http://dx.doi.org/10.1016/j.cemconcomp.2012.05.007.

Kreppelt, Fritz, Martin Weibel, Davide Zampini, and Michael Romer. 2002. “Influence of Solution Chemistry on the Hydration of Polished Clinker Surfaces - A Study of Different Types of Polycarboxylic Acid-Based Admixtures.” *Cement and Concrete Research* 32(2): 187–98.

Krishnya, Siventhirarajah et al. 2022. “Modeling of Hydration Products and Strength Development for High-Volume Fly Ash Binders.” *Construction and Building Materials* 320: 126228.

Krishnya, Siventhirarajah, Yuya Yoda, and Yogarajah Elakneswaran. 2021. “A Two-Stage Model for the Prediction of Mechanical Properties of Cement Paste.” *Cement and Concrete Composites* 115: 103853.

Kwan, A. K.H., and J. J. Chen. 2013. “Adding Fly Ash Microsphere to Improve Packing Density, Flowability and Strength of Cement Paste.” *Powder Technology* 234: 19–25.

Lam, L., Y. L. Wong, and C. S. Poon. 2000. “Degree of Hydration and Gel/Space Ratio of High-Volume Fly Ash/Cement Systems.” *Cement and Concrete Research* 30(5): 747–56.

Law, David W., Andi Arham Adam, Thomas K. Molyneaux, and Indubhushan Patnaikuni. 2012. “Durability Assessment of Alkali Activated Slag (AAS) Concrete.” *Materials and Structures/Materiaux et Constructions* 45(9): 1425–37.

Li, Ning et al. 2018. “A Mixture Proportioning Method for the Development of Performance-Based Alkali-Activated Slag-Based Concrete.” *Cement and Concrete Composites* 93: 163–74.

Li, Ying, Chunyu Qiao, and Wen Ni. 2020. “Green Concrete with Ground Granulated Blast-Furnace Slag Activated by Desulfurization Gypsum and Electric Arc Furnace Reducing Slag.” *Journal of Cleaner Production* 269: 122212.

Lin, Run Sheng, Han Seung Lee, Yi Han, and Xiao Yong Wang. 2021. “Experimental Studies on Hydration–Strength–Durability of Limestone-Cement-Calcined Hwangtoh Clay Ternary Composite.” *Construction and Building Materials* 269: 121290.

Liu, Jun et al. 2020. “Effect of Fly Ash as Cement Replacement on Chloride Diffusion, Chloride Binding Capacity, and Micro-Properties of Concrete in a Water Soaking Environment.” *Applied Sciences (Switzerland)* 10(18).

Lollini, Federica, and Elena Redaelli. 2021. “Carbonation of Blended Cement Concretes after 12 Years of Natural Exposure.” *Construction and Building Materials* 276: 122122. https://doi.org/10.1016/j.conbuildmat.2020.122122.

Loser, Roman, Barbara Lothenbach, Andreas Leemann, and Martin Tuchschmid. 2010. “Chloride Resistance of Concrete and Its Binding Capacity - Comparison between Experimental Results and Thermodynamic Modeling.” *Cement and Concrete Composites* 32(1): 34–42. http://dx.doi.org/10.1016/j.cemconcomp.2009.08.001.

Lothenbach, Barbara et al. 2019. “Cemdata18: A Chemical Thermodynamic Database for Hydrated Portland Cements and Alkali-Activated Materials.” *Cement and Concrete Research* 115: 472–506.

Lothenbach, Barbara, Gwenn Le Saout, Emmanuel Gallucci, and Karen Scrivener. 2008. “Influence of Limestone on the Hydration of Portland Cements.” *Cement and Concrete Research* 38(6): 848–60.

Luan, Yao, Tetsuya Ishida, Toyoharu Nawa, and Sagawa Takahiro. 2012. “Enhanced Model and Simulation of Hydration Process of Blast Furnace Slag in Blended Cement.” *Journal of Advanced Concrete Technology*: 10–2012.

Lumley, J. S., R. S. Gollop, G. K. Moir, and H. F.W. Taylor. 1996. “Degrees of Reaction of the Slag in Some Blends with Portland Cements.” *Cement and Concrete Research* 26(1): 139–51.

Luping, Tang, and Lars Olof Nilsson. 1993. “Chloride Binding Capacity and Binding Isotherms of OPC Pastes and Mortars.” *Cement and Concrete Research* 23(2): 247–53.

Machner, Alisa et al. 2022. “Effect of Leaching on the Composition of Hydration Phases during Chloride Exposure of Mortar.” *Cement and Concrete Research* 153(January).

Maltais, Y., E. Samson, and J. Marchand. 2004. “Predicting the Durability of Portland Cement Systems in Aggressive Environments - Laboratory Validation.” *Cement and Concrete Research* 34(9): 1579–89.

Maraghechi, Hamed et al. 2018. “Performance of Limestone Calcined Clay Cement (LC3) with Various Kaolinite Contents with Respect to Chloride Transport.” *Materials and Structures/Materiaux et Constructions* 51(5): 1–17. https://doi.org/10.1617/s11527-018-1255-3.

Matschei, T., B. Lothenbach, and F. P. Glasser. 2007. “The Role of Calcium Carbonate in Cement Hydration.” *Cement and Concrete Research* 37(4): 551–58.

Melo Neto, Antonio A., Maria Alba Cincotto, and Wellington Repette. 2008. “Drying and Autogenous Shrinkage of Pastes and Mortars with Activated Slag Cement.” *Cement and Concrete Research* 38(4): 565–74.

Mohammed, T. U., and H. Hamada. 2003. “Relationship between Free Chloride and Total Chloride Contents in Concrete.” *Cement and Concrete Research* 33(9): 1487–90.

Monkman, Sean, and Yixin Shao. 2010. “Carbonation Curing of Slag-Cement Concrete for Binding CO2 and Improving Performance.” *Journal of Materials in Civil Engineering* 22(4): 296–304.

Moon, Han Young, Hong Sam Kim, and Doo Sun Choi. 2006. “Relationship between Average Pore Diameter and Chloride Diffusivity in Various Concretes.” *Construction and Building Materials* 20(9): 725–32.

Morandeau, A., M. Thiéry, and P. Dangla. 2014. “Investigation of the Carbonation Mechanism of CH and C-S-H in Terms of Kinetics, Microstructure Changes and Moisture Properties.” *Cement and Concrete Research* 56: 153–70. http://dx.doi.org/10.1016/j.cemconres.2013.11.015.

Morandeau, Antoine E., and Claire E. White. 2015. “In Situ X-Ray Pair Distribution Function Analysis of Accelerated Carbonation of a Synthetic Calcium-Silicate-Hydrate Gel.” *Journal of Materials Chemistry A* 3(16): 8597–8605.

Nedeljković, Marija, Yibing Zuo, Kamel Arbi, and Guang Ye. 2018. “Carbonation Resistance of Alkali-Activated Slag Under Natural and Accelerated Conditions.” *Journal of Sustainable Metallurgy* 4(1): 33–49.

Nochaiya, Thanongsak, Watcharapong Wongkeo, and Arnon Chaipanich. 2010. “Utilization of Fly Ash with Silica Fume and Properties of Portland Cement-Fly Ash-Silica Fume Concrete.” *Fuel* 89(3): 768–74.

Noguchi, Natsumi et al. 2021. “Hydration of Ferrite-Rich Portland Cement: Evaluation of Fe-Hydrates and Fe Uptake in Calcium-Silicate-Hydrates.” *Construction and Building Materials* 288: 123142.

Ogirigbo, Okiemute Roland, and Leon Black. 2016. “Influence of Slag Composition and Temperature on the Hydration and Microstructure of Slag Blended Cements.” *Construction and Building Materials* 126: 496–507. http://dx.doi.org/10.1016/j.conbuildmat.2016.09.057.

———. 2017. “Chloride Binding and Diffusion in Slag Blends: Influence of Slag Composition and Temperature.” *Construction and Building Materials* 149: 816–25. http://dx.doi.org/10.1016/j.conbuildmat.2017.05.184.

Okpala, D. C. 1989. “Pore Structure of Hardened Cement Paste and Mortar.” *International Journal of Cement Composites and Lightweight Concrete* 11(4): 245–54.

Otieno, Mike, Hans Beushausen, and Mark Alexander. 2014. “Effect of Chemical Composition of Slag on Chloride Penetration Resistance of Concrete.” *Cement and Concrete Composites* 46: 56–64. http://dx.doi.org/10.1016/j.cemconcomp.2013.11.003.

Palacios, M., and F. Puertas. 2006. “Effect of Carbonation on Alkali-Activated Slag Paste.” *Journal of the American Ceramic Society* 89(10): 3211–21.

Palacios, M., F. Puertas, P. Bowen, and Y. F. Houst. 2009. “Effect of PCs Superplasticizers on the Rheological Properties and Hydration Process of Slag-Blended Cement Pastes.” *Journal of Materials Science* 44(10): 2714–23.

Park, Joon Woo, Ki Yong Ann, and Chang Geun Cho. 2015. “Resistance of Alkali-Activated Slag Concrete to Chloride-Induced Corrosion.” *Advances in Materials Science and Engineering* 2015.

Parkhurst, David L, and C.A.J. Appelo. 1999. “A Computer Program for Speciation, Batch-Reaction, One-Dimensional Transport and Inverse Geochemical Calculations.” *USGS Report*.

Paulini, P. 1990. “Reaction Mechanisms of Concrete Admixtures.” *Cement and Concrete Research* 20(6): 910–18.

Peng, Sheng, Qinhong Hu, Stefan Dultz, and Ming Zhang. 2012. “Using X-Ray Computed Tomography in Pore Structure Characterization for a Berea Sandstone: Resolution Effect.” *Journal of Hydrology* 472–473: 254–61.

Peter, M. A., A. Muntean, S. A. Meier, and M. Böhm. 2008. “Competition of Several Carbonation Reactions in Concrete: A Parametric Study.” *Cement and Concrete Research* 38(12): 1385–93. http://dx.doi.org/10.1016/j.cemconres.2008.09.003.

Phung, Quoc Tri et al. 2015. “Effect of Limestone Fillers on Microstructure and Permeability Due to Carbonation of Cement Pastes under Controlled CO2 Pressure Conditions.” *Construction and Building Materials* 82: 376–90. http://dx.doi.org/10.1016/j.conbuildmat.2015.02.093.

Provis, John L., Angel Palomo, and Caijun Shi. 2015. “Advances in Understanding Alkali-Activated Materials.” *Cement and Concrete Research* 78: 110–25.

Qi, Chongchong et al. 2019. “Understanding Cement Hydration of Cemented Paste Backfill: DFT Study of Water Adsorption on Tricalcium Silicate (111) Surface.” *Minerals* 9(4): 10–12.

Qiao, Chunyu et al. 2019. “Chloride Binding of Cement Pastes with Fly Ash Exposed to CaCl2 Solutions at 5 and 23 °C.” *Cement and Concrete Composites* 97(June 2018): 43–53. https://doi.org/10.1016/j.cemconcomp.2018.12.011.

Rakhimova, Nailia R. et al. 2016. “Influence of Limestone Content, Fineness, and Composition on the Properties and Microstructure of Alkali-Activated Slag Cement.” *Cement and Concrete Composites* 72: 268–74.

Ramachandran, V. S. 1971. “Possible States of Chloride in the Hydration of Tricalcium Silicate in the Presence of Calcium Chloride.” *Matériaux et Constructions* 4(1): 3–12.

Ramezanianpour, Amir Mohammad, and R. Douglas Hooton. 2014. “A Study on Hydration, Compressive Strength, and Porosity of Portland-Limestone Cement Mixes Containing SCMs.” *Cement and Concrete Composites* 51: 1–13.

Sanjuán, Miguel Ángel, Esteban Estévez, Cristina Argiz, and Daniel del Barrio. 2018. “Effect of Curing Time on Granulated Blast-Furnace Slag Cement Mortars Carbonation.” *Cement and*

Concrete Composites 90(September 2017): 257–65. https://doi.org/10.1016/j.cemconcomp.2018.04.006.

Santhanam, Manu, Menashi D. Cohen, and Jan Olek. 2001. "Sulfate Attack Research." *Cement and Concrete Research* 31(6): 845–51.

Le Saoût, Gwenn, Mohsen Ben Haha, Frank Winnefeld, and Barbara Lothenbach. 2011. "Hydration Degree of Alkali-Activated Slags: A 29 Si NMR Study." *Journal of the American Ceramic Society* 94(12): 4541–47.

Šavija, Branko, and Mladena Luković. 2016. "Carbonation of Cement Paste: Understanding, Challenges, and Opportunities." *Construction and Building Materials* 117: 285–301.

Scherer, George W. 2015. "Drying, Shrinkage, and Cracking of Cementitious Materials." *Transport in Porous Media* 110(2): 311–31.

Schöler, Axel, Barbara Lothenbach, Frank Winnefeld, and Maciej Zajac. 2015. "Hydration of Quaternary Portland Cement Blends Containing Blast-Furnace Slag, Siliceous Fly Ash and Limestone Powder." *Cement and Concrete Composites* 55: 374–82.

Shah, Vineet, Karen Scrivener, Bishwajit Bhattacharjee, and Shashank Bishnoi. 2018. "Changes in Microstructure Characteristics of Cement Paste on Carbonation." *Cement and Concrete Research* 109(April): 184–97. https://doi.org/10.1016/j.cemconres.2018.04.016.

Shanahan, Natalya, and Abla Zayed. 2007. "Cement Composition and Sulfate Attack. Part I." *Cement and Concrete Research* 37(4): 618–23.

Shao, Yixin, Vahid Rostami, Zhen He, and Andrew J. Boyd. 2014. "Accelerated Carbonation of Portland Limestone Cement." *Journal of Materials in Civil Engineering* 26(1): 117–24.

Shi, Xianming, Ning Xie, Keith Fortune, and Jing Gong. 2012. "Durability of Steel Reinforced Concrete in Chloride Environments: An Overview." *Construction and Building Materials* 30: 125–38. http://dx.doi.org/10.1016/j.conbuildmat.2011.12.038.

Shi, Zhenguo et al. 2017. “Friedel’s Salt Profiles from Thermogravimetric Analysis and Thermodynamic Modelling of Portland Cement-Based Mortars Exposed to Sodium Chloride Solution.” *Cement and Concrete Composites* 78: 73–83.

Skibsted, Jørgen, and Ruben Snellings. 2019. “Reactivity of Supplementary Cementitious Materials (SCMs) in Cement Blends.” *Cement and Concrete Research* 124: 105799.

Snellings, Ruben et al. 2022. “Hydration Kinetics of Ternary Slag-Limestone Cements: Impact of Water to Binder Ratio and Curing Temperature.” *Cement and Concrete Research* 151: 106647.

Song, S., D. Sohn, H. M. Jennings, and T. O. Mason. 2000. “Hydration of Alkali-Activated Ground Granulated Blast Furnace Slag.” *Journal of Materials Science* 35(1): 249–57.

Sui, S. et al. 2019. “Quantification Methods for Chloride Binding in Portland Cement and Limestone Systems.” *Cement and Concrete Research* 125(August): 105864. https://doi.org/10.1016/j.cemconres.2019.105864.

Suryavanshi, A. K., J. D. Scantlebury, and S. B. Lyon. 1995. “The Binding of Chloride Ions by Sulphate Resistant Portland Cement.” *Cement and Concrete Research* 25(3): 581–92.

Tang, Chenxi, Tung Chai Ling, and Kim Hung Mo. 2021. “Raman Spectroscopy as a Tool to Understand the Mechanism of Concrete Durability—A Review.” *Construction and Building Materials* 268: 121079.

Tariq, F., R. Haswell, P. D. Lee, and D. W. McComb. 2011. “Characterization of Hierarchical Pore Structures in Ceramics Using Multiscale Tomography.” *Acta Materialia* 59(5): 2109–20.

Taylor, H.F.W. 1997. “Cement Chemistry.” *Cement chemistry*.

Taylor, R., I. G. Richardson, and R. M.D. Brydson. 2010. “Composition and Microstructure of 20-Year-Old Ordinary Portland Cement–Ground Granulated Blast-Furnace Slag Blends Containing 0 to 100% Slag.” *Cement and Concrete Research* 40(7): 971–83.

Tennis, Paul D, and Hamlin M Jennings. 2000. “A Model for Two Types of Calcium Silicate Hydrate in the Microstructure of Portland Cement Pastes.” *Cement and Concrete Research* 30(6): 855–63.

Tsivilis, S. et al. 2000. “Properties and Behavior of Limestone Cement Concrete and Mortar.” *Cement and Concrete Research* 30(10): 1679–83.

Villagrán-Zaccardi, Yury A., Anya Vollpracht, Elke Gruyaert, and Nele De Belie. 2018. “Recommendation of RILEM TC 238-SCM: Determination of the Degree of Reaction of Siliceous Fly Ash and Slag in Hydrated Cement Paste by the Selective Dissolution Method.” *Materials and Structures/Materiaux et Constructions* 51(1).

Vuk, T., V. Tinta, R. Gabrovšek, and V. Kaučič. 2001. “The Effects of Limestone Addition, Clinker Type and Fineness on Properties of Portland Cement.” *Cement and Concrete Research* 31(1): 135–39.

Wang, Xiao Yong. 2017. “Modeling of Hydration, Compressive Strength, and Carbonation of Portland-Limestone Cement (PLC) Concrete.” *Materials* 10(2).

Wang, Yuli et al. 2019. “Effects of Calcium Bicarbonate on the Properties of Ordinary Portland Cement Paste.” *Construction and Building Materials* 225: 591–600.

De Weerdt, K., B. Lothenbach, and M. R. Geiker. 2019. “Comparing Chloride Ingress from Seawater and NaCl Solution in Portland Cement Mortar.” *Cement and Concrete Research* 115(October 2018): 80–89. https://doi.org/10.1016/j.cemconres.2018.09.014.

De Weerdt, K., D. Orsáková, and M. R. Geiker. 2014. “The Impact of Sulphate and Magnesium on Chloride Binding in Portland Cement Paste.” *Cement and Concrete Research* 65: 30–40. http://dx.doi.org/10.1016/j.cemconres.2014.07.007.

De Weerdt, Klaartje et al. 2016. “Towards the Understanding of Chloride Profiles in Marine Exposed Concrete, Impact of Leaching and Moisture Content.” *Construction and Building Materials* 120: 418–31. http://dx.doi.org/10.1016/j.conbuildmat.2016.05.069.

De Weerdt, Klaartje, Harald Justnes, and Mette R. Geiker. 2014. “Changes in the Phase Assemblage of Concrete Exposed to Sea Water.” *Cement and Concrete Composites* 47: 53–63. http://dx.doi.org/10.1016/j.cemconcomp.2013.09.015.

Yajun, Ji, and Jong Herman Cahyadi. 2003. “Effects of Densified Silica Fume on Microstructure and Compressive Strength of Blended Cement Pastes.” *Cement and Concrete Research* 33(10): 1543–48.

Yan, Xiancui et al. 2020. “Using EDTA-2Na to Inhibit Sulfate Attack in Slag Cement Mortar under Steam Curing.” *Construction and Building Materials* 265: 120324.

Yang, Jin et al. 2019. “Eco-Friendly Treatment of Low-Calcium Coal Fly Ash for High Pozzolanic Reactivity: A Step towards Waste Utilization in Sustainable Building Material.” *Journal of Cleaner Production* 238: 117962.

Yang, Keun Hyeok, Ah Ram Cho, Jin Kyu Song, and Sang Ho Nam. 2012. “Hydration Products and Strength Development of Calcium Hydroxide-Based Alkali-Activated Slag Mortars.” *Construction and Building Materials* 29: 410–19.

Ye, Hailong, and Aleksandra Radlińska. 2016. “Shrinkage Mechanisms of Alkali-Activated Slag.” *Cement and Concrete Research* 88: 126–35.

Younsi, A., Ph Turcry, A. Aït-Mokhtar, and S. Staquet. 2013. “Accelerated Carbonation of Concrete with High Content of Mineral Additions: Effect of Interactions between Hydration and Drying.” *Cement and Concrete Research* 43(1): 25–33. http://dx.doi.org/10.1016/j.cemconres.2012.10.008.

Yu, Zhuqing, and Guang Ye. 2013. “The Pore Structure of Cement Paste Blended with Fly Ash.” *Construction and Building Materials* 45: 30–35.

Yuan, Qiang et al. 2009. “Chloride Binding of Cement-Based Materials Subjected to External Chloride Environment - A Review.” *Construction and Building Materials* 23(1): 1–13. http://dx.doi.org/10.1016/j.conbuildmat.2008.02.004.

Zajac, Maciej et al. 2018. “Impact of Microstructure on the Performance of Composite Cements: Why Higher Total Porosity Can Result in Higher Strength.” *Cement and Concrete Composites* 90: 178–92.

Zajac, MacIej, Anne Rossberg, Gwenn Le Saout, and Barbara Lothenbach. 2014. “Influence of Limestone and Anhydrite on the Hydration of Portland Cements.” *Cement and Concrete Composites* 46: 99–108.

Zhang, Duo, Zaid Ghouleh, and Yixin Shao. 2017. “Review on Carbonation Curing of Cement-Based Materials.” *Journal of CO2 Utilization* 21(July): 119–31. https://doi.org/10.1016/j.jcou.2017.07.003.

Zhang, Jian, Caijun Shi, and Z. Zhang. 2019. “Chloride Binding of Alkali-Activated Slag/Fly Ash Cements.” *Construction and Building Materials* 226: 21–31. https://doi.org/10.1016/j.conbuildmat.2019.07.281.

Zhang, Jingxiao et al. 2022. “Review on Chloride Transport in Alkali-Activated Materials: Role of Precursors, Activators and Admixtures.” *Construction and Building Materials* 328(January): 127081.

Zhang, Zengqi, Bo Zhang, and Peiyu Yan. 2016. “Comparative Study of Effect of Raw and Densified Silica Fume in the Paste, Mortar and Concrete.” *Construction and Building Materials* 105: 82–93.

Zhu, Xiaohong et al. 2018. “Effect of Ca(OH)2 on Shrinkage Characteristics and Microstructures of Alkali-Activated Slag Concrete.” *Construction and Building Materials* 175: 467–82.

Zhu, Yaguang et al. 2022. “Solidification of Chloride Ions in Alkali-Activated Slag.” *Construction and Building Materials* 320(August 2021).